UNIVERSITY OF OKLAHOMA

GRADUATE COLLEGE

A Heat Wave Definition Employed across the Southern Great Plains for Trend Analysis from 1979-2019

A THESIS

SUBMITTED TO THE GRADUATE FACULTY

in partial fulfillment of the requirements for the

Degree of

MASTER OF SCIENCE IN METEOROLOGY

By

Taylor Grace

Norman, Oklahoma

2021

A Heat Wave Definition Employed across the Southern Great Plains for Trend Analysis from 1979-2019

A THESIS APPROVED FOR THE

SCHOOL OF METEOROLOGY

BY THE COMMITTEE CONSISTING OF

Dr. Jeffrey B. Basara, Chair

Dr. Elinor Martin

Dr. Jason Furtado

Acknowledgments

This work was supported by the National Science Foundation under Grant No. OIA-1946093 and NASA Water Resources Program under Grant 80NSSC19K1266. Any opinions, findings, and conclusions or recommendations expressed in this material are those of the authors and do not necessarily reflect the views of the National Science Foundation. Special thanks to Jordan Christian and Eric Hunt for their constructive feedback, comments, and guidance toward this work. Additionally, the data utilized from the NARR used in this study is available at https://www.esrl.noaa.gov/psd/data/gridded/data.narr.html. Lastly, particularly thankful for my family and friends for continued support.

Contents

Abstract

Subseasonal-to-seasonal (S2S) extremes occur frequently in the Southern Great Plains (SGP), more specifically heat waves. Heat waves are expected to increase in frequency, duration, and intensity in several regions globally, yet a single definition to identify heat wave events has not been established. This study focuses on proposing a novel comprehensive heat wave identification methodology and the application of this method to the SGP. Utilizing 2-meter temperatures from the North American Regional Reanalysis data set from 1979 through 2019, the heat wave definition was applied to complete an annual time series, duration, and seasonality analysis within the study spatial domain. Heat wave events in this study are identified when the daily maximum and minimum standardized temperature anomalies were greater than or equal to the 90^{th} percentile for a minimum of three consecutive days. The 90^{th} percentile was determined to be a more ideal relative threshold in comparison to the 95^{th} percentile through statistical analysis of the probability distribution functions of daily maximum, mean, and minimum standardized temperature anomalies across the Southern Great Plains throughout the study time period.

Spatially, a climatology of heat wave events was established on a climate division scale with the employment of three different spatial coverage percentages (i.e., 10%, 25%, and 50%) denoting the percentage of grid points within each climate division where the heat wave methodology was met. Temporal and spatial trends

were analyzed from the generated heat wave event climatologies within the annual time series, duration, and seasonality. This study found that the frequency of heat wave events is increasing over the study time period for all ten states within the SGP. Further, Louisiana and Mississippi are more susceptible to longer duration (i.e., 7-day or greater) heat wave events. Lastly, the frequency of heat wave events during all four seasons (i.e., fall, spring, summer, and winter) was increasing through all SGP states. Louisiana had the greatest increasing trend of fall, spring, and winter heat wave events, whereas Texas had the largest increasing trend in summer season heat waves. All relationships appeared within all three spatial coverage methods. The climatologies solved the need of a database of heat wave events in the Southern Great Plains, established on a climate division scale in this study. Furthermore, trends provided insight on the significance of particular years, locations, and future implications of heat wave events within the SGP. This work established the beginning steps in more expansive heat wave research to further analyze precursor, compound, and cascading events between multiple S2S extremes with heat wave events in order to mitigate socioeconomic losses.

1 Introduction

Extreme environmental events are common to the Southern Great Plains (SGP) of the United States, including extreme heat and heat waves. In recent years, flash droughts have impacted much of the SGP (Christian et al. 2019; Basara et al. 2019; Hunt 2020). Dong et al. (2011) as well as Christian et al. (2015) found that drought and extreme precipitation whiplash events have caused detrimental losses within this region. Additionally, Mullens and McPherson (2019) stated that an increase in hydrologic extremes in the SGP can be expected in the future. Even though past heat wave events have occurred in the SGP (Namias 1982; Cowan et al. 2017), unfortunately, a unified definition for extreme heat remains elusive (Souch and Grimmond 2004).

Figure 1.1 displays heat wave definitions used in prior studies (Smith et al. 2013) comprised of multiple variables: (1) maximum temperature (Meehl and Tebaldi 2004; Peng et al. 2011), (2) maximum and minimum temperature (Robinson 2001), (3) mean temperature (Anderson and Bell 2011), and (4) heat index (Steadman 1979, 1984). Further, the thresholds used were either relative or absolute (i.e., percentile or set value) while duration criteria varied from one to five days. Additionally, the United States National Weather Service utilizes a heat index to issue heat advisories to the general public and applies absolute thresholds dependent on the location of the National Weather Service office and the associated local climate variability. In

each study and application, given that a single definition for heat waves has not been defined, the methodologies were determined based on the individual study focus. The World Meteorological Organization (WMO) defines a heat wave as a period in which the daily maximum temperatures exceeds the daily normal maximum temperature by more then nine degrees Fahrenheit (five degrees Celsius) for more than five days consecutively. Yet, within literature this WMO definition is not primarily used. Therefore, a comprehensive definition for heat waves spanning local to global scales is needed.

Multiple socioeconomic sectors are impacted by such extreme heat events including agriculture (Lobell and Field 2007; Schlenker and Roberts 2009; van der Velde et al. 2012; Otkin et al. 2013; Hunt et al. 2014; Hunt 2020), energy (White et al. 2003; Marx et al. 2006; Miller et al. 2008), human health (Steadman 1979; Marx et al. 2006; Kovats and Hajat 2008; Anderson and Bell 2011; Gasparrini and Armstrong 2011; Barnett et al. 2012), water resources, infrastructure, and ecosystems (McKechnie and Wolf 2010; Teskey et al. 2015). Zuo et al. (2015) outlined the effects and connections of heat waves (Figure 1.2) between several socioeconomic sectors listed above. Additionally, in 2019, the National Weather Service found that heat was the number two weather-related killer in the United States. Moreover, in the last decade as well as the past 30 years in the United States, heat has been the leading weather phenomena of human mortality (Figure 1.3; National Weather Service 2020). Previous studies have researched past heat wave events to discuss potential

atmospheric drivers of extreme heat events (Meehl and Tebaldi 2004; Parker et al. 2014; Schubert et al. 2014), yet these findings were specific to the temporal periods studied and the definitions used. The heat wave event dates dependency on the heat wave definition utilized was further illustrated by Anderson and Bell (2011) who studied human mortality trends due to heat waves in several regional communities using multiple definitions. Their results found that the dates of the heat wave event depended on the classification (Figure 1.4).

Overall, past heat wave events have been studied across the world in Australia (Pezza et al. 2012; Perkins and Alexander 2013; Australian Bureau Of Meteorology 2013; Lewis and Karoly 2013; Cowan et al. 2014; Parker et al. 2014; Zuo et al. 2015), Europe (Hajat et al. 2002; Fischer et al. 2007; Della-Marta et al. 2007; Barriopedro et al. 2011; Schubert et al. 2014), China (Bai et al. 2014; Chen and Li 2017; Wu et al. 2020), and Russia (Barriopedro et al. 2011; Trenberth and Fasullo 2012). Additionally, Russo et al. (2014a) and Perkins (2015) focused their studies on a global scale. Within the United States, California has been a hot spot for heat wave research (Miller et al. 2008; Tamrazian et al. 2008; Gershunov et al. 2009; Knowlton et al. 2009; Gershunov et al. 2011; Gershunov and Guirguis 2012a). Further, Kunkel et al. (1996) and Whitman et al. (1997) focused on atmospheric patterns that were present during the July 1995 historical heat wave event in Chicago, whereas Karl and Quayle (1981) studied the 1980 summer heat wave with connection to drought conditions across the Central United States. Lastly, Bumbaco et al. (2013) captured

a historical record of heat wave events for the Pacific Northwest region in the United States. Various other studies employed different heat wave definitions either studying trends, impacts, future projections, or atmospheric drivers of extreme heat events across the entire United States (Robinson 2001; Meehl and Tebaldi 2004; Gershunov et al. 2009; Wu et al. 2012; Oswald and Rood 2014; Allen and Sheridan 2016; Schoof et al. 2017; Oswald 2018). While many of these previous studies have databases of heat wave events that have occurred with respect to each individual heat wave definition utilized, there is no consensus on a general climatology of heat wave events in specific regions.

A warming climate also raises the concern of an increase in frequency and intensity of extreme events associated with rising surface temperatures. For example, heat waves have been increasing in frequency over the past several decades (Peterson et al. 2013) and, in general, an increase in heat waves is expected over time (Karl et al. 2000; Meehl and Tebaldi 2004; Hao et al. 2013; Mazdiyasni and AghaKouchak 2015). Smith et al. (2013) found that from 1979-2011, an increase in heat wave frequency was observed for 14 out of the 15 heat wave definitions shown in Figure 1.1 across the Great Plains. In addition, Meehl and Tebaldi (2004) simulated a positive trend in worst-3 day (i.e., 3 consecutive days of the warmest daily minimum temperatures determined annually) heat waves from 2080 to 2099 in the Southern Great Plains.

However, the seasonality of heat waves has been neglected in a majority of studies. Numerous studies specifically limited their period of interest to the summer

and/or warm season (i.e., May through September). A few studies focused on specific cases (Karl and Quayle 1981; Barriopedro et al. 2011), whereas most of the studies that were interested in trends or drivers concentrated strictly on the warm season (Kunkel et al. 1996; Stefanon et al. 2012; Bumbaco et al. 2013; Cowan et al. 2014; Parker et al. 2014; Mo and Lettenmaier 2015; Perkins-Kirkpatrick and Lewis 2020). While heat waves are mostly associated with the warm season, these extreme events can occur all year round (Nissan et al. 2017; Oswald 2018). Therefore, understanding the seasonality of heat wave events within the SGP would provide insight on differing impacts dependent on the timing of the heat wave event.

As such, this study will focus on the development of a definition for heat waves to generate a climatology of heat wave events across the SGP. The objectives include: (1) define heat waves, (2) generate a climatology of heat waves from 1979-2019, and (3) understand any spatial and temporal trends. To complete the analysis, a novel definition for heat waves is outlined in Chapter 2. This definition will be used to develop a climatology of heat waves in Chapter 3, followed by a discussion on trends in heat wave events across the SGP.

1.1 Figures

Table 1 Definitions of heat wave indices. *HI16 did not have enough data to include in this analysis.

Heat Wave Indices (HI)	Temperature Metric	Threshold	Duration	HI Type	Reference(s)
HI01	Mean daily temperature	>95th percentile	2+ consecutive days	Relative	Anderson and Bell (2011)
HI02	Mean daily temperature	>90th percentile	2+ consecutive days	Relative	Anderson and Bell (2011)
HI03	Mean daily temperature	>98th percentile	2+ consecutive days	Relative	Anderson and Bell (2011)
HI04	Mean daily temperature	>99th percentile	2+ consecutive days	Relative	Anderson and Bell (2011)
HI05	Minimum daily temperature	>95th percentile	2+ consecutive days	Relative	Anderson and Bell (2011)
HI06	Maximum daily temperature	>95th percentile	2+ consecutive days	Relative	Anderson and Bell (2011)
HI07	Maximum daily temperature	T1: >81st percentile T2: >97.5th percentile	Everyday, >T1; 3+ consecutive days, >T2; Avg T_{max}>T1 for whole time period	Relative	Peng et al. (2011); Meehl and Tebaldi (2004)
HI08	Maximum daily apparent temperature	>85th percentile	1 day	Relative	Steadman (1984)
HI09	Maximum daily apparent temperature	>90th percentile	1 day	Relative	Steadman (1984)
HI10	Maximum daily apparent temperature	>95th percentile	1 day	Relative	Steadman (1984)
HI11	Maximum daily temperature	>35 °C	1 day	Absolute	Tan et al. (2007)
HI12	Minimum & maximum daily temperature	T_{min}>26.7 °C T_{max}>40.6 °C	≥1 threshold for 2+ consecutive days	Absolute	Robinson (2001)
HI13	Maximum daily heat index	>80 °F	1 day	Absolute	National Weather Service, Rothfusz and Scientific Services Division (1990); Steadman (1979)
HI14	Maximum daily heat index	>90 °F	1 day	Absolute	National Weather Service, Rothfusz and Scientific Services Division (1990); Steadman (1979)
HI15	Maximum daily heat index	>105 °F	1 day	Absolute	National Weather Service, Rothfusz and Scientific Services Division (1990); Steadman (1979)
HI16*	Maximum daily heat index	>130 °F	1 day	Absolute	National Weather Service, Rothfusz and Scientific Services Division (1990); Steadman (1979)

Figure 1.1: Table displaying the various heat wave definitions that have been used in previous studies. Table outlines the mode, threshold, duration, and reference of each definition. Figure courtesy of Smith et al. (2013).

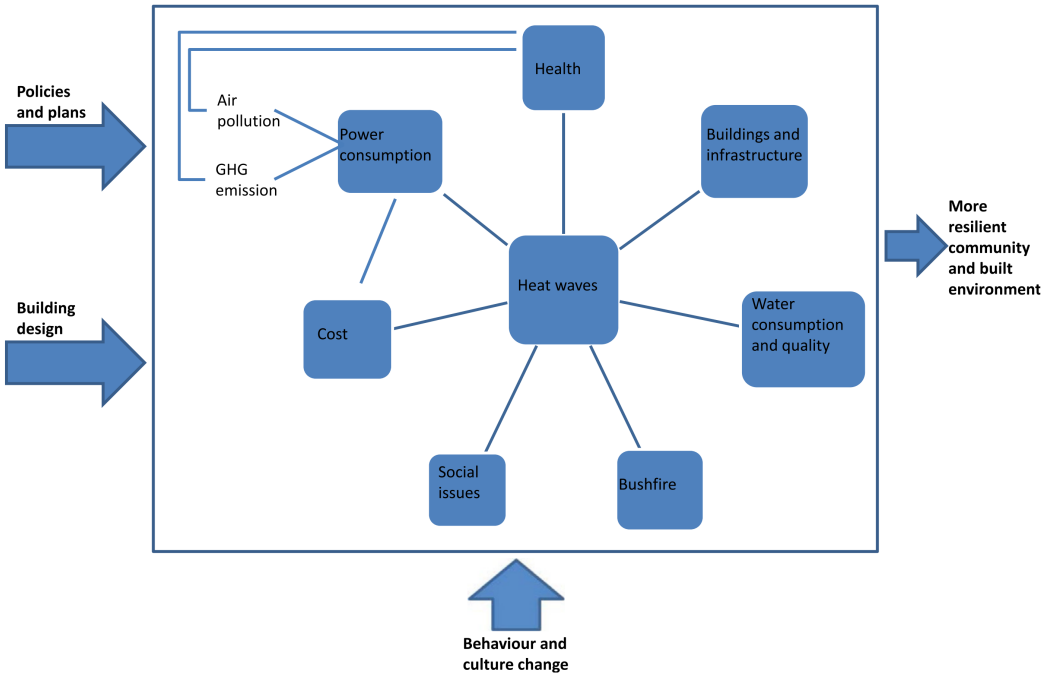

Fig. 1. Effects and mechanisms for heat waves.

Figure 1.2: Schematic outlining the impacts of heat waves on several socioeconomic sectors. Figure from Zuo et al. (2015).

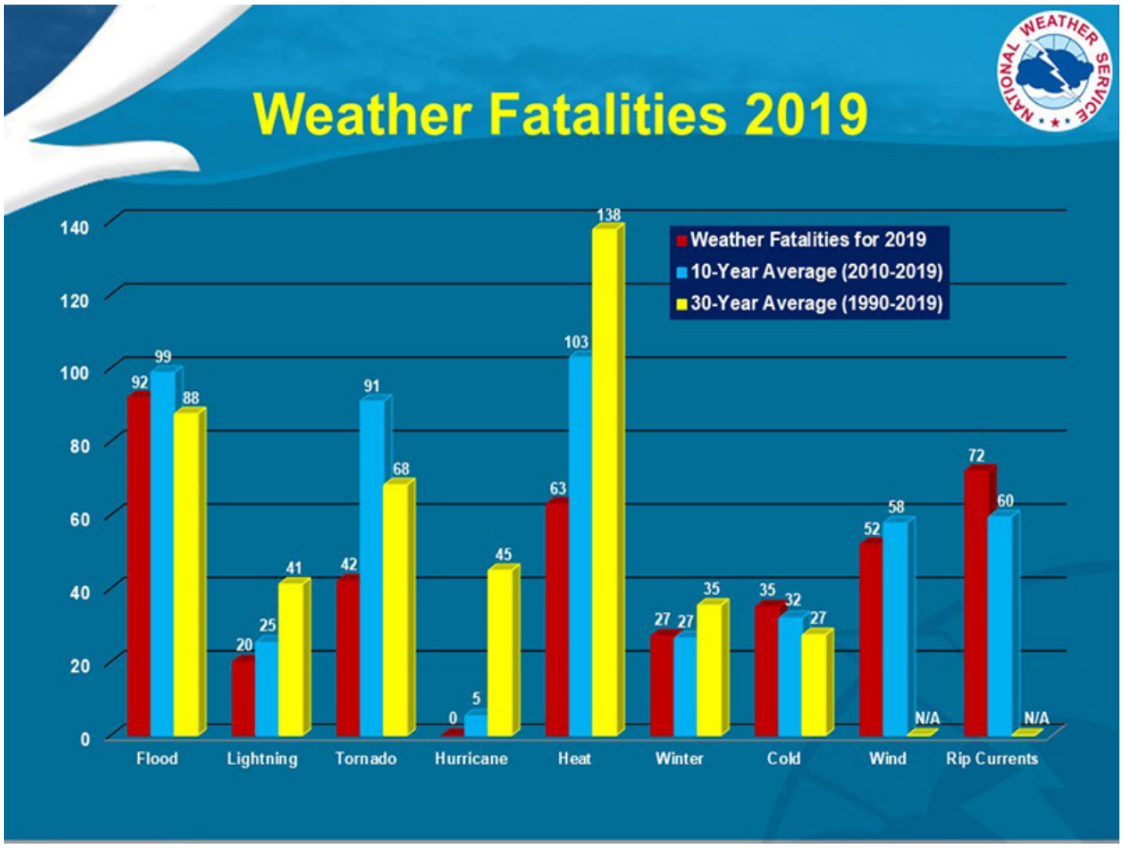

Figure 1.3: Chart illustrating the survey conducted by the National Weather Service in 2019 determining the number of fatalities due to multiple weather phenomena for the year 2019 compared to the 10-year average and 30-year average. Figure from National Weather Service (2020).

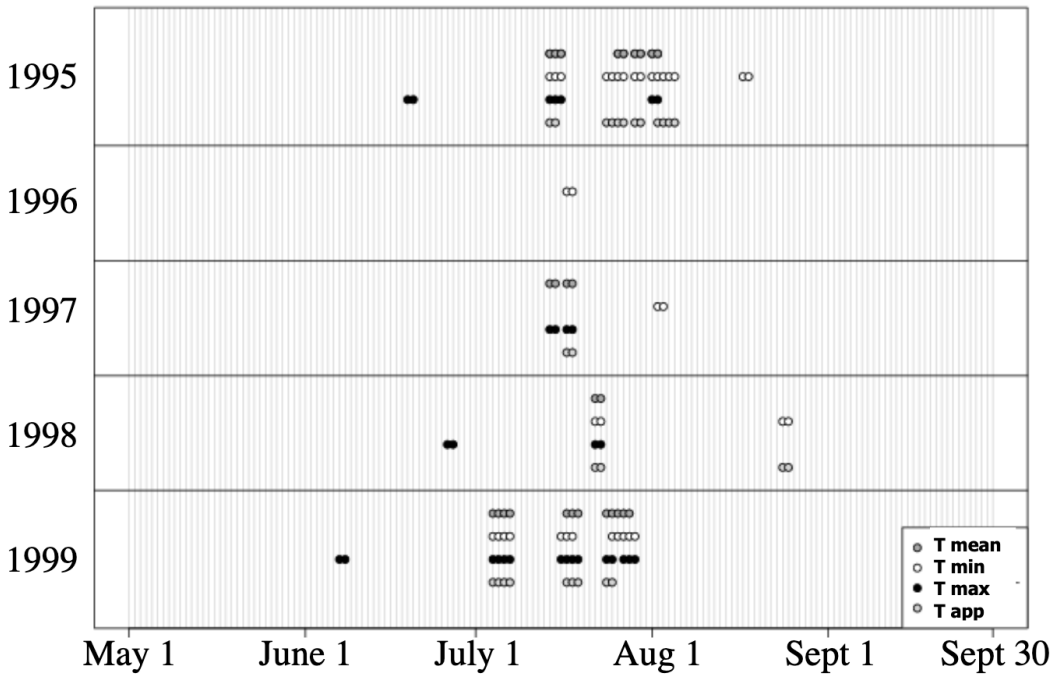

Figure 1.4: Time series of summer days from 1995 through 1999 that met the following threshold: two or more consecutive days when daily values of specified variable was equal to or greater than the 95^{th} percentile in New York, NY. Figure from Anderson and Bell (2011).

2 Heat Wave Methodology

2.1 Data & Variables

The heat wave methodology in this study depends on several variables derived over the entire time and spatial domain. Reanalysis data was used in lieu of observational to limit the amount of missing data, as well as, not needing to accommodate for homogeneity in observational temperature data (Oswald and Rood 2014). Furthermore, with the use of a percentile-base threshold, Zhang et al. (2005) found extreme inhomogeneity of percentile-based indices with the use of observational data. Using the North American Regional Reanalysis (NARR; Mesinger et al. 2006), daily maximum and minimum temperatures were calculated from 2-meter temperature values at 3-hour intervals from 1 January, 1979 through 31 December, 2019 across the Southern Great Plains (SGP). In this study, the SGP spanned from 25°N to 40.1°N, 89.5°W to 107°W.

Utilizing the climatological period of 1981 through 2010, daily standardized maximum and minimum temperature anomalies were generated which subsequently became the two primary variables employed in the heat wave methodology developed as part of this work. For the statistical distribution analysis Chapter 2.2, the standardized anomalies were detrended (i.e., daily maximum, minimum, and mean standardized anomalies). Whereas, for the climatology analysis Chapter 3, the standardized anomalies (i.e., daily maximum and minimum standardized anomalies) were

not detrended.

To capture smaller scale heat wave events, the SGP domain was subdivided into the pre-established climate divisions with boundaries denoted by the National Climate for Environmental Information (National Center for Atmospheric Research 2021). Further, several spatial methods were tested to generate a climatology. Each spatial method represented the percentage of grid points within a climate division that eclipsed critical thresholds; 10%, 25%, and 50% of the spatial area. As such, three heat wave climatologies based on spatial coverage were derived for each climate division listed in Table 2.1.

Once the climatology of heat wave events was generated, further analysis was completed to understand any temporal and/or spatial relationships. Time series were created which calculated the number of heat wave events that occurred every year within the study time period for a single SGP state. This was completed by combining all climate divisions within each SGP state, meaning that heat wave events between climate divisions in a single SGP state could have overlapped one another. However, if a heat wave event in one climate division had the same exact start and end date as any other event in another climate division, it was logged as one singular event. Furthermore, time series were derived for each SGP state for all three spatial method criteria from the corresponding heat wave climatologies. Linear trends were then determined from the time series.

Another analysis focused on duration of heat wave events. Several duration

categories were chosen to quantify any signals as to prominent heat wave duration depending on the spatial method used in the heat wave identification methodology. The duration categories were as follows: 3-day to 5-day, 5-day to 7-day, 7-day to 10-day, and 10+-day. The number of heat wave events that fell within each duration category was determined for each state across all three spatial methods, which were pulled from the entire climatology (i.e., 1979 through 2019). Further, the percentage of heat wave events that fell into each duration category out of the entire quantity of heat wave events in the climatology was derived.

Heat waves can occur any time during the year. Even though most heat wave studies have focused on heat waves during the warm season (Schubert et al. 2014; Parker et al. 2014; Cowan et al. 2014; Mo and Lettenmaier 2015), understanding potential relationships during the winter season could provide insight on the variability and the true change in heat wave events within a region. Heat waves that occur during the winter season are more of a warm thermal shock. These warm thermal shocks have different, but potentially important, impacts in comparison to heat waves that occur during the typical heat wave season. For example, a winter thermal shock within a region could result in warming of the surface further facilitating an early growing season. Due to the timing of the winter thermal shock, a return to normal temperatures after the presence of this winter thermal shock would pose potential detrimental impacts on vegetation due to the early growing season that was induced by the winter thermal shock. Therefore, seasonality was of interest due to previous

research focusing on case studies during the warm season, further lacking the concern on seasonality of heat waves. For each SGP state and spatial method, the frequency of heat wave events that occurred in each season per year was determined. Fall was categorized by September, October, and November values. Spring was determined with the values during the months of March, April, and May. The summer season distributions were derived from June, July, and August standardized temperature anomalies. Winter was analyzed for the months of December, January, and February. Therefore, time series of heat wave events for all four seasons across the study spatial domain from the climatology was derived and further the trend was calculated.

2.1.1 Statistical Significance Testing

Multiple significance tests were executed to quantify the robustness of the results. As stated, trends were derived for the time series and seasonality analyses. Each trend calculated was tested for statistical significance via the Mann-Kendall trend test (Mann 1945; Kendall 1957). The Mann-Kendall trend test is mostly used to identify statistically significant monotonic trends. The Mann-Kendall test has been used to justify statistical significance in flash drought (Hu et al. 2021), drought (Joshi et al. 2016; Yilmaz 2019; Tosunoglu and Kisi 2017; Bari Abarghouei and Safari Zarch 2011; Mazdiyasni and AghaKouchak 2015), and temperature (Karmeshu Supervisor Frederick Scatena 2015; Gavrilov et al. 2016; Alhaji et al. 2018) trends. Each trend was tested against two different alpha values; $\alpha = 0.05$ and $\alpha = 0.10$. The null

hypothesis (H_0) of the Mann-Kendall trend test was there was no trend present in the data set (e.g., time series), whereas the alternative hypothesis (H_a) was that there was a trend (either positive or negative) present in the data set. As such, if the trend of each had p <0.05, then the trend present in that data set was statistically significant to the 95% confidence interval; these trends were noted with two asterisks next to the trend value (i.e., heat wave events/year **). Yet, if 0.05 <p <0.10, then the trend calculated within that data was statistically significant to the 90% confidence interval and denoted by a single asterisk (i.e., heat wave events/year *).

2.2 Statistical Distribution Analysis

As shown by Figure 1.1, several different thresholds have been used in previous scientific research to study heat waves. Thus, an analysis on the distribution of daily maximum, minimum, and mean standardized temperature anomalies was completed for all climate divisions within the SGP spatial domain. These distributions were categorized by season to minimize any noise due to seasonality of surface temperatures. All of the values of each variable for the period spanning 1979 through 2019 were plotted. Once each histogram was plotted, several statistical distributions were fitted to the season data set and statistical significance testing was completed to test goodness-of-fit. Of the Gumbel, Skewed Normal, and Normal distribution possibilities, the Kolmogorov-Smirnov (ks-test) fitness test determined that the Normal distribution fitted all three variables the best. For the ks-test, the null hypothesis

(H_0) was that the sample comes from the statistical distribution tested, while the alternative hypothesis (H_a) was that the sample does not come from the statistical distribution tested. Each climate division histograms were plotted for the variable of interest with the mean (black dashed line), 90^{th} percentile threshold (blue solid line), 95^{th} percentile threshold (red dashed line), and the fitted Normal distribution outlined (grey solid line).

2.2.1 Fall

Beginning with the fall season values (Figures 2.2, 2.3, and 2.4), fitted distributions were derived for daily maximum, mean, and minimum standardized temperature anomalies for each state within the study spatial domain. Figure 2.2a-k illustrate that with 95% confidence, the combined daily maximum standardized temperature anomalies came from a Normal distribution (i.e., p ¿ 0.05). The main point from this analysis was to determine the ideal relative threshold to use within the heat wave methodology. As such, Figure 2.2l represents the difference between the number of values that fell above the 90^{th} percentile and 95^{th} percentile thresholds for each state. Note that states that had fewer climate divisions within the SGP spatial domain will naturally have smaller magnitudes in the count differences. Similarly, the daily mean standardized temperature anomalies during the fall season (Figure 2.3) yielded a Normal distribution. The count of the difference between the number of daily mean standardized temperature anomalies that were greater than the 90^{th} and 95^{th}

percentile thresholds (Figure 2.3l) were approximately the same range for each state compared to the fall daily maximum standardized temperature anomalies (Figure 2.2l). Additionally, the daily minimum standardized temperature anomalies during the months within the fall season were fitted for each state and displayed in Figure 2.4. Similar to daily maximum and mean standardized temperature anomalies, the ks-test indicates that the daily minimum standardized temperature anomalies during the months of September, October, and November from 1979 through 2019 came from a Normal distribution for all states in the SGP spatial domain. Again, the range in the number of daily minimum standardized temperature anomalies between the 90^{th} and 95^{th} percentile thresholds (Figure 2.4l) were approximately the same for each state compared to daily maximum and mean standardized temperature anomalies. In general, for a majority of the states the number of values during the fall months across the entire study time period was greater than 800. Furthermore, with the use of the 95^{th} percentile as the relative threshold in the heat wave event identification could be too extreme for the fall season, missing out on some heat wave events that still had an impact on socioeconomic sectors.

2.2.2 Spring

Utilizing the same analysis as the fall season, Figures 2.5, 2.6, and 2.7 demonstrated that all three standardized anomalies of air temperature during the spring season were consistent with a Normal distribution for all of the SGP states. For

the number of values for each variable that fell between the 90^{th} and 95^{th} percentile thresholds, Figures 2.5l, 2.6l, and 2.7l, identified similar conditions as the fall season. Despite the fact that the magnitude of the number of values in between the two percentile thresholds for eight out of the eleven states for at least two of the three study variables was less during the spring months compared to the fall months, a majority of the SGP states still had overall difference values greater than 800. Therefore, the 95^{th} percentile as the relative threshold could yield several heat wave events to be missed during the spring season, thus the 90^{th} percentile was chosen.

2.2.3 Summer

The summer months (i.e., June, July, and August) are most associated with a higher probability of heat waves to occur (Kunkel et al. 1996; Barriopedro et al. 2011; Stefanon et al. 2012; Bumbaco et al. 2013; Parker et al. 2014). Therefore, understanding the distribution of daily maximum, mean, and minimum standardized temperature anomalies during the summer season would be most crucial for heat wave events. Employing the same methodology as the fall and spring seasons, the ks-test proved that summertime daily standardized temperature anomalies for all three variables were consistent with a Normal distribution in all SGP states (Figures 2.8a-k, 2.9a-k, and 2.10a-k). Further within the analysis, the quantity of the count difference between both test relative thresholds for each variable (i.e., daily maximum, mean, or minimum standardized temperature anomalies) was still relatively large in a general

sense; most states had count values greater than 700 as displayed in Figures 2.8l, 2.9l, and 2.10l. In comparison to the spring season months, the count difference magnitude for many of the SGP states was less during the summer season. Starting with daily maximum standardized temperature anomalies, illustrated by Figures 2.5l and 2.8l, Arkansas, Mississippi, Tennessee, and Illinois are the only SGP states that had a larger magnitude in count difference between the 90^{th} and 95^{th} percentile threshold during the summer months than the spring season. Figures 2.6l and 2.9l illustrated the contrary, where Kansas, Oklahoma, and Illinois had a larger count difference for daily mean standardized temperature anomalies during the summer than the spring season. Finally, even fewer states had a larger count difference between the two relative thresholds when the spring and summer seasons were compared for the daily minimum standardized temperature anomalies; Kansas had a larger quantity of daily minimum standardized temperature anomalies between the 90^{th} and 95^{th} percentile thresholds (Figure 2.10l) during the summer months than the spring season (Figure 2.7l). Additionally, the variability during the spring season in the SGP was larger for all three variables compared to the summer months. However, within the summer season, the daily maximum temperatures had more variability than mean and minimum daily temperatures for states included in the study spatial domain. Moreover, because the count of the number of daily maximum, mean, or minimum standardized temperature anomalies that fell between the 90^{th} and 95^{th} percentile thresholds was greater than 700 for majority of the SGP states, further supports the

use of the 90^{th} percentile as the relative threshold versus the 95^{th} percentile.

2.2.4 Winter

The last season of focus, winter, followed the same trend set by the previous seasons discussed. Thus, the ks-test showed that, with 95% confidence, daily maximum, mean, and minimum standardized temperature anomalies derived from the winter months came from a Normal distribution (Figures 2.11a-k, 2.12a-k, 2.13a-k). Further, the magnitude of the difference count between the 90^{th} and 95^{th} percentile thresholds were greater than 800 for the SGP states (Figure 2.11l). Texas, Louisiana, Arkansas, and Mississippi were some of the SGP states that had a largest increase in count difference quantities for daily minimum standardized temperature anomalies (Figures 2.13l) compared to the summer season counts (Figure 2.10l), while Texas and Louisiana had the largest increase in the number of daily mean standardized temperature anomaly values that fell between the 90^{th} and 95^{th} percentile thresholds in the winter season (Figure 2.12l) compared to the summer month (Figure 2.9l) analysis. In short, the winter season analysis for all three variables further showed that the use of the 95^{th} percentile may be too restrictive in the heat wave methodology due to the large magnitude of the quantity of each variable that fell within the two test threshold boundaries.

2.2.5 General Summary

From the statistical distribution analysis for daily maximum, mean, and minimum standardized temperature anomalies, the use of the 90^{th} percentile as the relative threshold within this heat wave methodology proposed was strongly supported by the Normal distribution for all four seasons as well as the count difference quantities which demonstrated that the 95^{th} percentile may not be representative of the true number of heat waves that would have occurred. Therefore, for this heat wave methodology the 90^{th} percentile was selected as the relative threshold to fully capture heat wave events that may have occurred in each region within the study time period (i.e., 1979 through 2019).

2.3 Heat Wave Identification Definition

A single, comprehensive heat wave definition has not been adopted within the scientific literature (Souch and Grimmond 2004), so this study proposes a novel definition. For a heat wave event to begin within a region (i.e., a single climate division), two criteria needed to be met:

(1) daily maximum standardized temperature anomaly was greater than or equal to the 90^{th} percentile

(2) daily minimum standardized temperature anomaly was greater than or equal to the 90^{th} percentile

This threshold must be met for three consecutive days to initialize the start of a heat wave event. Once the minimum temporal threshold for any heat wave event was identified, the end point was determined. If the heat wave threshold was not met for more than three days, the heat wave event ended on the last date the threshold was met. This allowed for a three-day buffer to end a heat wave event and takes into account short-term modification of surface temperatures that could temporally mask long-term heat wave events. An example of determining the start and end dates of a heat wave event is outlined in Table 2.2. Via this identification methodology, the start and end dates of each heat wave event that occurred in each climate division within the SGP for each spatial method was determined for the study data set. Figure 2.1 outlines all of the steps taken to complete this heat wave methodology.

2.4 Tables and Figures

State	Climate Division (CD)
TX	CD1, CD2, CD3, CD4, CD5, CD6, CD7, CD8, CD9, CD10
OK	CD1, CD2, CD3, CD4, CD5, CD6, CD7, CD8, CD9
KS	CD1, CD2, CD3, CD4, CD5, CD6, CD7, CD8, CD9
NM	CD2, CD3, CD5, CD6, CD7, CD8
CO	CD1, CD2, CD3, CD4, CD5
LA	CD1, CD2, CD3, CD4, CD5, CD6, CD7, CD8, CD9
AR	CD1, CD2, CD3, CD4, CD5, CD6, CD7, CD8, CD9
MO	CD1, CD2, CD3, CD4, CD5, CD6
MS	CD1, CD2, CD3, CD4, CD5, CD7, CD8
IL	CD3, CD4, CD6, CD8

Table 2.1: Climate Divisions included in the Southern Great Plains spatial domain (25 °N to 40.1 °N, 89.5 °W to 107 °W).

Date Threshold Met	Heat Wave Start Date	Heat Wave End Date
7/1	7/1	7/8
7/2		
7/3		
7/4		
7/7		
7/8		
7/12		

Table 2.2: Example of determining a heat wave event through the identification methodology.

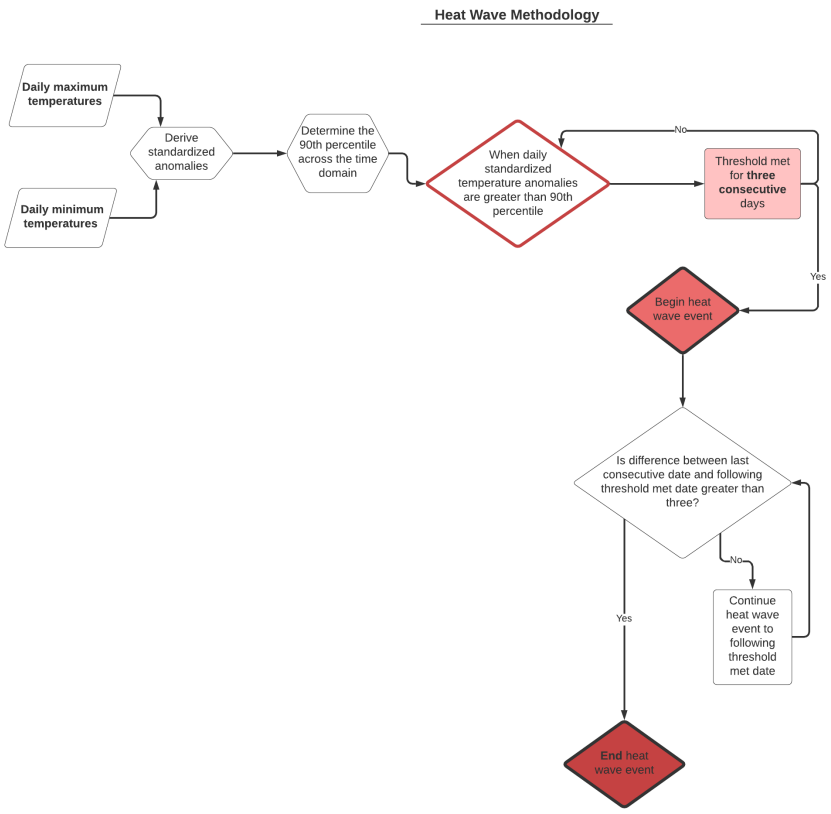

Figure 2.1: Flowchart outlining the procedures and steps in the heat wave identification methodology. Important steps in determining the start and end dates of each heat wave event are highlighted in red colors.

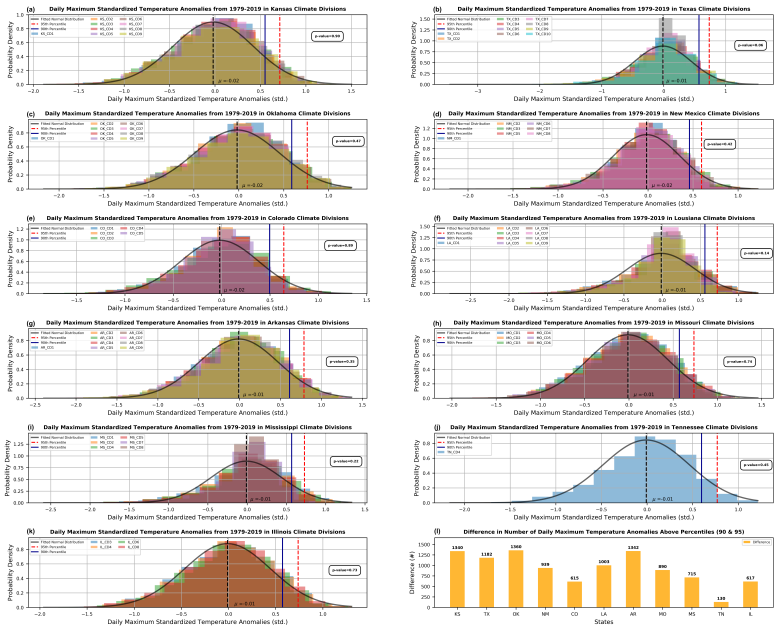

Figure 2.2: Statistical distributions of daily maximum standardized temperature anomalies during the fall season (September, October, and November) from 1979 through 2019. (a) Histograms of daily maximum standardized temperature anomalies for each climate division in Kansas in the SGP spatial domain overlaid (various colors). Fitted Normal distribution outlined in grey; mean (dashed black), 90^{th} (solid blue), and 95^{th} (dashed red) percentile thresholds distinguished accordingly. P-value determined by the Kolmogorov-Smirnov goodness-of-fit test at the 95% confidence interval printed. (b-k) Same as (a), but for Texas, Oklahoma, New Mexico, Colorado, Louisiana, Arkansas, Missouri, Mississippi, Tennessee, and Illinois, respectively. (l) Number of daily maximum standardized temperature anomalies that fall between the 90^{th} and the 95^{th} percentile thresholds for each SGP state. Total count displayed in bold black number above each bar.

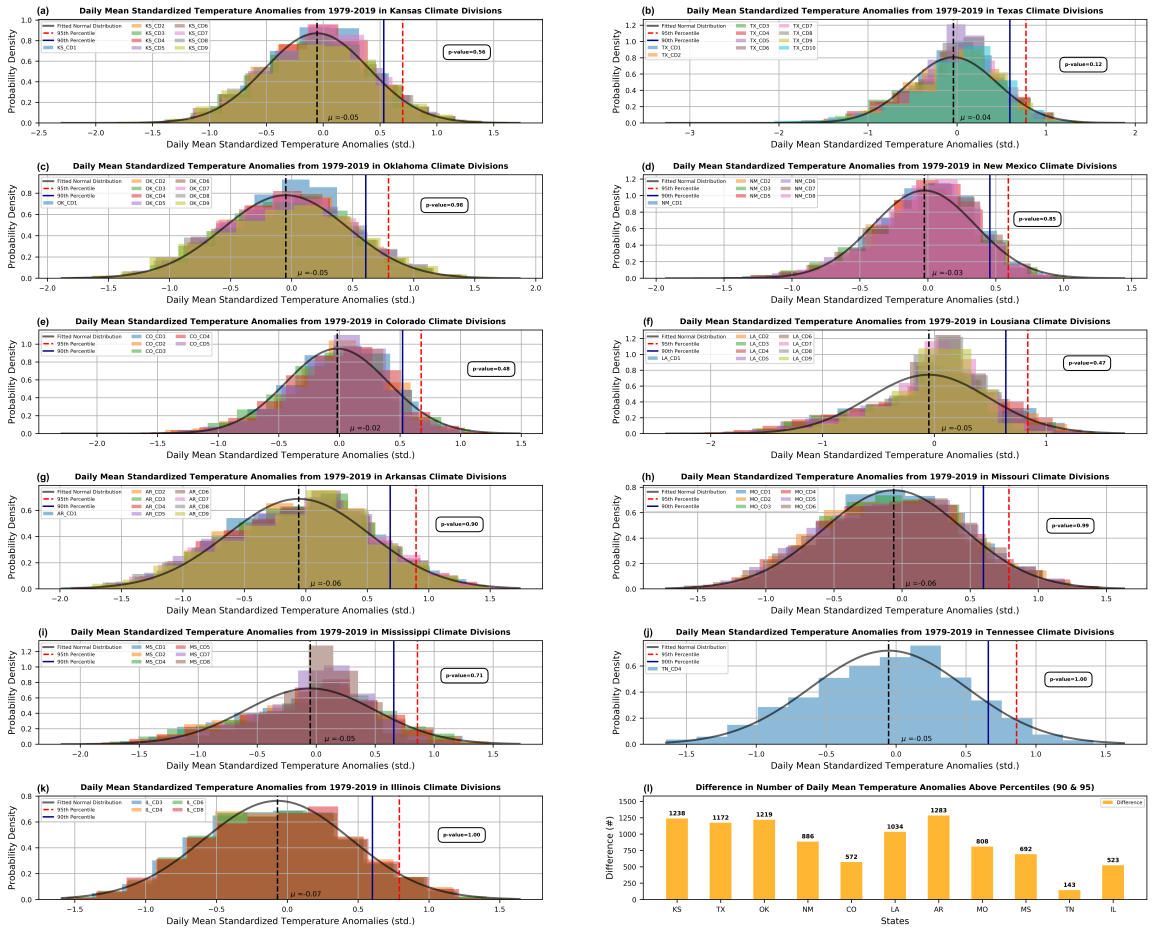

Figure 2.3: Same as Figure 2.2, but analysis on daily mean standardized temperature anomalies during the fall season from 1979 through 2019.

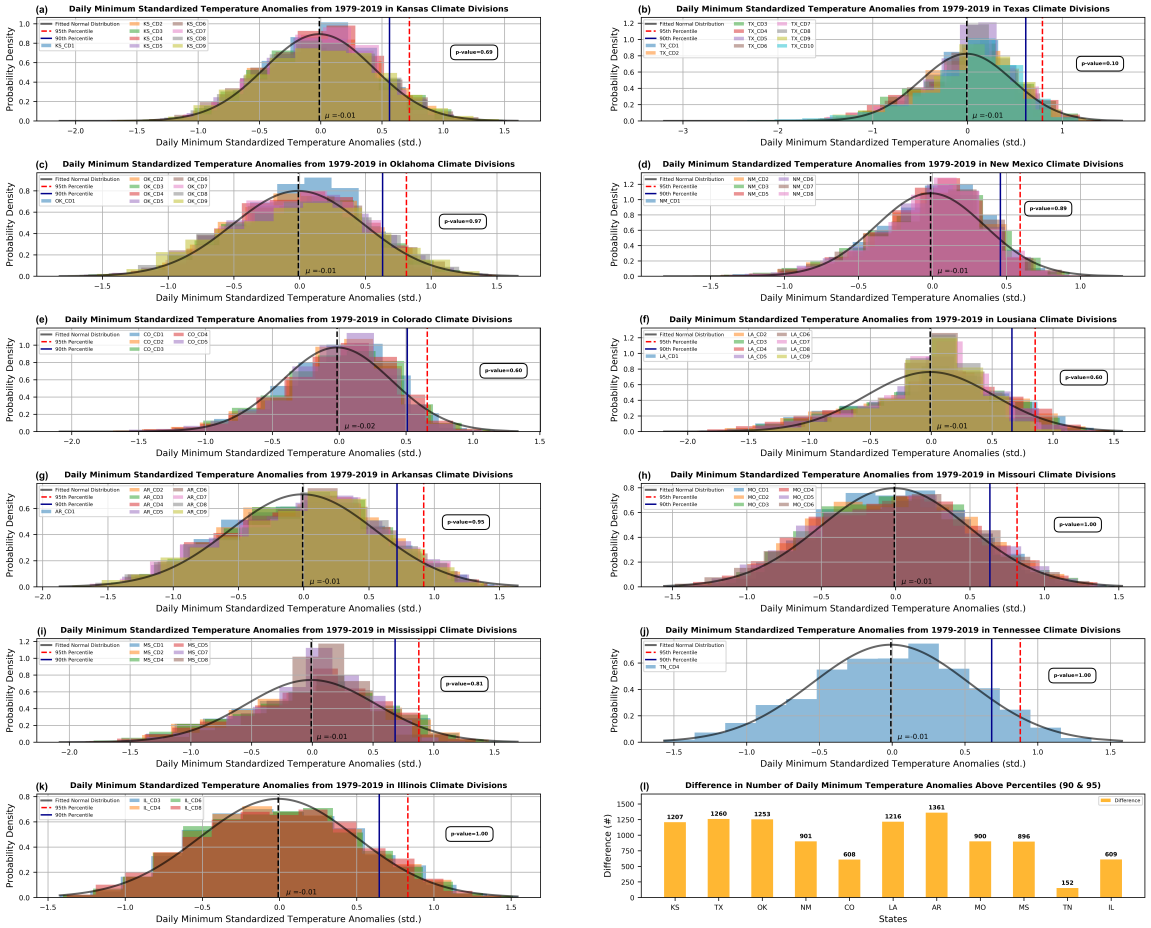

Figure 2.4: Same as Figure 2.2, but utilizing daily minimum standardized temperature anomalies during the fall season from 1979 through 2019.

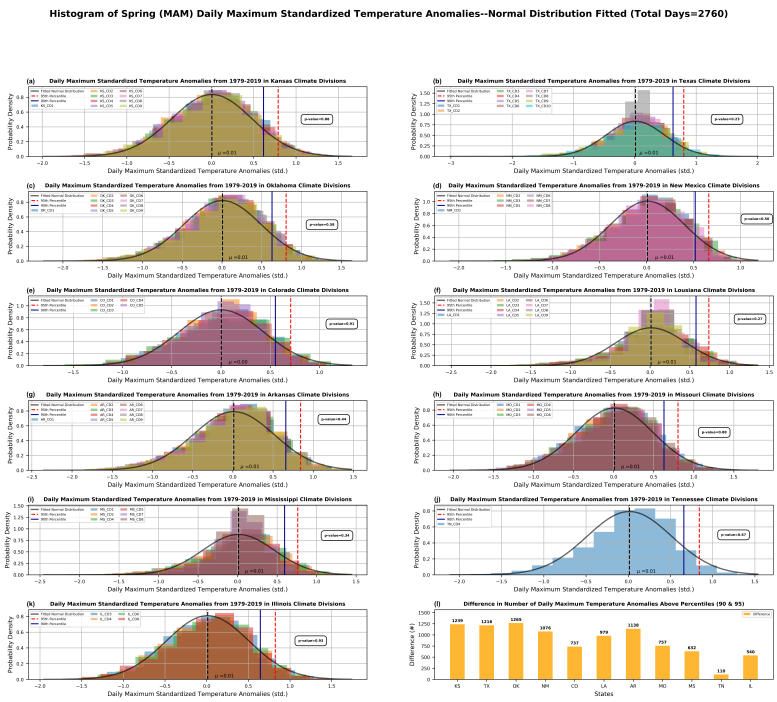

Figure 2.5: Statistical distributions of daily maximum standardized temperature anomalies during the spring season (March, April, and May) from 1979 through 2019. (a) Histograms of daily maximum standardized temperature anomalies for each climate division in Kansas in the SGP spatial domain overlaid (various colors). Fitted Normal distribution outlined in grey; mean (dashed black), 90^{th} (solid blue), and 95^{th} (dashed red) percentile thresholds distinguished accordingly. P-value determined by the Kolmogorov-Smirnov goodness-of-fit test at the 95% confidence interval printed. (b-k) Same as (a), but for Texas, Oklahoma, New Mexico, Colorado, Louisiana, Arkansas, Missouri, Mississippi, Tennessee, and Illinois, respectively. (l) Number of daily maximum standardized temperature anomalies that fall between the 90^{th} and the 95^{th} percentile thresholds for each SGP state. Total count displayed in bold black number above each bar.

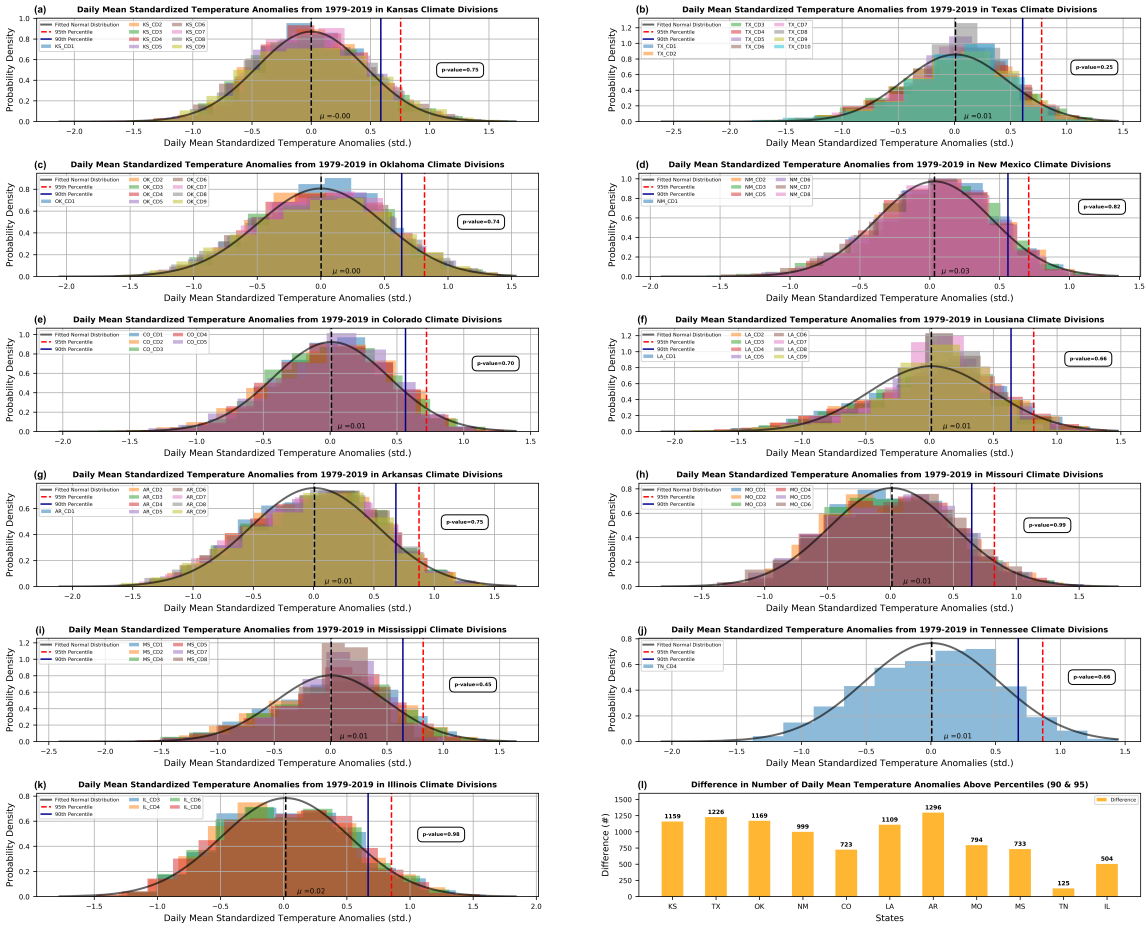

Figure 2.6: Same as Figure 2.5, but using daily mean standardized temperature anomalies during the spring season from 1979 through 2019.

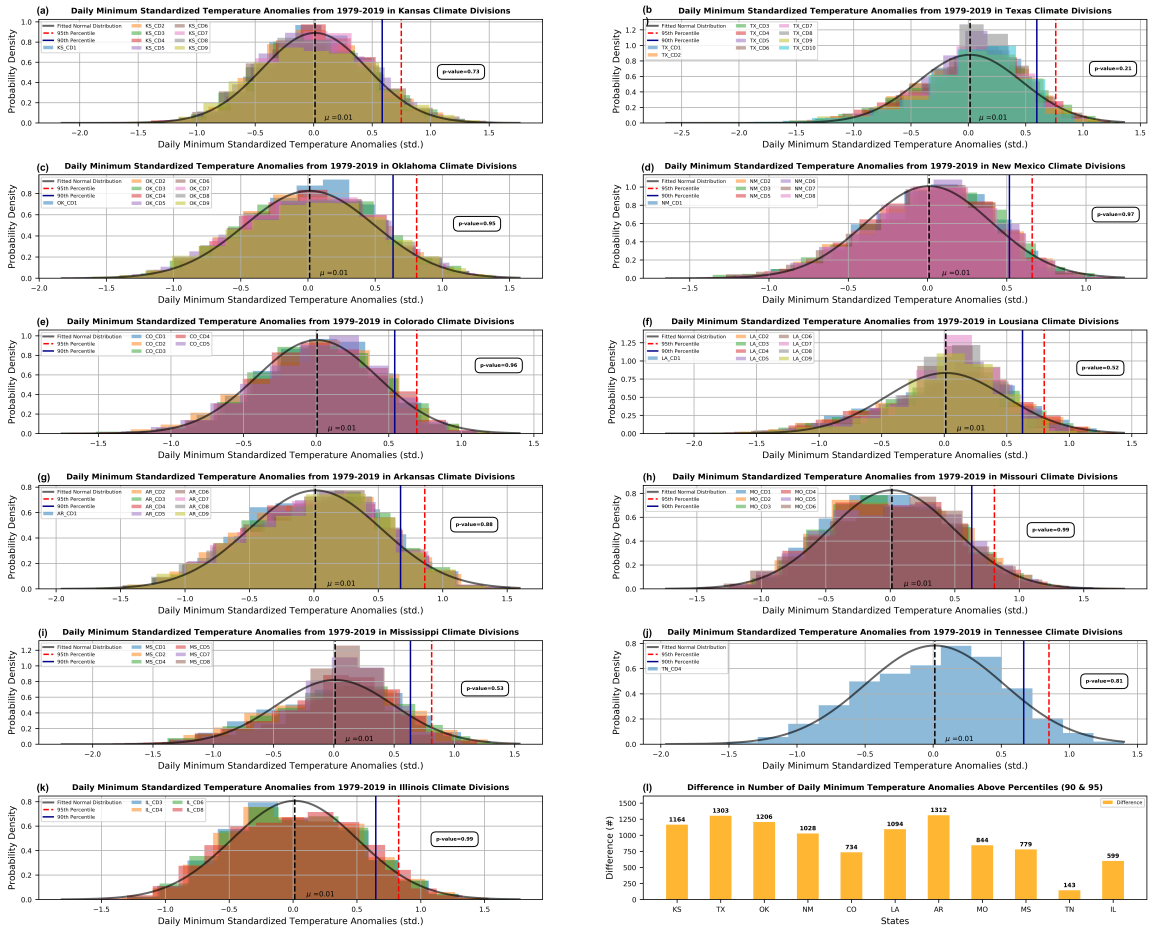

Figure 2.7: Same as Figure 2.7, instead with daily minimum standardized temperature anomalies during the spring months from 1979 through 2019.

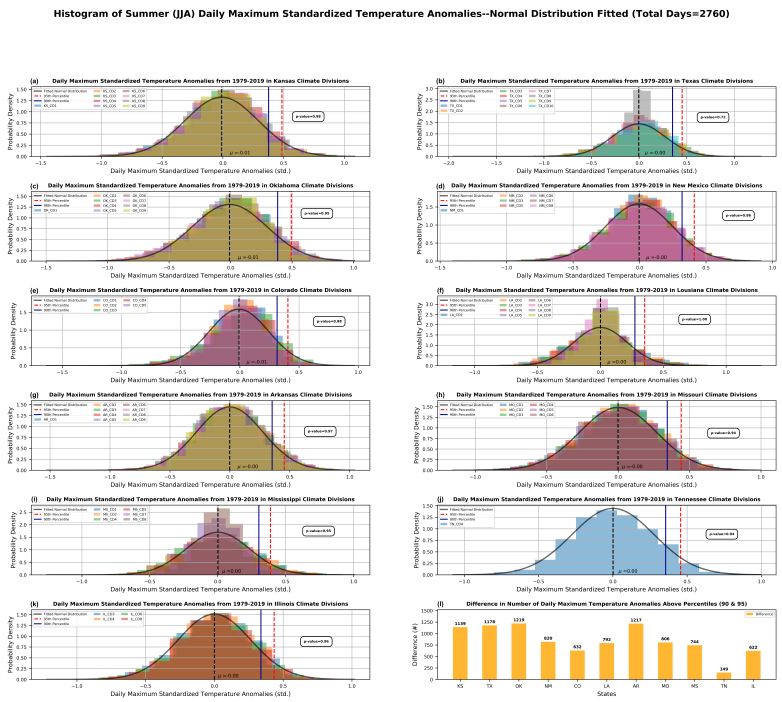

Figure 2.8: Statistical distributions of daily maximum standardized temperature anomalies during the summer season (June, July, and August) from 1979 through 2019. (a) Histograms of daily maximum standardized temperature anomalies for each climate division in Kansas in the SGP spatial domain overlaid (various colors). Fitted Normal distribution outlined in grey; mean (dashed black), 90^{th} (solid blue), and 95^{th} (dashed red) percentile thresholds distinguished accordingly. P-value determined by the Kolmogorov-Smirnov goodness-of-fit test at the 95% confidence interval printed. (b-k) Same as (a), but for Texas, Oklahoma, New Mexico, Colorado, Louisiana, Arkansas, Missouri, Mississippi, Tennessee, and Illinois, respectively. (l) Number of daily maximum standardized temperature anomalies that fall between the 90^{th} and the 95^{th} percentile thresholds for each SGP state. Total count displayed in bold black number above each bar.

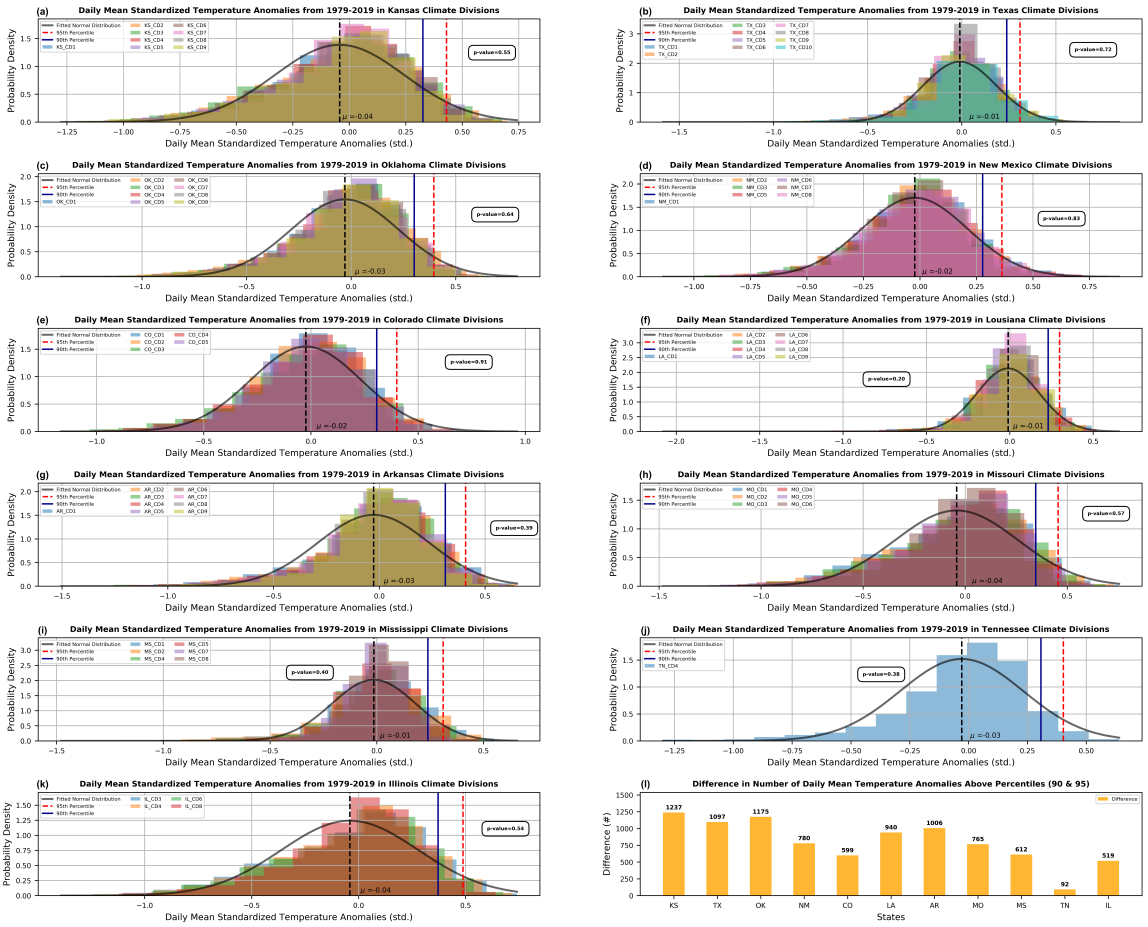

Figure 2.9: Same as Figure 2.8, but utilizing daily mean standardized temperature anomalies during the summer months from 1979 through 2019.

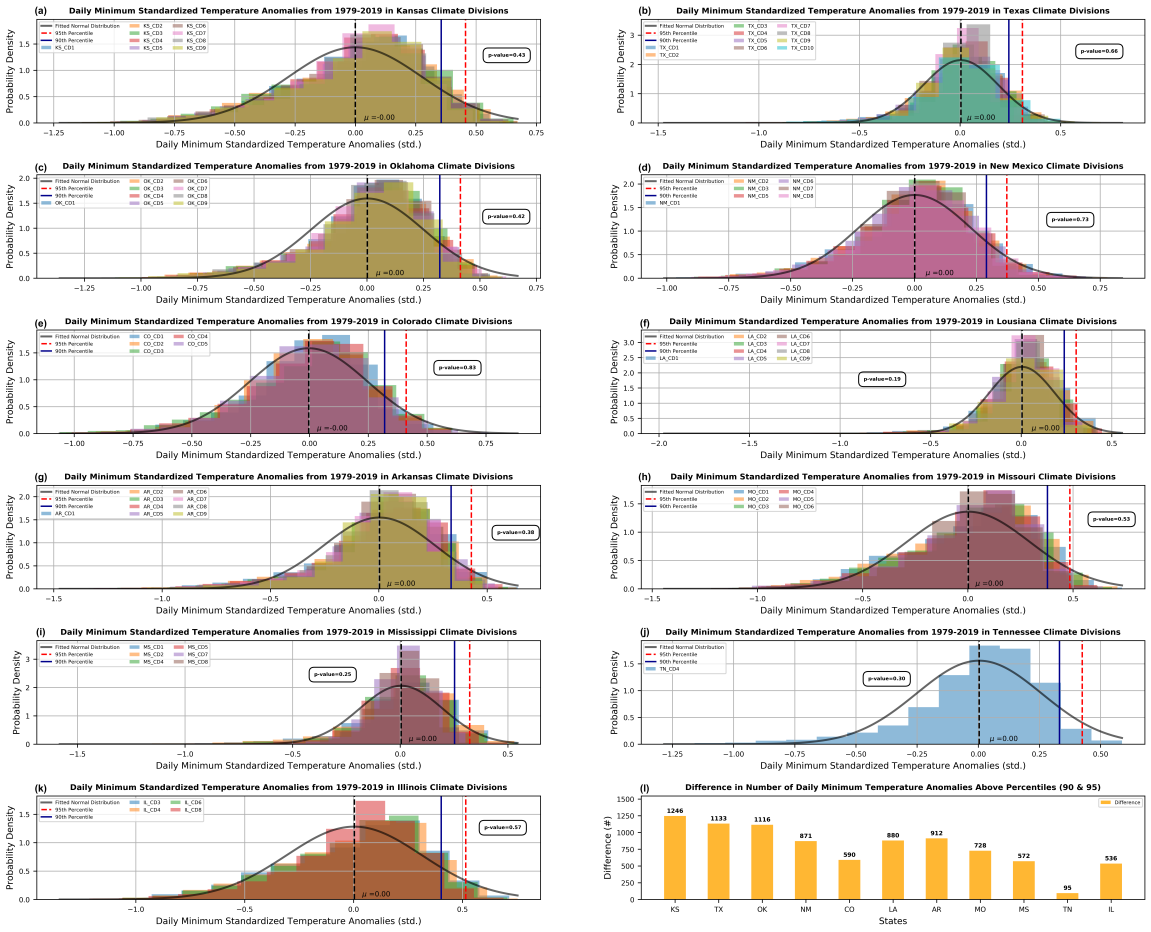

Figure 2.10: Same as Figure 2.8, but employing daily minimum standardized temperature anomalies during the summer season from 1979 through 2019.

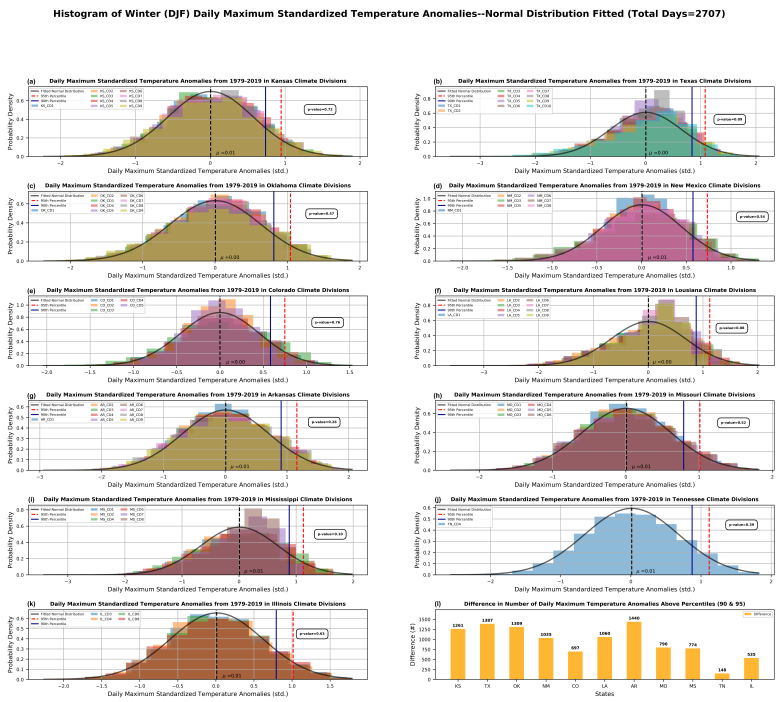

Figure 2.11: Statistical distributions of daily maximum standardized temperature anomalies during the winter season (December, January, and February) from 1979 through 2019. (a) Histograms of daily maximum standardized temperature anomalies for each climate division in Kansas in the SGP spatial domain overlaid (various colors). Fitted Normal distribution outlined in grey; mean (dashed black), 90^{th} (solid blue), and 95^{th} (dashed red) percentile thresholds distinguished accordingly. P-value determined by the Kolmogorov-Smirnov goodness-of-fit test at the 95% confidence interval printed. (b-k) Same as (a), but for Texas, Oklahoma, New Mexico, Colorado, Louisiana, Arkansas, Missouri, Mississippi, Tennessee, and Illinois, respectively. (l) Number of daily maximum standardized temperature anomalies that fall between the 90^{th} and the 95^{th} percentile thresholds for each SGP state. Total count displayed in bold black number above each bar.

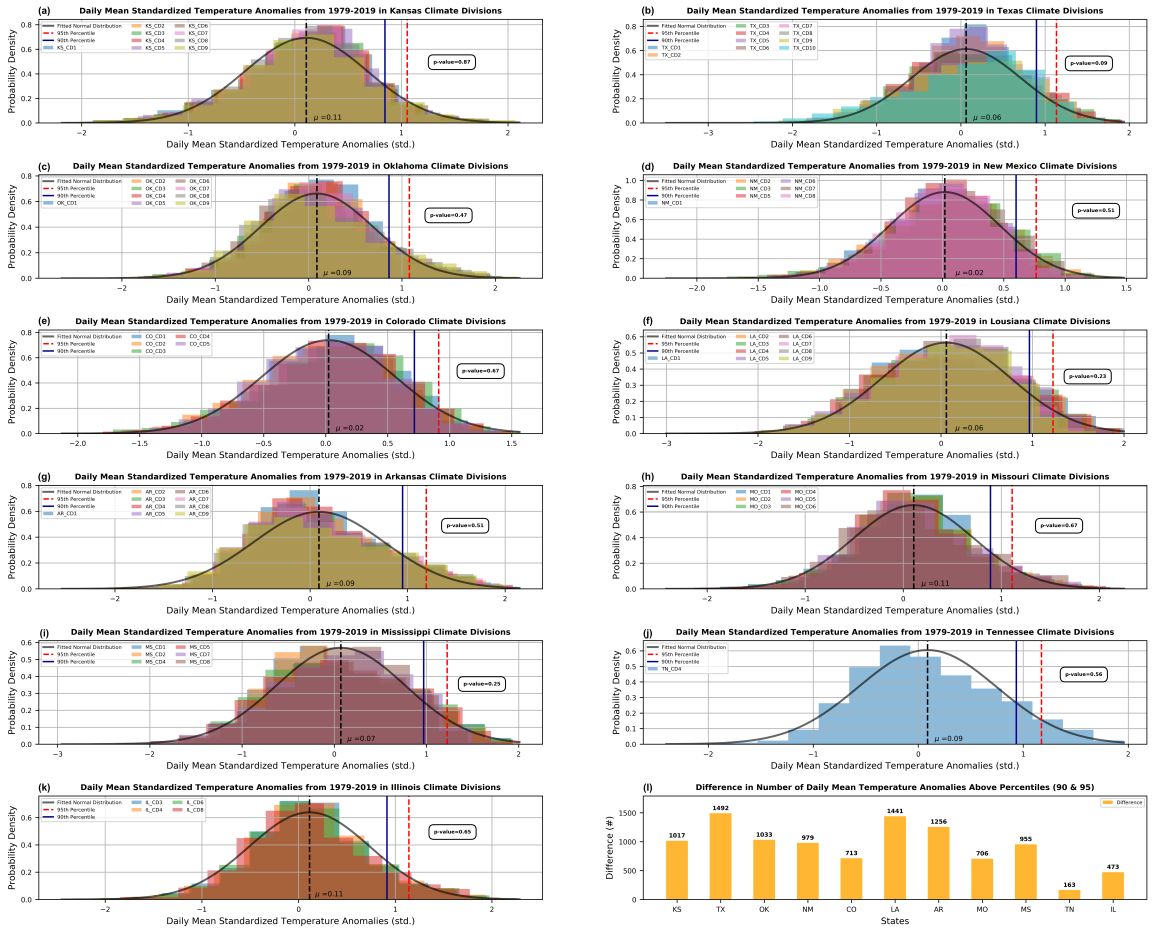

Figure 2.12: Same as Figure 2.11, but using daily mean standardized temperature anomalies during the winter season from 1979 through 2019.

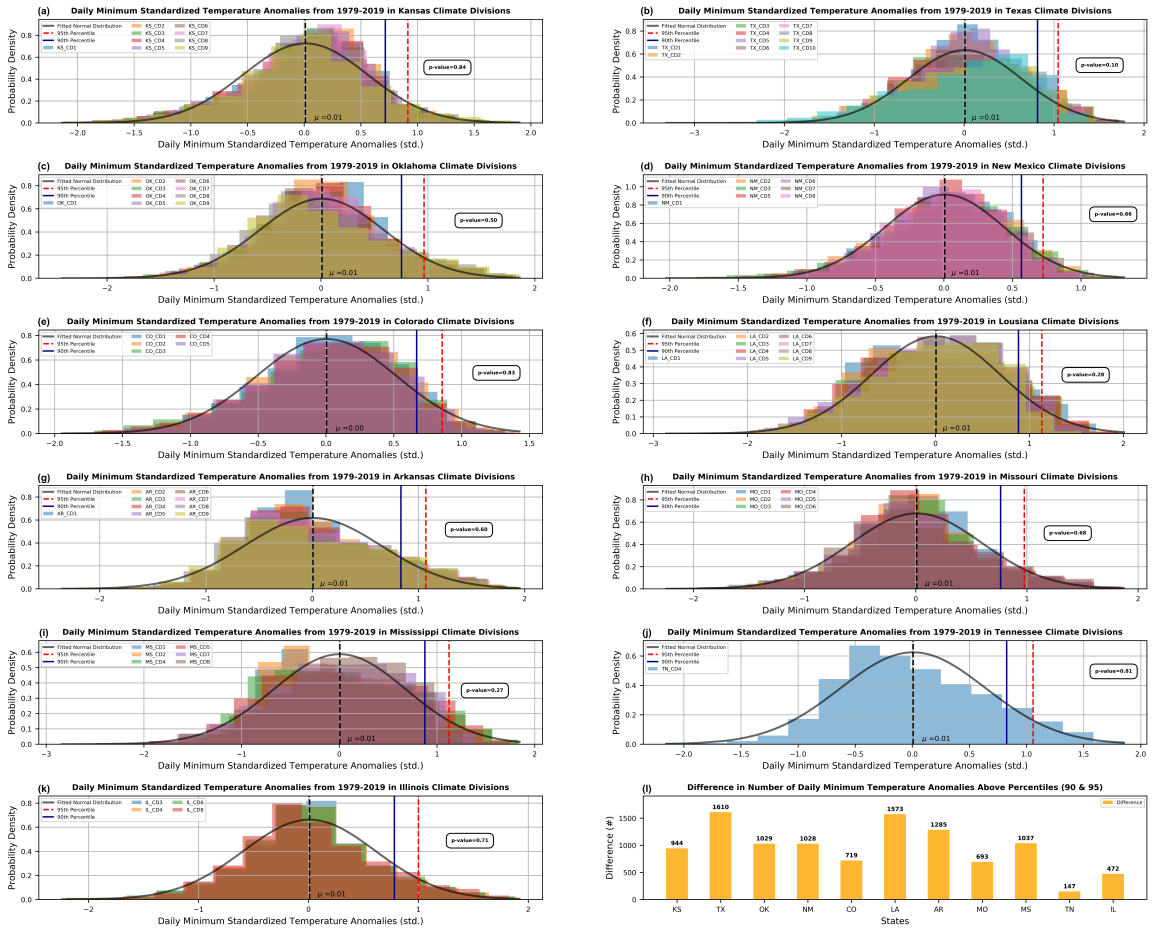

Figure 2.13: Same as Figure 2.11, instead utilizing daily minimum standardized temperature anomalies during the winter months from 1979 through 2019.

3 Climatology of Heat Waves

3.1 Time series

Using the heat wave methodology, a climatology of heat wave events from 1979 through 2019 was completed for the SGP. Figures 3.1 and Appendix-A display the annual time series for each spatial method for each state within and bordering the SGP; corresponding trends are outlined by the black line. All three spatial methods (10%, 25%, and 50%) for each state, displayed an increasing trend from 1979 through 2019 demonstrating that the number of heat waves per year has increased with time. For eight out of the ten states, individual trends were greater than one heat wave per year with the 10% and 25% spatial method. Further, all of the trends derived for each time series was statistically significant ($p < 0.05$). Within the three spatial methods, the frequency of heat waves that meet the 50% spatial method was far less than the frequency on the 10% spatial method. Yet, the trend at 50% spatial method was still significant. The average approximate trend across the entire SGP domain for 10%, 25%, and 50% spatial methods were 2, 1.6, and 1 heat wave events per year respectively. Additionally, years that included the largest number of heat waves in all three spatial methods were: 1998, 2004, 2012, 2016, and 2017. These years not only had a large magnitude of heat wave events in comparison to other years, but were signaled in the 50% spatial method, meaning these heat waves had a large spatial footprint.

From a statewide perspective, Louisiana had the highest magnitude trend for each spatial method compared to all other SGP states. During the last five years within the study time period, Louisiana experienced a higher number of heat wave events in all three spatial methods (Figure 3.1). Moreover, these heat wave events were not only more frequent but included a larger spatial footprint as well. Again, the trends were all significant ($p < 0.05$) and the 10% spatial method trend concluded an annual increase of approximately three heat wave events per year. Colorado and Illinois held the two smallest magnitude trends across each spatial method (Figures A.5 and A.9, respectively). Both states had the smallest number of climate divisions that were included in the study spatial domain. Furthermore, this could have resulted in a lower magnitude with respect to the trend with the potential of missing key heat wave events within each state during the study time period.

3.2 Duration

While the annual climatology time series is of great importance to study, understanding the duration of each heat wave within the climatology is also crucial to gain knowledge on the impacts of heat waves. For example, heat waves of longer duration would have a larger impact on human health (Anderson and Bell 2011; Guirguis et al. 2014), the energy sector (Zamuda et al. 2013), and agriculture (Castillo et al. 2021). As such, duration categories for all heat wave events from 1979 through 2019, and for all three spatial methods within each SGP state, are displayed in Figures 3.2, 3.3,

3.4, 3.5, and Appendix-B. In general, as the duration increased the number of heat waves within each duration category decreased. Additionally, the magnitude in the number of heat waves decreased as the spatial method percentage increased within each duration category. However, while the frequency of heat wave events that are between 3-day to 5-day duration using the 50% spatial method is less than using the 10% spatial method, the percentage of those duration events within the climatology was higher with the 50% spatial method (Figures B.1, 3.2, B.2, B.3, B.4, 3.3, 3.4, B.5, 3.5, and B.6). The percent decrease in the number of heat wave events between the 10% and 50% spatial methods for the 3-day to 5-day duration category averaged across the entire SGP spatial domain was 51.75%. While the average increase in the percentage within the climatology for this duration category between the 10% and 50% spatial method was 8.9%. Thus, the majority of the heat wave events that occurred when utilizing the 50% spatial method (i.e., spatially widespread) were shorter duration events in comparison to the other duration categories.

Additionally, Texas displayed a pattern whereby the same frequency of heat waves within the climatology in the 7-day and 10+-day categories were the same when the 10% spatial method was utilized (Figure 3.2). Similarly, in Louisiana and Mississippi, the percentage of heat waves within the 7-day through 10+-day categories across all three spatial methods were approximately the same (Figures 3.3 and 3.5). In other words, these regions are more susceptible to longer heat waves within this climatology window, and potentially, larger socioeconomic impacts. Arkansas had

the largest percentage of heat wave events from the climatology that were 3-day to 5-day duration across all three spatial methods (Figure 3.4), whereas Louisiana had the smallest percentage of heat wave events in the shortest duration category (Figure 3.3) compared to all the other SGP states.

Overall, over 40% of the heat waves events lasted 5-days or longer for eight out of all ten states for the 10% and 25% spatial methods (Figures 3.2, B.2, B.3, B.4, 3.3, B.5, 3.5, and B.6).

3.3 Seasonality

The analysis of the time series combined with the duration relationships provides several insights on heat waves experienced in the SGP. But studying the seasonality of heat waves within this region also allows for understanding of temporal dynamics of heat waves within a singular year. This section will be split up into each season discussing the results from all three spatial methods in all of the SGP states. Additional seasonality figures outlined by SGP state are listed in Appendix-C.

3.3.1 Fall

In all of the SGP states, there was an increasing trend in the number of heat wave events per year during the fall season at the 10% spatial coverage of the heat wave methodology (Figure 3.6). All of the increasing trends were statistically significant with 95% confidence. Texas held the largest trend of heat wave events per year within

the fall months, with an increase of 0.97 heat wave events per year between the study time period, as shown in Figure 3.6b. Additionally, Figures 3.6a, 3.6c, 3.6d, 3.6f, and 3.6g, illustrated an increasing significant trend of greater than 0.5 heat wave events per year in Kansas, Oklahoma, New Mexico, Louisiana, and Arkansas. Furthermore, this means that over two years, an increase of one heat wave event during the fall season would be expected in those states, represented by the trend associated between 1979 and 2019.

When the 25% spatial method was employed in the heat wave identification methodology, all trends of fall heat wave events per year were increasing (Figure 3.7). As such, all trends determined within this analysis (i.e., 25% spatial method in the fall season) were statistically significant ($p < 0.05$). The magnitude of each trend was less with the use of the 25% spatial method compared to the 10% spatial method. Louisiana and Texas derived the highest trend with both showing an increase of 0.70 heat wave events per year or greater (Figures 3.7b and 3.7f). Figures 3.6g and 3.7g displayed that in Arkansas the utilization of 10% and 25% spatial methods yielded the same trend value for heat wave events that occurred in the fall season during the climatological time period. The same pattern was seen in Missouri (Figure 3.6h and 3.7h). While all of the trends with the use of the 25% spatial method were increasing, the largest difference in trend value from the 10% spatial method climatology was in Oklahoma (Figure 3.6c and 3.7c).

Additionally, utilizing the 50% spatial method, the same increasing trends

were seen in all SGP states for heat wave events that occurred during the fall season from 1979 through 2019 (Figure 3.8). As expected, the trend values yielded with this spatial method were the smallest in magnitude for majority of the states within the study spatial domain. However, Arkansas (Figures 3.6g, 3.7g, and 3.8g) and Missouri (Figures 3.6h, 3.7h, and 3.8h) maintained the same trend value throughout all three spatial methods when applied to the heat wave identification methodology. Thus, heat waves during the fall season in these two SGP states (i.e., Arkansas and Missouri) show the same increase in the number of heat waves expected during this season. Arkansas produced the largest trend value using the 50% spatial method heat wave climatology; Louisiana was close second with a 0.55 heat wave events per year increase (Figure 3.8f). Additionally, Texas had the greatest difference in upward trend value between the 10% (Figure 3.6) and 50% (Figure 3.8) spatial method. Texas exhibited a 0.6 heat wave event per year difference between the two spatial methods (i.e., 10% and 50%). Furthermore, this could mean that during the fall season in the future, increased heat wave events are most likely smaller spatial impacting heat waves within the Texas region. Meanwhile, Louisiana featured one of the top trends through all three spatial methods for heat wave events occurring during the fall season.

3.3.2 Spring

Gershunov and Guirguis (2012b) used a similar heat wave definition applied to California, but the time period of focus was between the months of May through

September. Therefore, the understanding of potential heat waves during the spring season needs to be studied. If heat waves combined with normal to above normal precipitation, could result in a faster green-up of the ecosystem, but could be bad if whiplash events (i.e., drastic shifts between high-impact weather events) begin to become more common after the green-up. The results of the 10% spatial method in the heat wave methodology while only analyzing heat wave events that occurred during March, April, and May for each year in all the SGP states are outlined in Figure 3.9. Similar to the fall season trends, all trends in each SGP state were positive as well as statistically significant at the $\alpha = 0.05$ level, except Colorado which was statistically significant with 90% confidence (Figure 3.9e). Louisiana yielded the highest trend value of all regions within the study spatial domain (0.86 heat waves per year; Figure 3.9f). Texas and Kansas had the next largest increasing trend in spring season heat wave events per year (Figure 3.9b and 3.9a, respectively). Additionally, approximately seven out of ten SGP states resulted in an increase of around one heat wave event every two years during the spring season. One year that seems to stand out as having an abundance of heat wave events during the spring months (i.e., March, April, and May) was 2012 across majority of the SGP states in comparison to the other climatological time period years. In 2012, an early green-up occurred due to the abundance of warm temperatures allowing for natural growth, but by the summer of 2012 the onset of a flash drought quickly escalated (Basara et al. 2019) and resulted in crop desiccation and impact to the agriculture sector (Wolf et al. 2016).

Via the 25% spatial method, all trends for each SGP state, excluding Mississippi, were reduced compared to the use of the 10% spatial method. Even so, the trends of spring season heat wave events over time with the 25% spatial method were positive (Figure 3.10). Again, the trend for each state within the study spatial domain was statistically significant at the $\alpha = 0.05$ level, with the exception of Colorado (Figure 3.10e). Similar to the 10% spatial method spring analysis, Louisiana yielded the largest trend value (0.74 heat wave events per year). This trend value (i.e., 0.74) was almost double the trend value of five out of the ten SGP states. In Louisiana, Figure 3.10f, five years within the last fifteen years had the highest frequency of heat wave events during the spring season out of the entire climatological time period. Meanwhile, Texas had the largest difference in trend value between 10% (Figure 3.9b) and 25% (Figure 3.10b) spatial method, which this relationship was similarly present during the fall season. Furthermore, Arkansas and Missouri had the same trend value in both the 10% and 25% spatial methods.

Figure 3.11 displays the time series of spring season heat waves when the 50% spatial method was utilized. As shown in the fall and previous spring analysis, all trends remained positive resulting in an increase in the number of heat waves during the spring months over time. Furthermore, a positive trend with the 50% spatial method yields an increase in larger heat waves, spatially. Louisiana continued to have the greatest magnitude in trend value in comparison to other SGP states (Figure 3.11f). Additionally, with the exception of Colorado, the 50% spatial method

resulted in statistically significant trend values with 95% confidence. Even though Louisiana had the highest trend in spring season heat wave events for all three spatial methods, Louisiana along with Texas had the largest change in trend (~ 0.4) when the 10% and 50% spatial methods were compared. Once again, the year 2012 stood out as the year with the most number of heat wave events during the spring months (i.e., March, April, and May), further supporting the impact of these heat waves during the spring season could have on the socioeconomic sector.

3.3.3 Summer

Meehl and Tebaldi (2004) as well as Smith et al. (2013) have found that an increase in the frequency of heat waves that occur during the summer season would be expected over time; Figure 3.12 supports those findings. All trends for heat waves that occurred during the summer months between 1979 and 2019 were statistically significant to the 95% confidence level for all the SGP states within the study domain. Texas had the highest trend, with an increase of 1.03 heat wave events per year (Figure 3.12b) for the 10% spatial method. In addition, Texas, Oklahoma, New Mexico, Colorado, and Mississippi, all yielded a higher trend value in summer heat waves (Figure 3.12) than the spring (Figure 3.9). However, Kansas and Arkansas were the only two SGP states that had a large difference in the value of the derived trend when the fall season and summer season were compared; otherwise, the trends in both seasons were approximately the same (Figures 3.6 and 3.12). Heat wave events

that only occurred during the summer months between 1979 and 2019 in Arkansas, yielded a trend that was 0.16 heat wave events per year less in comparison to the fall season (Figure 3.6g). In Kansas (Figure 3.12a) and Oklahoma (Figure 3.12c), 2011 had the highest frequency of heat wave events during the summer months (i.e., June, July, and August) out of the entire time series within those two states.

The 25% spatial method in the heat wave identification methodology is illustrated in Figure 3.13. Trend values across the SGP decreased when compared to the trend values from the 10% spatial method application, but still all remained positive. Kansas had the least difference in trends between the 10% (Figures 3.12a) and 25% (Figure 3.13a) spatial methods, whereas the other trends for the SGP states within the study spatial domain decreased in the range of 0.06 and 0.24 heat wave events per year. Similar to the fall and spring season, the summer heat wave trends for Arkansas and Missouri yield no change between the use of the 10% and 25% spatial method. Additionally, Texas remained the state with the largest trend in summer season heat wave events over time with 25% spatial method applied to the heat wave identification methodology (Figure 3.13b). Furthermore, all trends derived for each SGP state during the summer season with 25% spatial method applied, were statistically significant ($p < 0.05$), excluding Colorado (Figure 3.13e).

Lastly, when the 50% spatial method was applied in the heat wave methodology, it yielded time series climatologies for each SGP state displayed in Figure 3.14. As expected, the trend values continued to decrease as the spatial method increased

for all states, excluding Arkansas (Figure 3.14g) and Missouri (Figure 3.14h). Most of the trends were statistically significant ($p < 0.05$) when the 10% and 25% spatial methods were used; whereas, the trends from the summer season climatology when the 50% spatial method was utilized resulted in more trends that were only statistically significant with 90% confidence or less (e.g., Kansas, Colorado, Arkansas, Missouri, and Illinois). Continued through all three spatial methods, Texas remained having the largest trend value out of all of the SGP states (Figure 3.14b), which was also the state that had the highest difference in trend values from 10% (Figure 3.12b) to 50% (Figure 3.14b) spatial method. Furthermore, this means that majority of the heat waves in the summer season in Texas were mostly on shorter spatial scales (i.e., 10% and 25%). Additionally, the year 2011 in Oklahoma, Figure 3.14c, had almost 3 times the number of heat wave events in that singular year during the summer season in comparison to majority of the other climatological study years (i.e., 1979 through 2019).

3.3.4 Winter

Beginning with the 10% spatial method for thermal shock events that occurred during the winter months (i.e., December, January, and February), the results are displayed in Figure 3.15. The first thing to note is the comparison of the scale in the number of heat wave events (i.e., y-axis) between the summer and winter season. Kansas, Texas, Oklahoma, Louisiana, and Arkansas had at least one year within

the climatological time study that had the frequency of winter season thermal shock events greater than the frequency of summer season heat wave events. Figure 3.15f, shows that the trend for Louisiana winter season thermal shock events was the largest compared to the other SGP states. Furthermore, the winter thermal shock trend for Louisiana was the highest in this season compared to the other seasons and six out of the ten SGP states yielded winter month thermal shock trends above 0.5 thermal shock events per year (Figure 3.15). Two years that stood out as the having the most warm thermal shock events during the winter season within each SGP state were 2012 and 2017 when the 10% spatial method was used in the heat wave methodology.

Figure 3.16 outlines each state's winter climatology of warm thermal shocks using the 25% spatial method in the heat wave identification. All of the trends, except for Colorado, were statistically significant with 95% confidence using the Mann-Kendall statistical test. Out of all ten states studied, Louisiana had the largest trend in the winter season (Figure 3.16f) yet again. Similar to the other seasons, as the spatial method increased the trend values decreased across majority of the SGP states. One state that didn't have much of a change in the winter season thermal shock trend was in Oklahoma. Figures 3.15c and 3.16c show that there was a decrease of only 0.03 thermal shock events per year between the 10% and 25% spatial methods. Furthermore, this means that winter season thermal shock events in Oklahoma in the future could impact more spatially in comparison to the other seasonal increases in heat wave events over time.

Lastly, the 50% spatial method was applied to the heat wave identification methodology and results are displayed in Figure 3.17. Similar relationships that were seen in the other seasons were also seen in the winter season; majority of the trends derived for each state using the 50% spatial method to generate the thermal shock time series were statistically significant at the 95% confidence. Throughout all three spatial methods, Louisiana yielded the highest trend of thermal shock events per year on the 50% spatial method (Figure 3.17f). The impressive trend of 0.67 heat wave events per year for Louisiana further shows that winter season thermal shocks are of importance for future study. Figures 3.15g, 3.16g, and 3.17g show that the winter season thermal shocks in Arkansas were mostly large-scale given the frequency of events only slightly decreased as the spatial methods increased. Additionally, the year that was dominant in most of the SGP states for yielding the largest number of events during the winter months was 2017 when the 50% spatial method was utilized in the heat wave methodology.

3.4 Figures

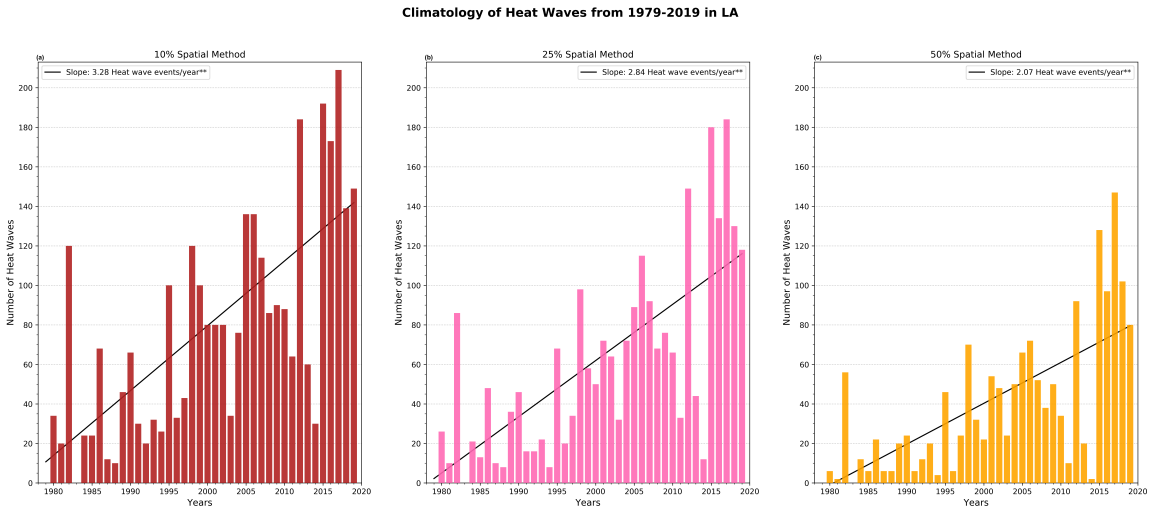

Figure 3.1: Time Series from the climatology of heat wave events for Louisiana. (a) Time Series of the climatology heat wave events established using the 10% spatial method. Trend marked with ** indicates statistical significance at p <0.05, while * indicates significance at p <0.10. (b) Same as (a), but utilizing the 25% spatial method to produce the heat wave climatology. (c) Same as (a), but employing the 50% spatial method in the heat wave identification methodology.

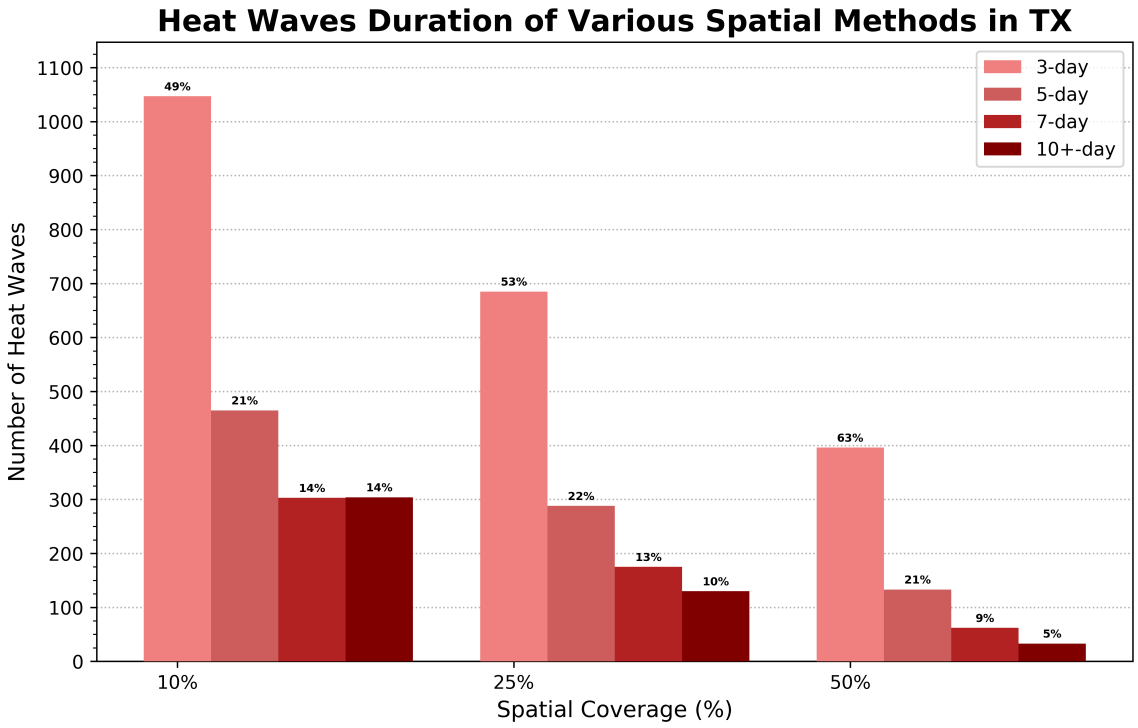

Figure 3.2: Number of heat wave events from the study time period in each duration category for the state of Texas for all three spatial methods (10%, 25%, and 50%). Percentage of heat wave events within the overall climatology that fall in each duration category displayed on top of each bar.

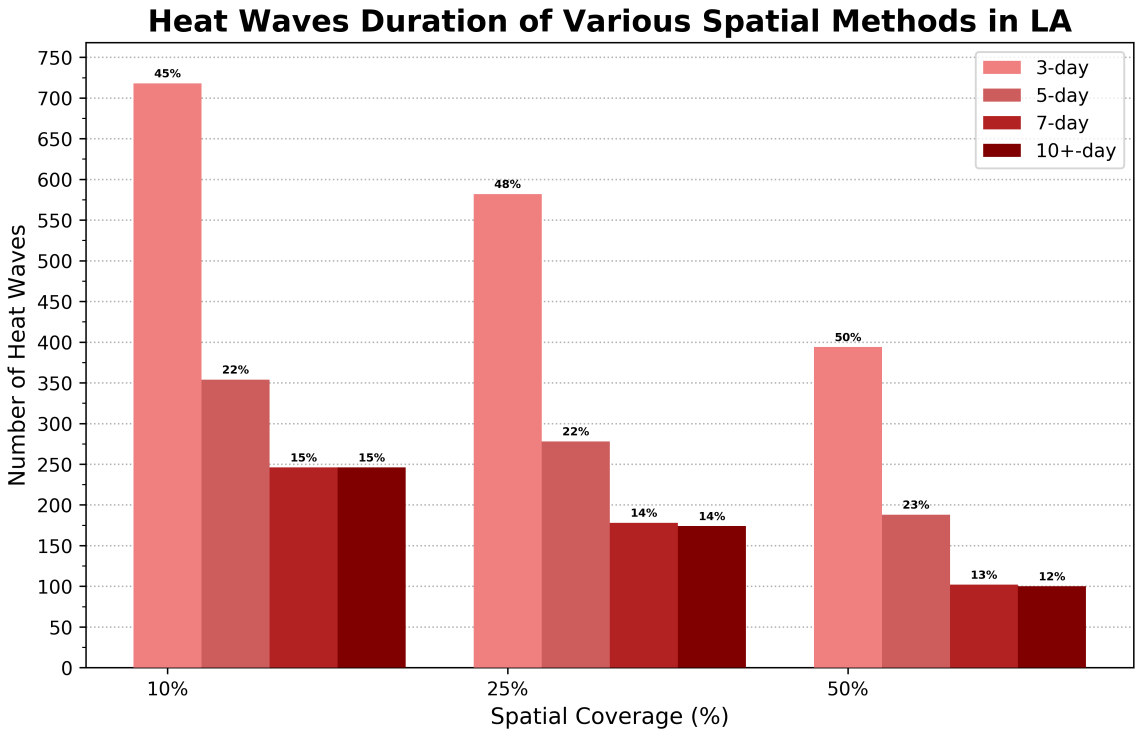

Figure 3.3: Same as Figure 3.2, but for heat wave events in Louisiana.

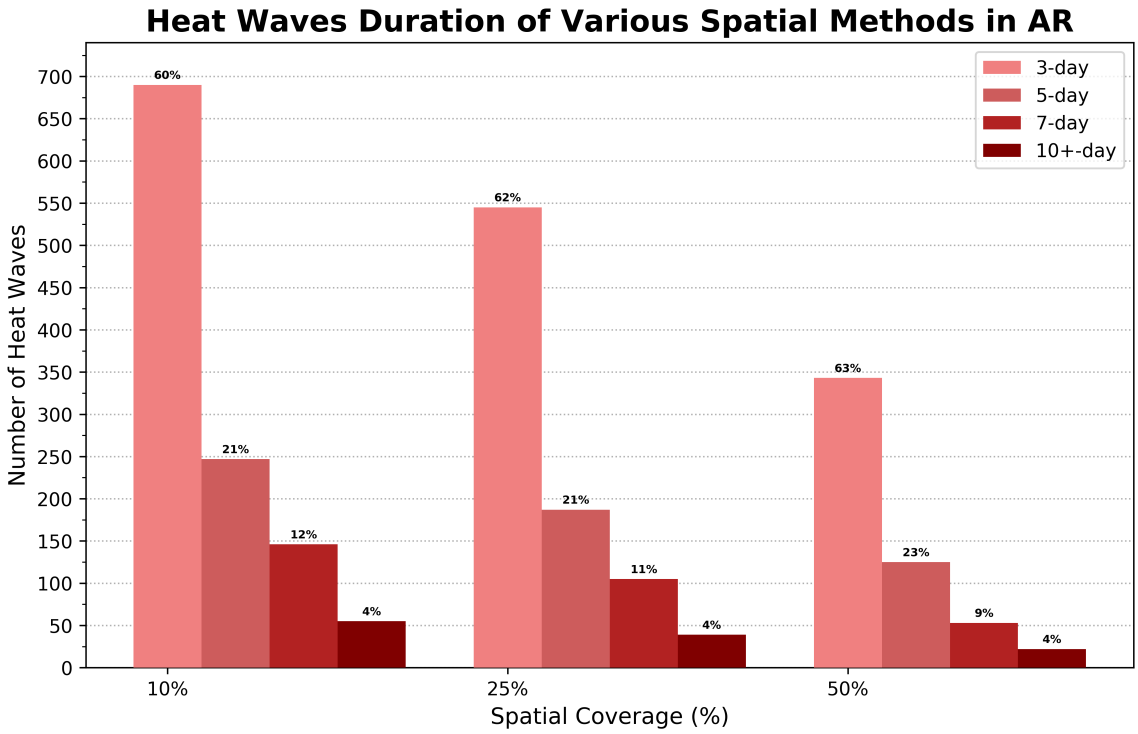

Figure 3.4: Same as Figure 3.2, but for heat wave events in Arkansas.

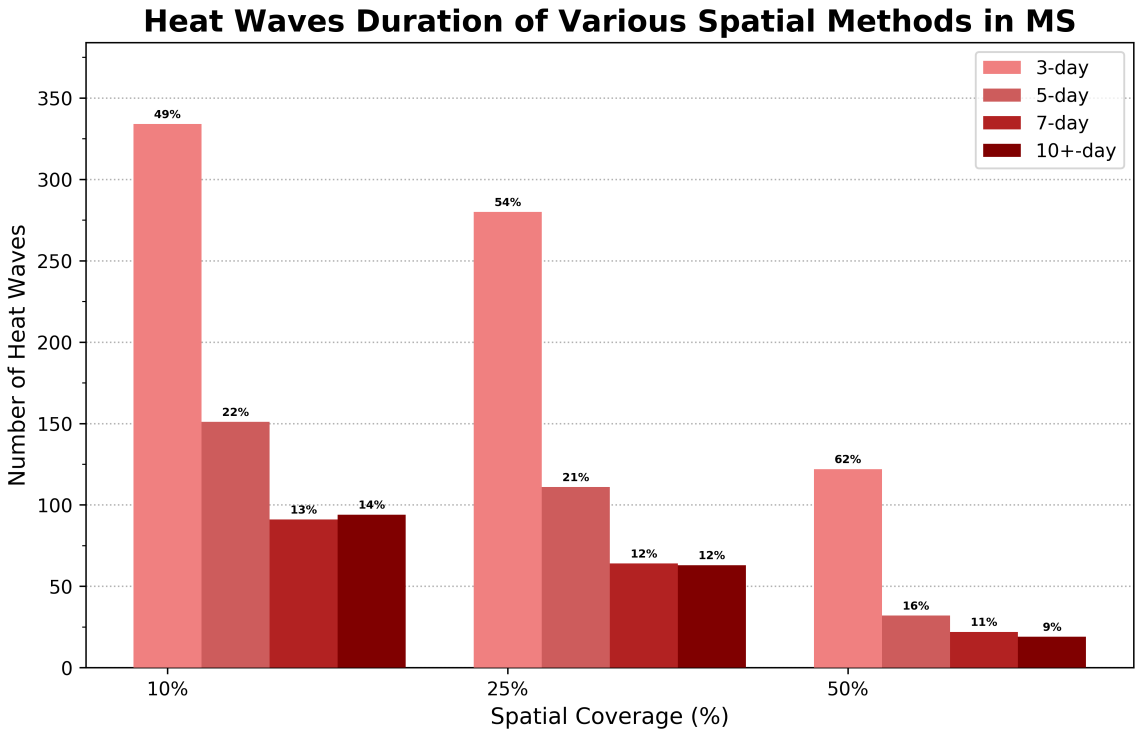

Figure 3.5: Same as Figure 3.2, instead for heat wave events in Mississippi.

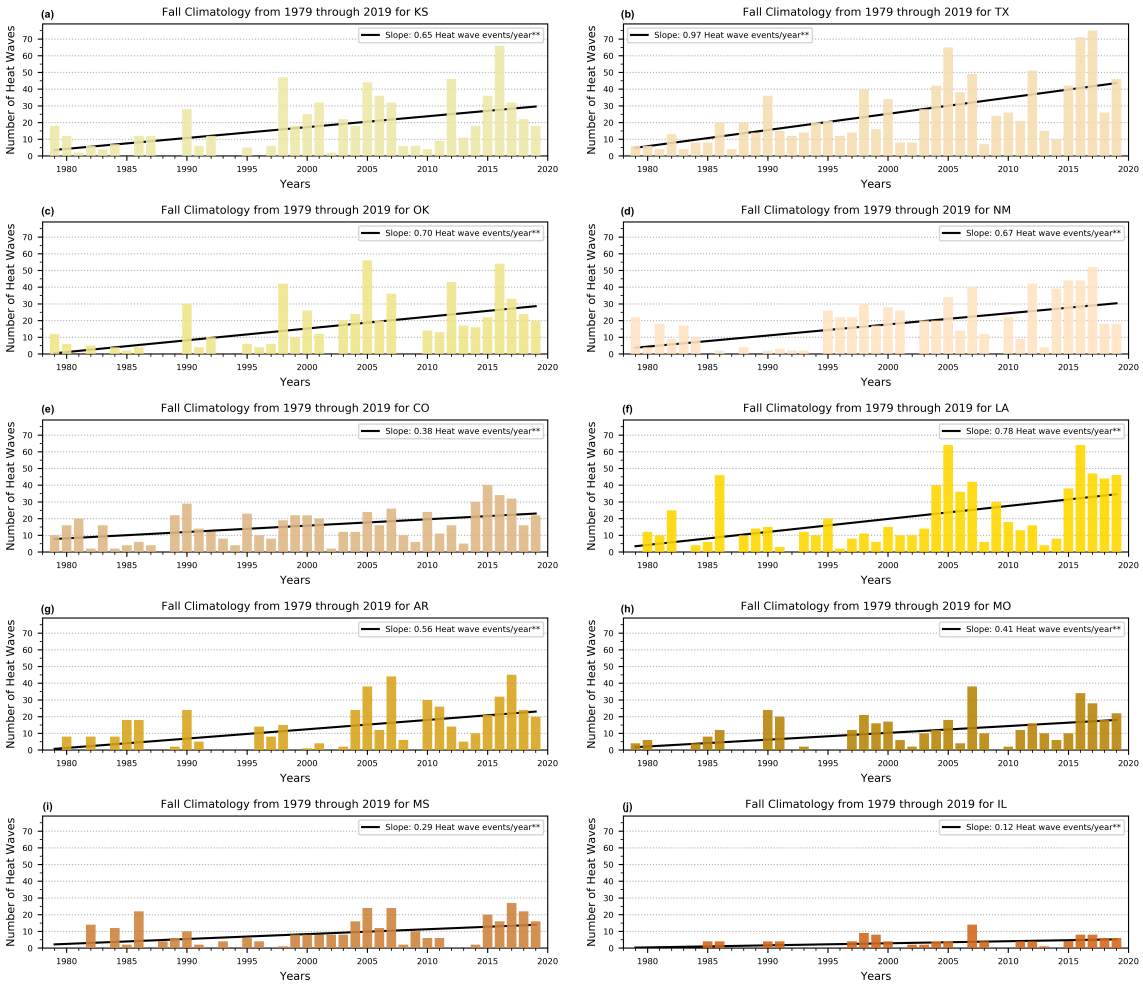

Figure 3.6: Annual frequency of heat wave events that occurred during the fall season (September, October, and November) between the years of 1979 through 2019 with 10% spatial method in heat wave identification methodology. (a) Analysis for Kansas. (b-j) Same as (a), but for Texas, Oklahoma, New Mexico, Colorado, Louisiana, Arkansas, Missouri, Mississippi, and Illinois, respectively. Trends indicated with single asterisk (*) are significant at the p <0.10 level, while those marked with a double asterisk (**) are significant at the p <0.05 level.

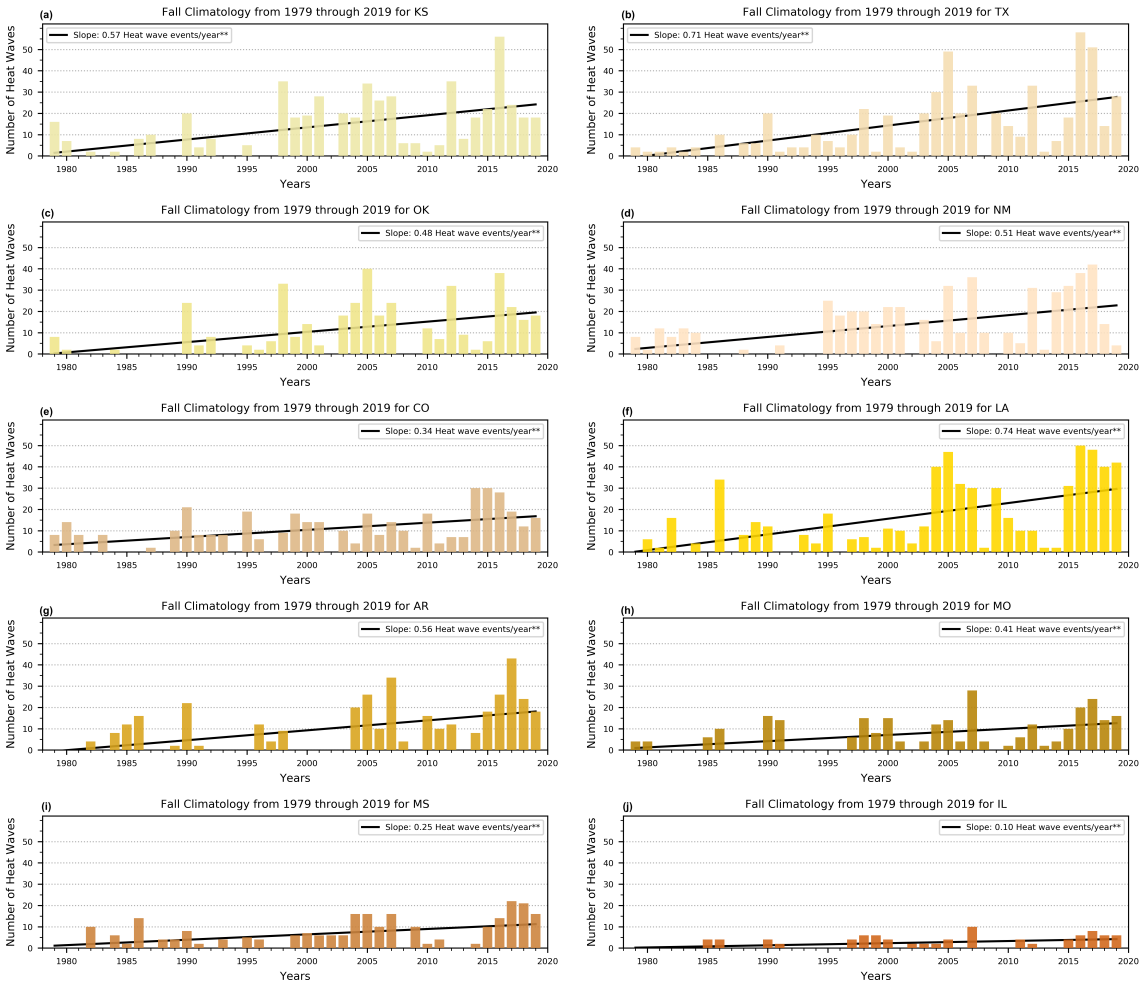

Figure 3.7: Same as Figure 3.6, but utilizing the 25% spatial method.

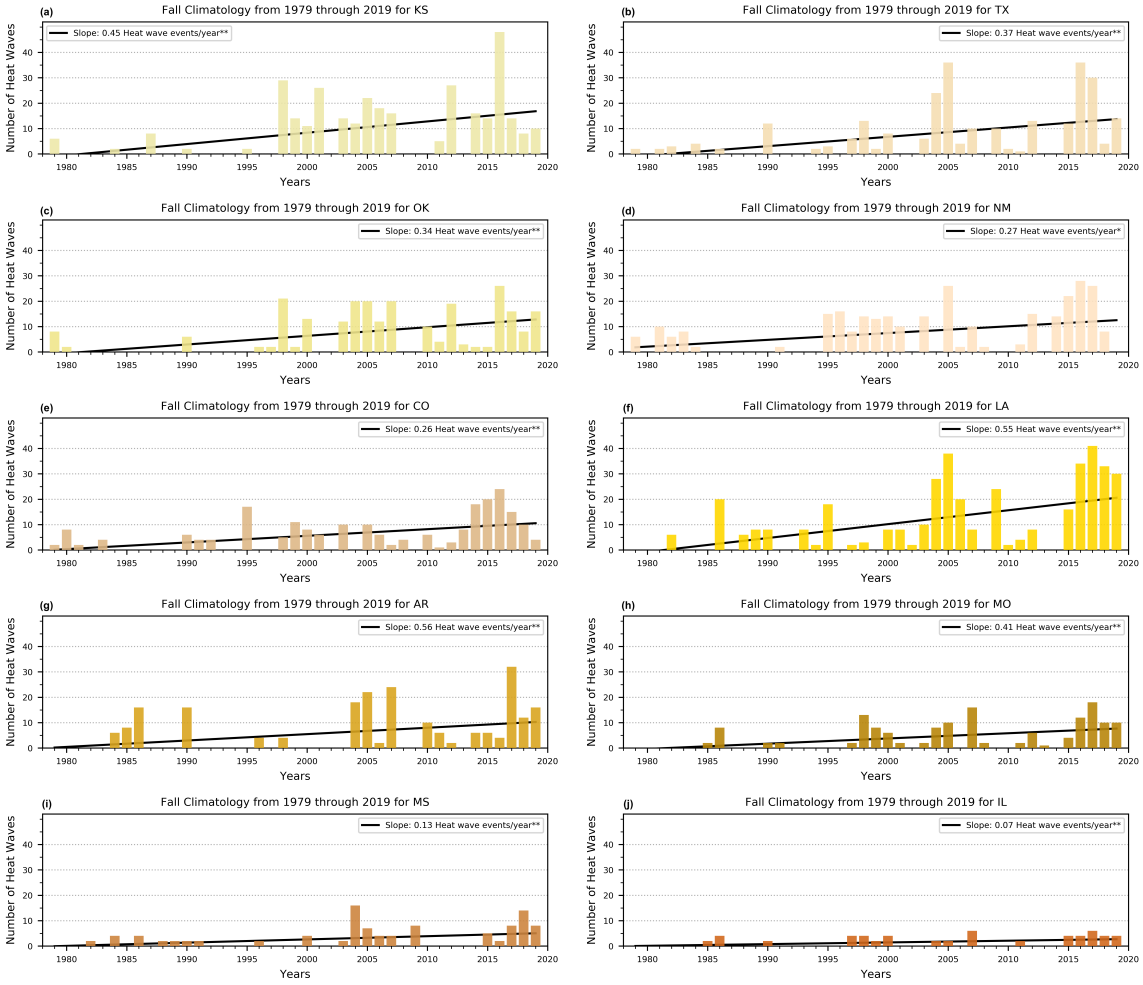

Figure 3.8: Same as Figure 3.6, instead using the 50% spatial method.

Figure 3.9: Annual frequency of heat wave events that occurred during the spring season (March, April, and May) between the years of 1979 through 2019 with 10% spatial method in heat wave identification methodology. (a) Analysis for Kansas. (b-j) Same as (a), but for Texas, Oklahoma, New Mexico, Colorado, Louisiana, Arkansas, Missouri, Mississippi, and Illinois, respectively.Trends indicated with single asterisk (*) are significant at the p <0.10 level, while those marked with a double asterisk (**) are significant at the p <0.05 level.

Figure 3.10: Same as Figure 3.9, instead employing the 25% spatial coverage method.

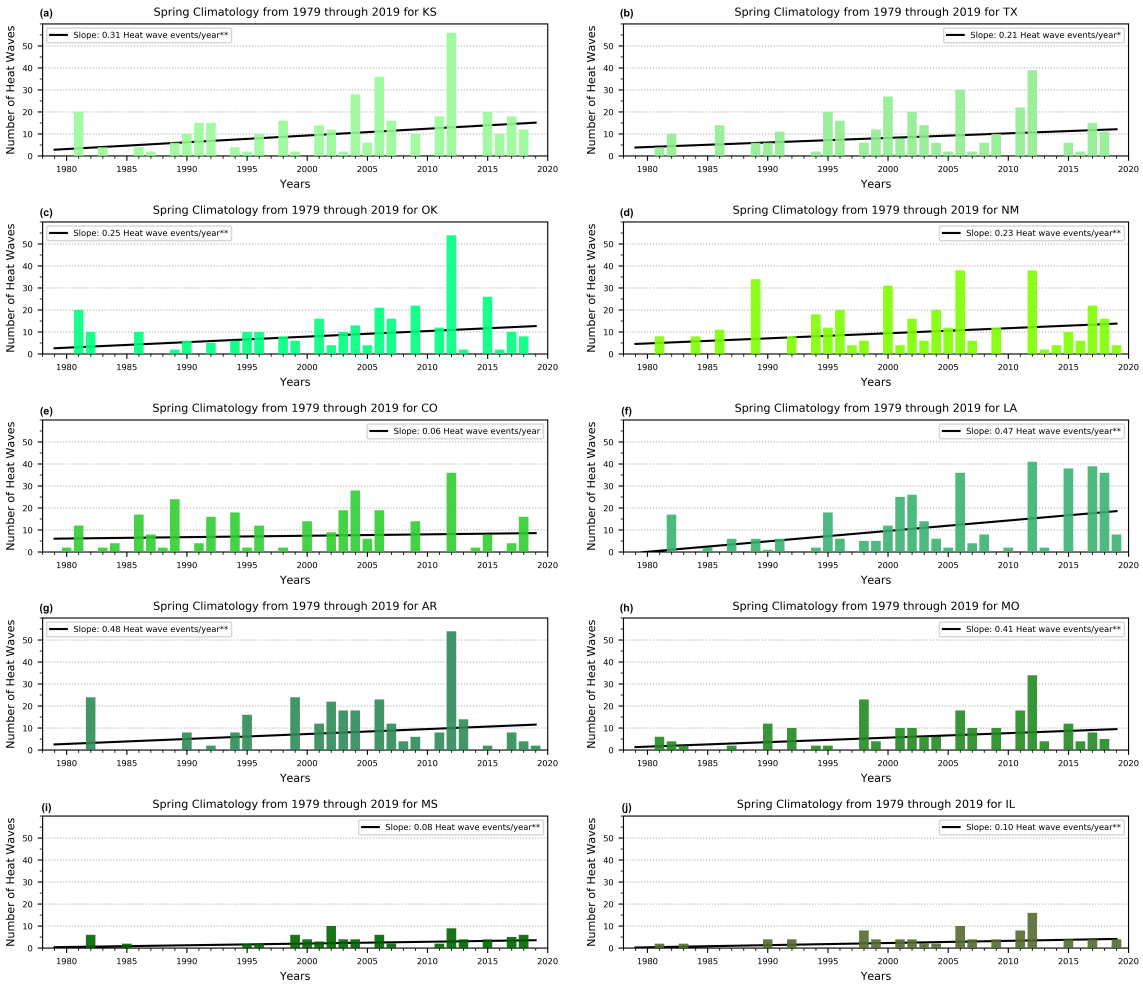

Figure 3.11: Same as Figure 3.9, but using the 50% spatial method.

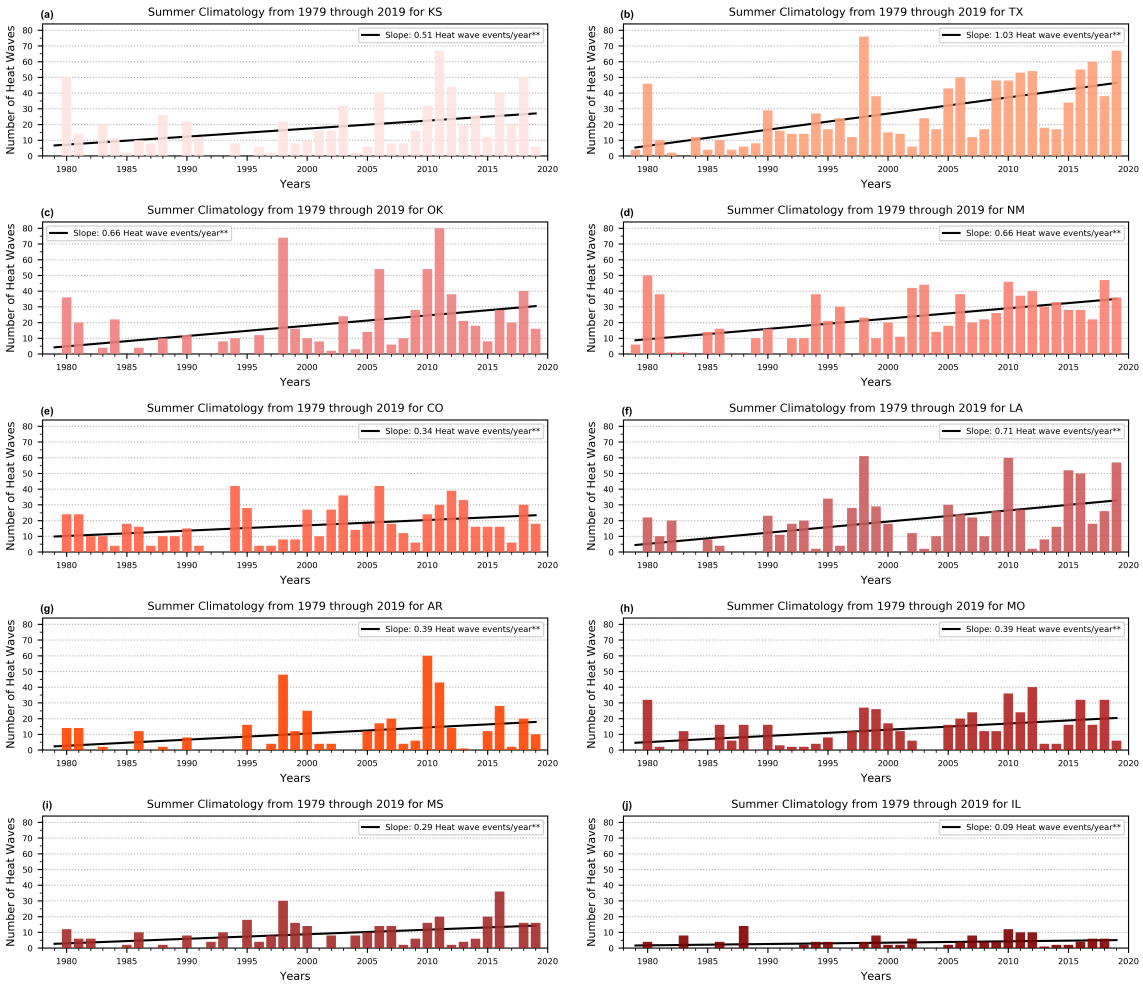

Figure 3.12: Annual frequency of heat wave events that occurred during the summer season (June, July, and August) between the years of 1979 through 2019 with 10% spatial method in heat wave identification methodology. (a) Analysis for Kansas. (b-j) Same as (a), but for Texas, Oklahoma, New Mexico, Colorado, Louisiana, Arkansas, Missouri, Mississippi, and Illinois, respectively.Trends indicated with single asterisk (*) are significant at the p <0.10 level, while those marked with a double asterisk (**) are significant at the p <0.05 level.

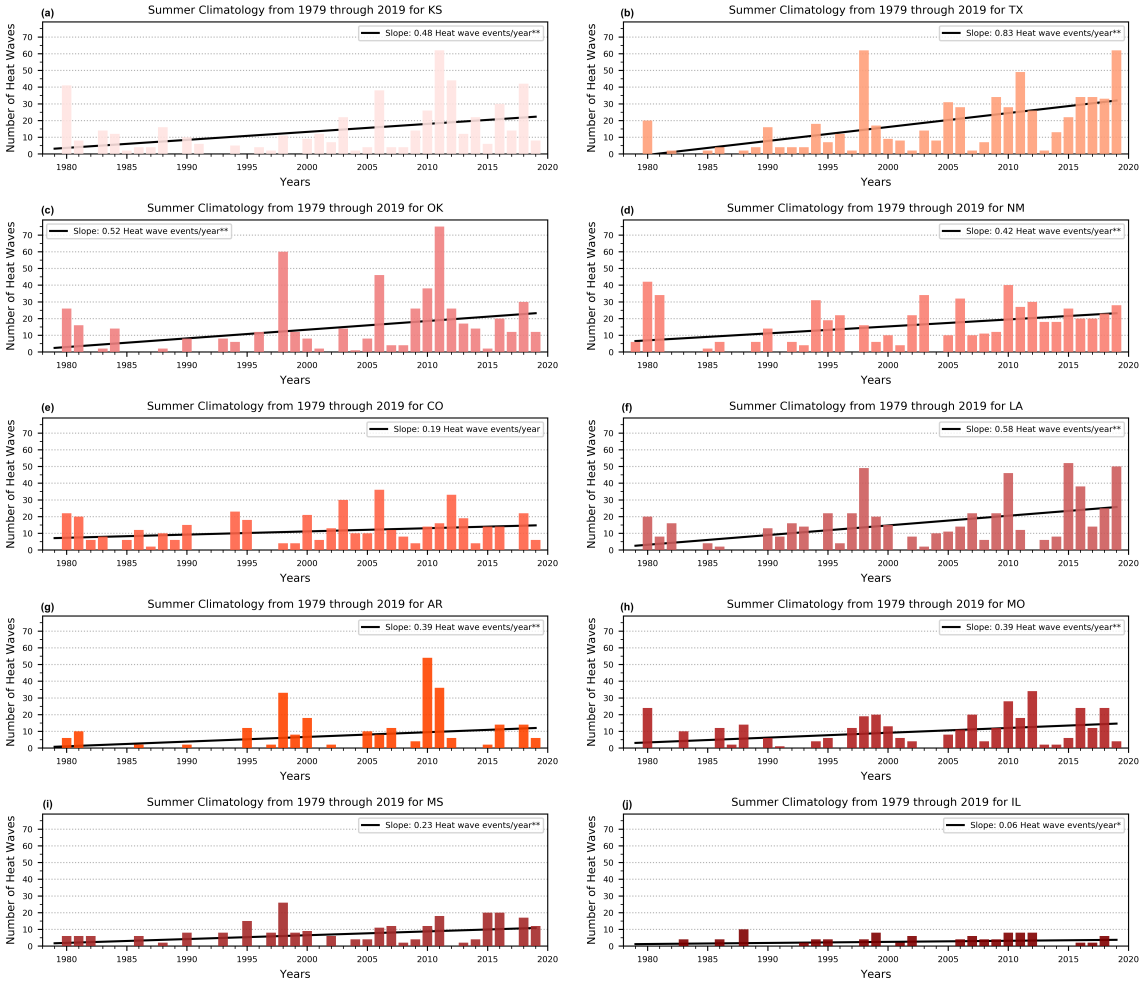

Figure 3.13: Same as Figure 3.12, but utilizing the 25% spatial method.

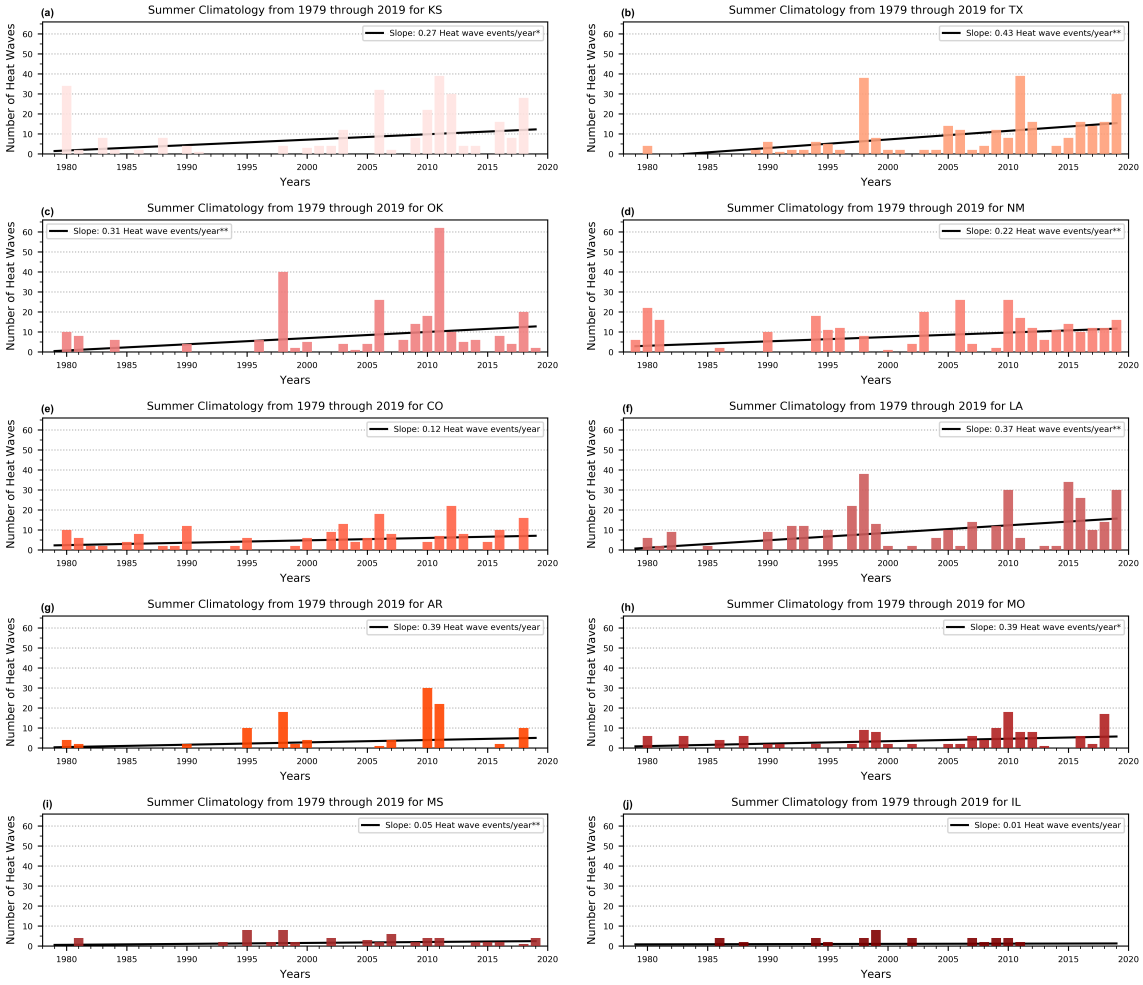

Figure 3.14: Same as Figure 3.12, instead using the 50% spatial coverage method.

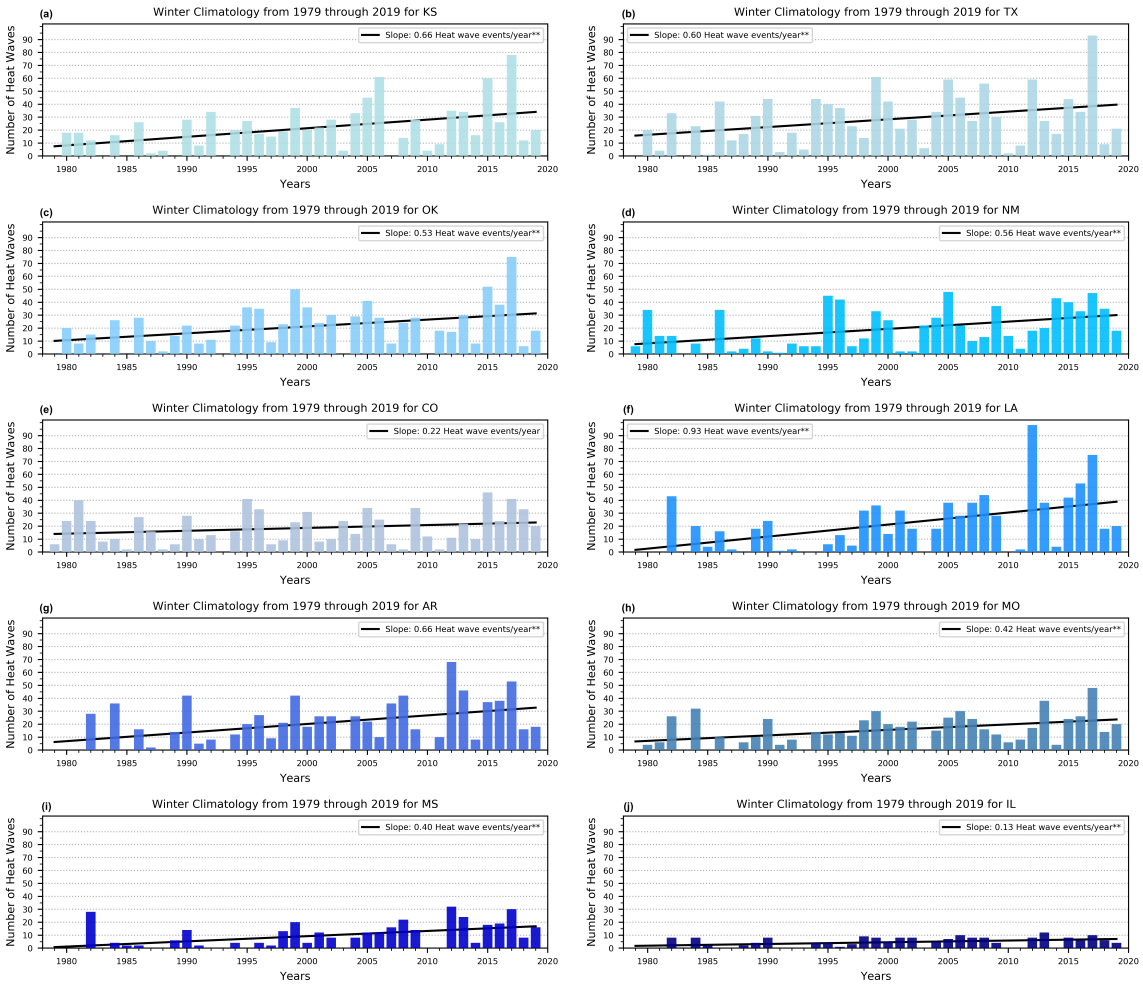

Figure 3.15: Annual frequency of heat wave events that occurred during the winter season (December, January, and February) between the years of 1979 through 2019 with 10% spatial method in heat wave identification methodology. (a) Analysis for Kansas. (b-j) Same as (a), but for Texas, Oklahoma, New Mexico, Colorado, Louisiana, Arkansas, Missouri, Mississippi, and Illinois, respectively. Trends indicated with single asterisk (*) are significant at the p <0.10 level, while those marked with a double asterisk (**) are significant at the p <0.05 level.

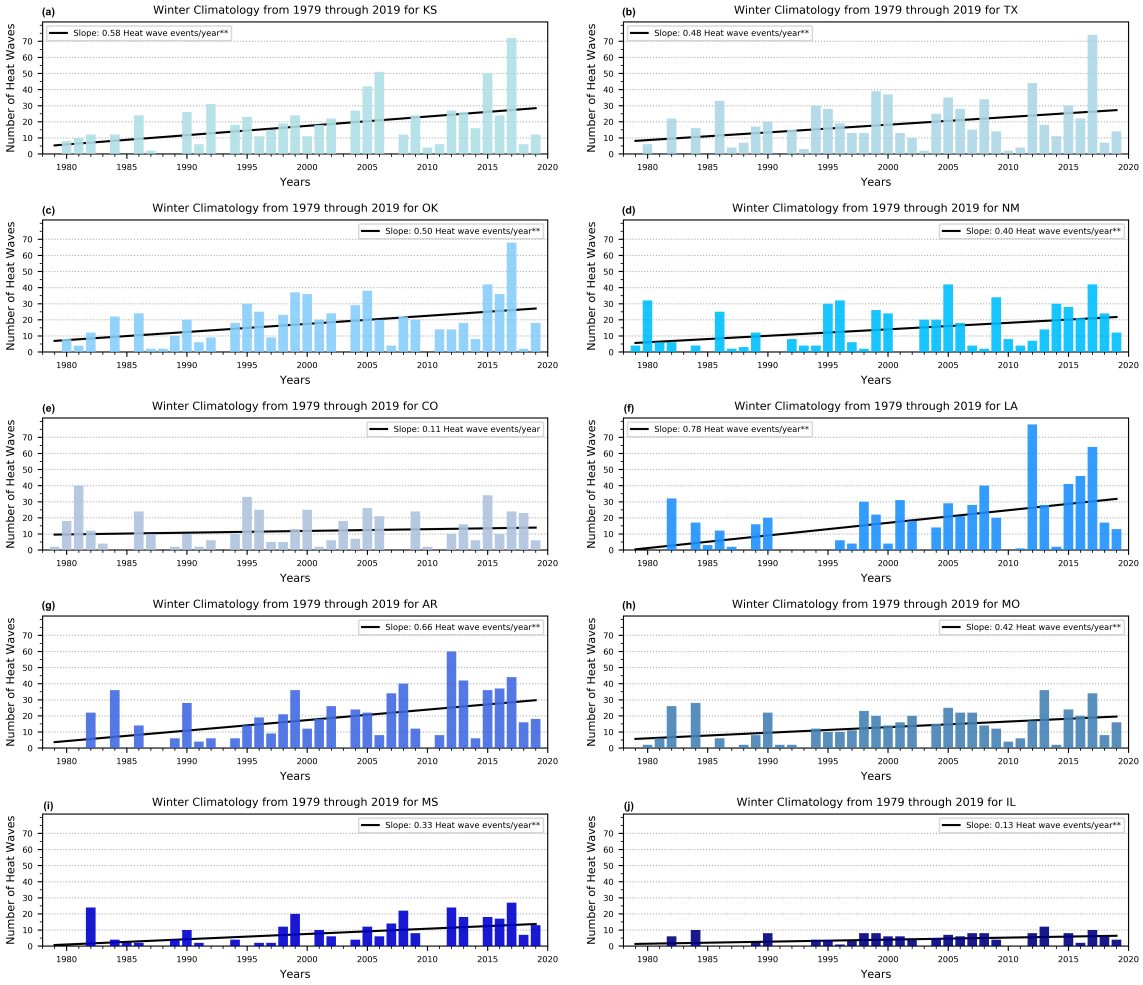

Figure 3.16: Same as Figure 3.15, instead using 25% spatial coverage method.

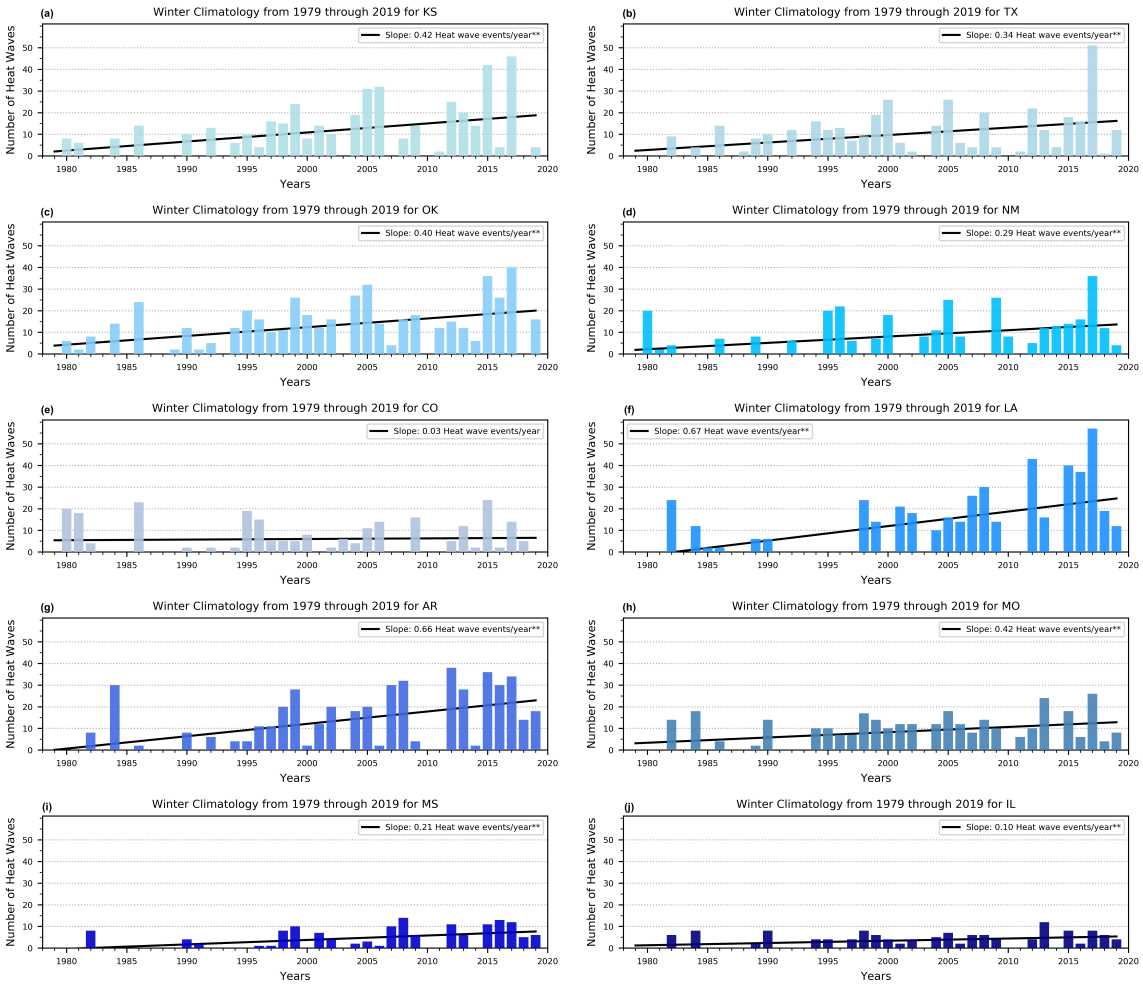

Figure 3.17: Same as Figure 3.15, but employing the 50% spatial method.

4 Discussion

The first purpose of this study was to generate a novel but comprehensive identification methodology for heat wave events across the SGP that compliments definitions used in previous heat wave studies (Figure 1.1). The use of a relative threshold within the heat wave methodology accounts for climate variability in a region, rather than an absolute threshold. For example, the 90^{th} percentile of daily maximum temperatures in Texas is different than the 90^{th} percentile of daily maximum temperature in Missouri. Even within a state, the average temperature can vary (Figure 4.1). Utilizing a relative threshold allows for this heat identification methodology to be applicable to other regions outside of the SGP. Furthermore, Figures 2.2 through 2.13 suggest that the use of the 95^{th} percentile as that relative threshold would be too restrictive which disagrees with several previous studies (Karl and Quayle 1981; Gershunov and Guirguis 2012b; Stefanon et al. 2012; Nissan et al. 2017).

For all three daily standardized temperature anomaly variables (i.e., maximum, mean, and minimum), the ks-test showed that all values in all four seasons and for each climate division within each SGP state came from a Normal distribution. Examining the distribution of these daily variables within the study spatial region has not been done before to justify the heat wave definitions established prior to this study. The analysis of the distributions dictates the proper relative threshold that would be ideal within a heat wave identification methodology. With greater than 800

daily values in one state (Figures 2.2, 2.3, 2.4, 2.7, 2.12, and 2.13) that fall between the relative thresholds in question (i.e., 90^{th} and 95^{th}) the results demonstrate that heat wave events could be masked due to the relative threshold being too extreme.

Although, the heat wave identification methodology was applied to gridded reanalysis data set in this study, the methodology could be applied to observational data to determine the start of a heat wave event in close to real-time (i.e., three days after the actual start date). Furthermore, databases of heat wave events that have occurred across the entire Contiguous United States exist (Robinson 2001; Meehl and Tebaldi 2004; Gershunov et al. 2009; Wu et al. 2012; Oswald and Rood 2014; Allen and Sheridan 2016; Oswald 2018), a database using this proposed definition with multiple datasets (i.e., various reanalysis and observational) is a task planned for future work. Further, the generation of a database opens many opportunities for future research. One example would be to research relationships of precursor, compound, and cascading events with other subseasonal-to-seasonal (S2S) extremes (e.g., heat waves and flash droughts). Precursor events is when one S2S extreme event occurs prior to another, possibly resulting in the development of the second S2S extreme (i.e., focus in more on the first S2S event). A compound event is when two S2S events occur simultaneously. Lastly, a cascading event is the same as a precursor event, but the focus is on the second S2S extreme event. The connection between heat waves and drought in past events have been studied (Karl and Quayle 1981; Namias 1982; Cowan et al. 2014), but further analysis of these compound events

could provide insight on predictability of detrimental S2S events to minimize the impacts experienced on the socioeconomic scale.

With the application of this heat wave identification methodology, a climatology of heat wave events across the SGP was created. Further analysis of annual time series, duration, and seasonality provided knowledge of relationship and trends for each SGP state within the study spatial domain. Within each analysis, three different spatial coverage methods were applied in the heat wave methodology (i.e., 10%, 25%, and 50%). Each spatial method denoted the percentage of grid points within a single climate division that had to meet the threshold and further follow the heat wave identification methodology outlined in Figure 2.1. All trends from all three spatial coverage percentages were statistically significant at the 95% confidence level as indicated by the Mann-Kendall test. Furthermore, all trends were positive, signifying that the number of heat waves will likely be more prominent over time, even heat waves that span across spatially large regions. Various studies have found an expected increase in the number of heat wave events in the future (Meehl and Tebaldi 2004; Fischer and Schär 2010; Hao et al. 2013; Peterson et al. 2013; Smith et al. 2013; Russo et al. 2014b; Mazdiyasni and AghaKouchak 2015; Perkins-Kirkpatrick and Lewis 2020). All of these studies had a different way of distinguishing heat wave events, and thus, the magnitude of the anticipated increase varied between these studies.

The use of a single heat wave definition would allow for the advancement of

predictability of these extreme events, which further gives more knowledge to stake holders and socioeconomic sectors to help mitigate losses from heat waves. This definition could be employed within models to signal when forecasted daily maximum and minimum standardized temperature anomalies would meet the heat wave identification methodology proposed in this study. Further providing advanced warning for socioeconomic sectors that are impacted by heat waves. One state within the SGP that may have high interest in future modeling of heat wave events would be Louisiana, supported by Figure 3.1. The last five years in the study time period (i.e., 1979 through 2019), displayed a higher frequency of heat waves to have occurred in Louisiana, further causing the trend to be highest compared to all of the other SGP states. If this trend outlined in Figure 3.1 continues to increase, this would result in large impacts seen on agriculture (Lobell and Field 2007; Wreford and Neil Adger 2010; Bindi and Olesen 2011; Pathak et al. 2018), water resources, and generation efficiencies in fossil and nuclear power plants (Añel et al. 2017).

As future trends are important to understand, past years that have been impacted by heat waves provide ways to learn how to adapt in the future. This analysis showed that 1998, 2004, 2012, 2016, and 2017 consistently had the largest number of heat wave events in all three spatial coverage methods. Two years that have been previously studied as being incorporated with other S2S extreme events are 2012 and 2017. In 2012, a flash drought evolved across the Central United States as early as May. Basara et al. (2019) showed that this flash drought did not develop

uniformly, but propagated throughout the growing season in 2012. The occurrence of heat waves in certain regions across the similar spatial domain may have helped inhibit the onset and intensification of the flash drought that impacted the Central United States in 2012. Land-atmosphere coupling during heat wave and drought compound events provide a positive feedback loop which enables the continuation of intensification and duration of both events as argued by Miralles et al. (2019). This same positive feedback may have occurred in the 2012 Central United States drought case, which is a topic of future work. Additionally, between 2016 and 2017 the SGP experienced multiple significant wildfires. The Starbuck wildfire started on 6 March 2017 in the panhandle of Oklahoma, further impacting Oklahoma and Kansas. Whereas, Perryton fire began on 6 March 2017 as well, but in the panhandle of Texas spreading through parts of Texas and Oklahoma. Steiner et al. (2020) studied how these wildfires affected the surrounding ecology and the recovery of the environment. The generation of a database of past heat wave events would allow this work to expand into how heat waves could have played a role in the ignition of these wildfires as well as the length of the wildfire.

While Section 3.1 provided insight on past years that had an abundance of heat wave events, the duration of these S2S extreme events is also important. Longer duration heat wave events cause substantial depletion to agriculture yields (Castillo et al. 2021), human health (Anderson and Bell 2011; Guirguis et al. 2014), and energy efficiency (Zamuda et al. 2013). Louisiana not only showed one of the largest trends in

heat wave events across all three spatial coverage methods, but also was a region that had the smallest percentage of short duration heat wave events (Figure 3.3). Louisiana (Figure 3.3) and Mississippi (Figure 3.5) had the same percentage of heat wave events in the 7-day through 10+-day categories in all three spatial methods, meaning these regions are more susceptible to longer heat waves within this climatology time period. Longer and more frequent heat wave events in Louisiana could yield drastic impacts in the state in the future. Between the two lowest spatial coverage methods (i.e., 10% and 25%), eight out of all ten SGP states had over 40% of heat wave events last 5-days or longer. Moreover, most past studies have only noted the duration of the heat wave event(s) within case studies (Tan et al. 2007; Anderson and Bell 2011; Khan et al. 2019; Perkins-Kirkpatrick and Lewis 2020) and further stated that longer duration heat wave events have a large impact on socioeconomic sectors (Rocklov et al. 2012). Spatial analysis on duration of heat wave events can highlight specific states that may be more sensitive to longer duration heat waves (e.g., Louisiana and Mississippi). Further analysis on the duration during the "prime" years (i.e., 1998, 2004, 2012, 2016, and 2017) within the annual time series is of interest to complete in future work. Anderson and Bell (2011) determined intensity of heat waves by the mean temperature throughout the heat wave event. Therefore, longer duration heat wave events may cause the intensity to be skewed, thus, determining an intensity scale that is independent of length of heat wave event is ideal for future research. While longer duration events increase the stress placed on an environment,

a shorter duration heat wave with extremely above normal temperatures could result in different detrimental impacts.

Primarily, heat wave studies have focused on events occurring during the warm season (i.e., May through September) (Della-Marta et al. 2007; Gershunov and Guirguis 2012b; Bumbaco et al. 2013; Cowan et al. 2014; Parker et al. 2014; Perkins-Kirkpatrick and Lewis 2020). Meanwhile, heat waves can occur any time during the year, especially during the winter months (i.e., December, January, and February). Thermal shock events (i.e., winter season heat wave events) could have significant impacts by disturbing the typical environmental cycle. For example, a thermal shock present in February may cause the ground to warm up enough to modify the growing season (earlier than typical) within a region. Yet, since cooler temperatures are still possible during those months, this may result in farmers losing crops if a cold snap follows the thermal shock event. Such events are known as whiplash events, which will be a topic of future research with respect to heat waves. Furthermore, knowing trends temporally and spatially with respect to the seasonality of heat waves within a region would provide knowledge for mitigation strategies. Two examples of heat waves occurring in the "off-season" are further discussed below.

Recalling the 2017 wildfire cases in Texas and Oklahoma (Steiner et al. 2020), the months leading up to the wildfires created a dry environment for the wildfires to thrive and propagate. Figures 3.6b and 3.7b display that the frequency of heat wave events during the fall season in Texas were high during the years of 2016 and 2017.

These two years within the analysis of fall heat wave events were more dominant than other years through the entire study time period. A similar relationship was seen for Oklahoma, but more strictly for 2016 (Figures 3.6c and 3.7c). Through the winter season analysis, 2017 had the largest number of heat wave events in Texas (Figures 3.15b and 3.16b) and Oklahoma (Figures 3.15c and 3.16c) compared to the rest of the study climatological time period (i.e., 1979 through 2019). The combination of several heat wave events that occurred in the fall season of 2016 into the winter season of 2017 could have created an ideal environment for the 6 March 2017 wildfires in Texas and Oklahoma. If heat waves were only studied during the warm season, then the contribution of heat waves on the 2017 wildfire events may be missed. As such, understanding the contributing factors of heat waves as precursor or compound events could have given these regions impacted by the 2017 wildfires advanced warning.

In 2012 heat waves were a precursor event but also a compound event with a summer drought that developed across the Central United States. During the spring season in 2012, there were higher frequencies of heat wave events that occurred in Kansas (Figure 3.9a), Oklahoma (Figure 3.9c), Texas (Figure 3.9b), Louisiana (Figures 3.9f), and Arkansas (Figure 3.9g). These spring season heat wave events allowed vegetation to grow earlier and flourish, further resulting in an increase in carbon uptake during March through early May (Wolf et al. 2016). Following this large uptake in carbon, a severe drought occurred during the summer which decreased the excess amount of carbon that was produced during the spring season (Wolf et al.

2016). Basara et al. (2019) found that the onset of several flash drought events began in May and further expanded spatially as time progressed. Furthermore, land-atmosphere feedbacks through the boundary layer contributed to anomalously dry air mass over the regions impacted by drought conditions during the summer months of 2012 (Basara et al. 2019). Figures 3.12 and 3.13 displayed that the summer of 2012 had a large number of heat wave events in Kansas and Oklahoma. This relates back to the findings from Basara et al. (2019) of a continued dry air mass over the Central United States. Furthermore, due to the positive feedback between drought and heat waves (Miralles et al. 2019), these S2S extreme events intensified during the summer, resulting in the worst drought since the Dust Bowl. This is a prime example of heat waves acting as precursor and compound event with drought, which forced severe and exceptional drought conditions across much of the Central United States through the beginning of October (Basara et al. 2019).

Through this study, multiple knowledge gaps have been addressed associated with heat wave research. First, with the application of this innovative comprehensive heat wave identification methodology, could be applied to most regions (i.e., local to global scale) to provide a full database of heat wave events. Furthermore, while case studies have been researched in several countries (i.e., Australia, Europe, China, Russia, and United States), this heat wave identification methodology would help identify additional case studies that have occurred in the past wherever applied across the globe.

Via case studies, general conclusions concerning potential atmospheric drivers of heat wave events have been made (Meehl and Tebaldi 2004; Schubert et al. 2004; Parker et al. 2014). With this methodology, more robust conclusions could be drawn on atmospheric drivers during heat wave events which may improve predictability of these S2S extreme events. Additionally, with a warming climate many recent studies have focused on modeling trends in heat wave events for the future (Karl et al. 2000; Meehl and Tebaldi 2004; Hao et al. 2013; Peterson et al. 2013; Mazdiyasni and AghaKouchak 2015). All studies found an increasing trend in future heat wave events in various regions (e.g., Europe, Australia, Russia, China, Western United States, and Southern United States). The annual time series and seasonality analyses of this study further agrees with the findings in past studies that the occurrence of heat wave events in the future may increase compared to the past few decades given the trends identified. Peterson et al. (2013) specifically found an increasing trend over the past several decades across the United States; this study supported an increase over the past several decades throughout the SGP region (Section 3.1).

Finally, a gap in the scientific literature with respect to heat wave research is the seasonality of heat waves within a region. In particular, heat waves outside of the warm season have not been studied heavily, yet still pose impacts on socioeconomic sectors and could improve the understanding of potential precursor, compound, and cascading events. Section 3.3 demonstrated the importance of analyzing these winter time thermal shocks, especially given the large magnitudes of trends shown in Figures

3.15, 3.16, and 3.17.

4.1 Figures

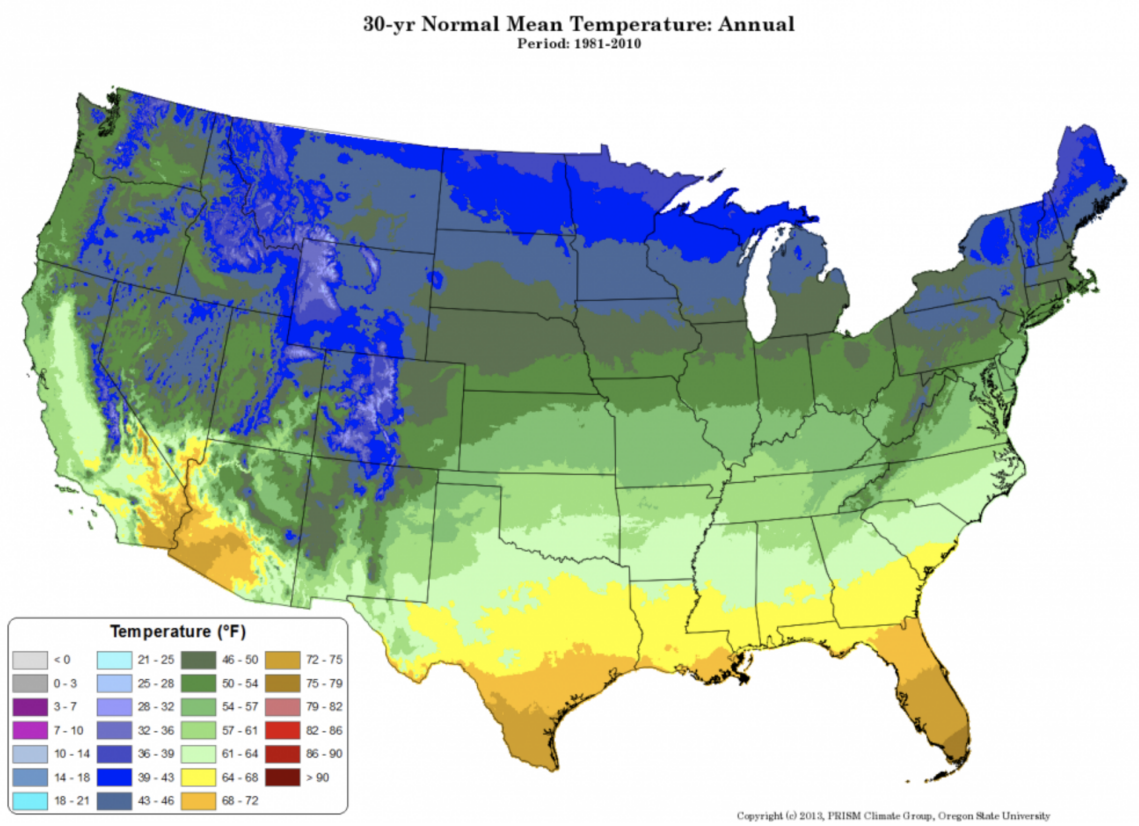

Figure 4.1: 30-year (1981-2010) normals for daily mean temperatures across the Contiguous United States. Figure from National Center for Atmospheric Research (2014).

5 Conclusion

This study developed a novel heat wave identification methodology to create a climatology of heat wave events in the SGP from 1979 through 2019. Daily maximum, mean, and minimum standardized temperature anomalies during all four seasons within the study time period came from a fitted Normal distribution as determined from the Kolmogorov-Smirnov significance test. From the distribution analysis, this study found the use of the 95^{th} percentile as the relative threshold to be too restrictive and resulted in heat wave events to be missed within the climatology. Therefore, the 90^{th} percentile was used. Within the literature, heat wave definitions have used many atmospheric variables to determine the start and end dates of heat wave events. This heat wave definition utilized daily maximum and minimum standardized temperature anomalies within a region over three consecutive days. Furthermore, thresholds had to not be met for more than three days after the last met date to account for surface air modification during a heat wave event.

Once the database of heat wave events from 1979 through 2019 was created, a more in-depth analysis was completed for each state within the SGP. Trends were derived for annual time series and time series for all four seasons. This study found increasing trends in all ten SGP states from the annual time series. Louisiana had the largest trend through all three spatial coverage methods (i.e., 10%, 25%, and 50%), which would be an area of future study. Additionally, Louisiana had the same

percentage of heat wave events within the climatology (i.e., 1979 through 2019) that lasted in either the 7-day to 10-day category or the 10+-day duration. Thus, these two analyses showed that Louisiana will not only experience an increase in the number of heat wave events, but is also susceptible to longer duration heat waves meaning detrimental impacts could be seen within this state in the future.

The seasonality of heat wave events has not been a large focus in previous studies. However, this study found several interesting results from researching the frequency of heat wave events that occur in each season (i.e., fall, spring, summer, and winter) in the SGP. Even though heat wave studies have focused during the warm season, winter season heat waves in all SGP states featured increasing trends. Further, 2017 was an example of how heat waves occurring outside of the warm season could act as precursor events to other extreme events. Further analysis of heat wave events outside of the warm season will be a topic in future work. Louisiana held the highest increasing trend in frequency of heat wave events in the fall, spring, and winter through the entire study time period. Whereas, Texas had the largest upward trend in frequency of heat wave events during the summer season. Similar to the trends in the annual time series, all trends for each SGP state in every season had positive trends in the number of heat wave events per year. Future analysis of heat wave event duration sub-sectioned for all four seasons will be completed. Lastly, an intensity scale is another heat wave event characteristic that remains elusive, which will be tackled in future work. The first step of establishing a single comprehensive

heat wave identification definition and successfully applied has been completed in this study.

References

Alhaji, U. U., A. S. Yusuf, C. O. Edet, C. O. Oche, and E. P. Agbo, 2018: Trend Analysis of Temperature in Gombe State Using Mann Kendall Trend Test. *Journal of Scientific Research and Reports*, **20**, doi:10.9734/jsrr/2018/42029.

Allen, M. J., and S. C. Sheridan, 2016: Spatio-temporal changes in heat waves and cold spells: an analysis of 55 U.S. cities. *Physical Geography*, doi: 10.1080/02723646.2016.1184078.

Anderson, G., and M. L. Bell, 2011: Heat waves in the United States: Mortality risk during heat waves and effect modification by heat wave characteristics in 43 U.S. communities. *Environmental Health Perspectives*, doi:10.1289/ehp.1002313.

Añel, J. A., M. Fernández-González, X. Labandeira, X. López-Otero, and L. de la Torre, 2017: Impact of cold waves and heat waves on the energy production sector. *Atmosphere*, **8**, doi:10.3390/atmos8110209.

Australian Bureau Of Meteorology, 2013: Annual Climate Report 2013. 31, URL `http://www.bom.gov.au/climate/annual`$_s um/2013/AnClimSum2013_H R1.0.pdf$.

Bai, L., G. Ding, S. Gu, P. Bi, B. Su, D. Qin, G. Xu, and Q. Liu, 2014: The effects of summer temperature and heat waves on heat-related illness in a coastal city of China, 2011-2013. *Environmental Research*, doi:10.1016/j.envres.2014.04.002.

Bari Abarghouei, A. Z. M. A. D. M. T. K. M. R., H., and M. Safari Zarch, 2011: The survey of climatic drought trend in Iran. *Stochastic Environmental Research and Risk Assessment*, **25**, 851–863, doi:10.1007/s00477-011-0491-7.

Barnett, A. G., S. Hajat, A. Gasparrini, and J. Rocklöv, 2012: Cold and heat waves in the United States. *Environmental Research*, doi:10.1016/j.envres.2011.12.010.

Barriopedro, D., E. M. Fischer, J. Luterbacher, R. M. Trigo, and R. García-Herrera, 2011: The hot summer of 2010: Redrawing the temperature record map of Europe. *Science*, doi:10.1126/science.1201224.

Basara, J. B., J. I. Christian, R. A. Wakefield, J. A. Otkin, E. H. Hunt, and D. P. Brown, 2019: The evolution, propagation, and spread of flash drought in the Central United States during 2012. *Environmental Research Letters*, doi:10.1088/1748-9326/ab2cc0.

Bindi, M., and J. E. Olesen, 2011: The responses of agriculture in Europe to climate change. *Regional Environmental Change*, S151–S158, doi:10.1007/s10113-010-0173-x.

Bumbaco, K. A., K. D. Dello, and N. A. Bond, 2013: History of Pacific Northwest Heat Waves: Synoptic pattern and trends. *Journal of Applied Meteorology and Climatology*, doi:10.1175/JAMC-D-12-094.1.

Castillo, F., A. S. Vargas, J. K. Gilless, and M. Wehner, 2021: The Impact of Heat

Waves on Agricultural Labor Productivity and Output. *Extreme Events and Climate Change*, 11–20, doi:10.1002/9781119413738.ch2.

Chen, Y., and Y. Li, 2017: An Inter-comparison of Three Heat Wave Types in China during 1961-2010: Observed Basic Features and Linear Trends. *Scientific Reports*, doi:10.1038/srep45619.

Christian, J., K. Christian, and J. B. Basara, 2015: Drought and pluvial dipole events within the great plains of the United States. *Journal of Applied Meteorology and Climatology*, **54 (9)**, 1886–1898, doi:10.1175/JAMC-D-15-0002.1.

Christian, J. I., J. B. Basara, J. A. Otkin, E. D. Hunt, R. A. Wakefield, P. X. Flanagan, and X. Xiao, 2019: A methodology for flash drought identification: Application of flash drought frequency across the United States. *Journal of Hydrometeorology*, doi:10.1175/JHM-D-18-0198.1.

Cowan, T., G. C. Hegerl, I. Colfescu, M. Bollasina, A. Purich, and G. Boschat, 2017: Factors contributing to record-breaking heat waves over the great plains during the 1930s Dust Bowl. *Journal of Climate*, **30**, 2437–2461, doi:10.1175/JCLI-D-16-0436.1.

Cowan, T., A. Purich, S. Perkins, A. Pezza, G. Boschat, and K. Sadler, 2014: More frequent, longer, and hotter heat waves for Australia in the Twenty-First Century. *Journal of Climate*, doi:10.1175/JCLI-D-14-00092.1.

Della-Marta, P. M., J. Luterbacher, H. von Weissenfluh, E. Xoplaki, M. Brunet, and H. Wanner, 2007: Summer heat waves over western Europe 1880-2003, their relationship to large-scale forcings and predictability. *Climate Dynamics*, doi: 10.1007/s00382-007-0233-1.

Dong, X., and Coauthors, 2011: Investigation of the 2006 drought and 2007 flood extremes at the Southern Great Plains through an integrative analysis of observations. *Journal of Geophysical Research Atmospheres*, **116**, doi:10.1029/2010JD014776.

Fischer, E. M., and C. Schär, 2010: Consistent geographical patterns of changes in high-impact European heatwaves. *Nature Geoscience*, **3**, 398–403, doi: 10.1038/ngeo866.

Fischer, E. M., S. I. Seneviratne, D. Lüthi, and C. Schär, 2007: Contribution of land-atmosphere coupling to recent European summer heat waves. *Geophysical Research Letters*, doi:10.1029/2006GL029068.

Gasparrini, A., and B. Armstrong, 2011: The impact of heat waves on mortality. *Epidemiology*, doi:10.1097/EDE.0b013e3181fdcd99.

Gavrilov, M. B., I. Tošić, S. B. Marković, M. Unkašević, and P. Petrović, 2016: Analysis of annual and seasonal temperature trends using the Mann-Kendall test in Vojvodina, Serbia. *Idojaras*, **120**, 183–198.

Gershunov, A., D. R. Cayan, and S. F. Iacobellis, 2009: The great 2006 heat wave

over California and Nevada: Signal of an increasing trend. *Journal of Climate*, doi:10.1175/2009JCLI2465.1.

Gershunov, A., and K. Guirguis, 2012a: California heat waves in the present and future. *Geophysical Research Letters*, doi:10.1029/2012GL052979.

Gershunov, A., and K. Guirguis, 2012b: California heat waves in the present and future. *Geophysical Research Letters*, **39**, doi:10.1029/2012GL052979.

Gershunov, A., Z. Johnston, H. G. Margolis, and K. Guirguis, 2011: The California heat wave 2006 with impacts on statewide medical emergency: A space-time analysis. *Geography Research Forum*.

Guirguis, K., A. Gershunov, A. Tardy, and R. Basu, 2014: The impact of recent heat waves on human health in California. *Journal of Applied Meteorology and Climatology*, **53**, 3–19, doi:10.1175/JAMC-D-13-0130.1.

Hajat, S., R. S. Kovats, R. W. Atkinson, and A. Haines, 2002: Impact of hot temperatures on death in London: A time series approach. *Journal of Epidemiology and Community Health*, doi:10.1136/jech.56.5.367.

Hao, Z., A. Aghakouchak, and T. J. Phillips, 2013: Changes in concurrent monthly precipitation and temperature extremes. *Environmental Research Letters*, doi:10.1088/1748-9326/8/3/034014.

Hu, C., J. Xia, D. She, L. Li, Z. Song, and S. Hong, 2021: A new framework for

the identification of flash drought: Multivariable and probabilistic statistic perspectives: Identification of flash drought. *International Journal of Climatology*, doi:10.1002/joc.7157.

Hunt, E., 2020: The flash drought of 1936. *Journal of Applied and Service Climatology*, **2020 (4)**, 1–15, doi:10.46275/joasc.2020.11.001.

Hunt, E. D., M. Svoboda, B. Wardlow, K. Hubbard, M. Hayes, and T. Arkebauer, 2014: Monitoring the effects of rapid onset of drought on non-irrigated maize with agronomic data and climate-based drought indices. *Agricultural and Forest Meteorology*, **191**, doi:10.1016/j.agrformet.2014.02.001.

Joshi, N., D. Gupta, S. Suryavanshi, J. Adamowski, and C. A. Madramootoo, 2016: Analysis of trends and dominant periodicities in drought variables in India: A wavelet transform based approach. *Atmospheric Research*, **182**, 200–220, doi:10.1016/j.atmosres.2016.07.030.

Karl, T. R., R. W. Knight, and B. Baker, 2000: The record breaking global temperatures of 1997 and 1998: Evidence for an increase in the rate of global warming? *Geophysical Research Letters*, **27 (5)**, 719–722, doi:10.1029/1999GL010877.

Karl, T. R., and R. G. Quayle, 1981: The 1980 summer heat wave and drought in historical perspective (USA). *Monthly Weather Review*, doi:10.1175/1520-0493(1981)109¡2055:TSHWAD¿2.0.CO;2.

Karmeshu Supervisor Frederick Scatena, N. N., 2015: Trend Detection in Annual Temperature & Precipitation using the Mann Kendall Test – A Case Study to Assess Climate Change on Select States in the Northeastern United States. *Mausam*, **66**.

Kendall, M. G., 1957: Rank Correlation Methods. *Biometrika*, **44 (1/2)**, 298, doi: 10.2307/2333282.

Khan, N., S. Shahid, T. Ismail, K. Ahmed, and N. Nawaz, 2019: Trends in heat wave related indices in Pakistan. *Stochastic Environmental Research and Risk Assessment*, **33**, 287–302, doi:10.1007/s00477-018-1605-2.

Knowlton, K., M. Rotkin-Ellman, G. King, H. G. Margolis, D. Smith, G. Solomon, R. Trent, and P. English, 2009: The 2006 California heat wave: Impacts on hospitalizations and emergency department visits. *Environmental Health Perspectives*, doi:10.1289/ehp.11594.

Kovats, R. S., and S. Hajat, 2008: Heat Stress and Public Health: A Critical Review. *Annual Review of Public Health*, doi: 10.1146/annurev.publhealth.29.020907.090843.

Kunkel, K. E., S. A. Changnon, B. C. Reinke, and R. W. Arritt, 1996: The July 1995 heat wave in the midwest: A climatic perspective and critical weather factors. *Bulletin of the American Meteorological Society*, doi:10.1175/1520-0477(1996)077¡1507:TJHWIT¿2.0.CO;2.

Lewis, S. C., and D. J. Karoly, 2013: Anthropogenic contributions to Australia's record summer temperatures of 2013. *Geophysical Research Letters*, doi: 10.1002/grl.50673.

Lobell, D. B., and C. B. Field, 2007: Global scale climate-crop yield relationships and the impacts of recent warming. *Environmental Research Letters*, **2 (1)**, doi: 10.1088/1748-9326/2/1/014002.

Mann, H. B., 1945: Mann Nonparametric test against trend. *Econometrica*, **13**, 245–259.

Marx, M. A., and Coauthors, 2006: Diarrheal illness detected through syndromic surveillance after a massive power outage: New York City, August 2003. *American Journal of Public Health*, **96 (3)**, doi:10.2105/AJPH.2004.061358.

Mazdiyasni, O., and A. AghaKouchak, 2015: Substantial increase in concurrent droughts and heatwaves in the United States. *Proceedings of the National Academy of Sciences of the United States of America*, doi:10.1073/pnas.1422945112.

McKechnie, A. E., and B. O. Wolf, 2010: Climate change increases the likelihood of catastrophic avian mortality events during extreme heat waves. *Biology Letters*, **6 (2)**, doi:10.1098/rsbl.2009.0702.

Meehl, G. A., and C. Tebaldi, 2004: More intense, more frequent, and longer lasting heat waves in the 21st century. *Science*, doi:10.1126/science.1098704.

Miller, N. L., K. Hayhoe, J. Jin, and M. Auffhammer, 2008: Climate, extreme heat, and electricity demand in California. *Journal of Applied Meteorology and Climatology*, doi:10.1175/2007JAMC1480.1.

Miralles, D. G., P. Gentine, S. I. Seneviratne, and A. J. Teuling, 2019: Land–atmospheric feedbacks during droughts and heatwaves: state of the science and current challenges. *Annals of the New York Academy of Sciences*, 19 – 33, doi:10.1111/nyas.13912.

Mo, K. C., and D. P. Lettenmaier, 2015: Heat wave flash droughts in decline. *Geophysical Research Letters*, doi:10.1002/2015GL064018.

Mullens, E. D., and R. A. McPherson, 2019: Quantitative scenarios for future hydrologic extremes in the U.S. Southern Great Plains. *International Journal of Climatology*, **39**, 2659 – 2676, doi:10.1002/joc.5979.

Namias, J., 1982: Anatomy of Great Plains Protracted Heat Waves (especially the 1980 U.S. summer drought). *Monthly Weather Review*, doi:10.1175/1520-0493(1982)110¡0824:aogpph¿2.0.co;2.

National Center for Atmospheric Research, 2014: PRISM 30-year normal temperature climatology. `https://climatedataguide.ucar.edu/climate-data/prism-high-resolution-spatial-climate-data-united-states-maxmin-temp-dewpoint`.

National Center for Atmospheric Research, 2021: NOAA/NCEI U.S. Climate Division Data Plotting Page: Division boundaries and county relationships. https://psl.noaa.gov/data/usclimdivs/boundaries.html.

National Weather Service, 2020: Weather Related Fatality and Injury Statistics. https://www.weather.gov/hazstat/.

Nissan, H., K. Burkart, E. C. de Perez, M. Van Aalst, and S. Mason, 2017: Defining and predicting heat waves in Bangladesh. *Journal of Applied Meteorology and Climatology*, **56**, 2653–2670, doi:10.1175/JAMC-D-17-0035.1.

Oswald, E. M., 2018: An analysis of the prevalence of heat waves in the United States between 1948 and 2015. *Journal of Applied Meteorology and Climatology*, doi:10.1175/JAMC-D-17-0274.1.

Oswald, E. M., and R. B. Rood, 2014: A trend analysis of the 1930-2010 extreme heat events in the continental United States. *Journal of Applied Meteorology and Climatology*, doi:10.1175/JAMC-D-13-071.1.

Otkin, J. A., M. C. Anderson, C. Hain, I. E. Mladenova, J. B. Basara, and M. Svoboda, 2013: Examining rapid onset drought development using the thermal infrared-based evaporative stress index. *Journal of Hydrometeorology*, **14 (4)**, 1057–1074, doi:10.1175/JHM-D-12-0144.1.

Parker, T. J., G. J. Berry, and M. J. Reeder, 2014: The structure and evolution of

heat waves in Southeastern Australia. *Journal of Climate*, doi:10.1175/JCLI-D-13-00740.1.

Pathak, T. B., M. L. Maskey, J. A. Dahlberg, F. Kearns, K. M. Bali, and D. Zaccaria, 2018: Climate change trends and impacts on California Agriculture: A detailed review. doi:10.3390/agronomy8030025.

Peng, R. D., J. F. Bobb, C. Tebaldi, L. McDaniel, M. L. Bell, and F. Dominici, 2011: Toward a quantitative estimate of future heat wave mortality under global climate change. *Environmental Health Perspectives*, doi:10.1289/ehp.1002430.

Perkins, S. E., 2015: A review on the scientific understanding of heatwaves-Their measurement, driving mechanisms, and changes at the global scale. doi: 10.1016/j.atmosres.2015.05.014.

Perkins, S. E., and L. V. Alexander, 2013: On the measurement of heat waves. *Journal of Climate*, doi:10.1175/JCLI-D-12-00383.1.

Perkins-Kirkpatrick, S. E., and S. C. Lewis, 2020: Increasing trends in regional heatwaves. *Nature Communications*, **11**, doi:10.1038/s41467-020-16970-7.

Peterson, T. C., and Coauthors, 2013: Monitoring and understanding changes in heat waves, cold waves, floods, and droughts in the United States: State of knowledge. *Bulletin of the American Meteorological Society*, doi:10.1175/BAMS-D-12-00066.1.

Pezza, A. B., P. van Rensch, and W. Cai, 2012: Severe heat waves in Southern

Australia: Synoptic climatology and large scale connections. *Climate Dynamics*, doi:10.1007/s00382-011-1016-2.

Robinson, P. J., 2001: On the definition of a heat wave. *Journal of Applied Meteorology*, doi:10.1175/1520-0450(2001)040¡0762:OTDOAH¿2.0.CO;2.

Rocklov, J., A. G. Barnett, and A. Woodward, 2012: On the estimation of heat-intensity and heat-duration effects in time series models of temperature-related mortality in Stockholm, Sweden. *Environmental Health: A Global Access Science Source*, **11 (23)**, doi:10.1186/1476-069X-11-23.

Russo, S., and Coauthors, 2014a: Magnitude of extreme heat waves in present climate and their projection in a warming world. *Journal of Geophysical Research Atmospheres*, doi:10.1002/2014JD022098.

Russo, S., and Coauthors, 2014b: Magnitude of extreme heat waves in present climate and their projection in a warming world. *Journal of Geophysical Research Atmospheres*, 12 500–12 512, doi:10.1002/2014JD022098.

Schlenker, W., and M. J. Roberts, 2009: Nonlinear temperature effects indicate severe damages to U.S. crop yields under climate change. *Proceedings of the National Academy of Sciences of the United States of America*, **106 (37)**, doi:10.1073/pnas.0906865106.

Schoof, J. T., T. W. Ford, and S. C. Pryor, 2017: Recent changes in U.S. regional heat

wave characteristics in observations and reanalyses. *Journal of Applied Meteorology and Climatology*, doi:10.1175/JAMC-D-16-0393.1.

Schubert, S. D., M. J. Suarez, P. J. Pegion, R. D. Koster, and J. T. Bacmeister, 2004: Causes of long-term drought in the U.S. Great Plains. *Journal of Climate*, **17 (3)**, 485–503, doi:10.1175/1520-0442(2004)017¡0485:COLDIT¿2.0.CO;2.

Schubert, S. D., H. Wang, R. D. Koster, M. J. Suarez, and P. Y. Groisman, 2014: Northern Eurasian heat waves and droughts. *Journal of Climate*, doi:10.1175/JCLI-D-13-00360.1.

Smith, T. T., B. F. Zaitchik, and J. M. Gohlke, 2013: Heat waves in the United States: Definitions, patterns and trends. *Climatic Change*, doi:10.1007/s10584-012-0659-2.

Souch, C., and C. S. Grimmond, 2004: Applied climatology: 'Heat waves'. *Progress in Physical Geography*, doi:10.1191/0309133304pp428pr.

Steadman, R. G., 1979: The assessment of sultriness. Part I. A temperature-humidity index based on human physiology and clothing science. *Journal of Applied Meteorology*, doi:10.1175/1520-0450(1979)018¡0861:TAOSPI¿2.0.CO;2.

Steadman, R. G., 1984: A universal scale of apparent temperature. *Journal of Climate & Applied Meteorology*, **23 (12)**.

Stefanon, M., F. Dandrea, and P. Drobinski, 2012: Heatwave classification over

Europe and the Mediterranean region. *Environmental Research Letters*, doi: 10.1088/1748-9326/7/1/014023.

Steiner, J. L., and Coauthors, 2020: Grassland wildfires in the southern great plains: Monitoring ecological impacts and recovery. *Remote Sensing*, **12 (619)**, doi:10.3390/rs12040619.

Tamrazian, A., S. LaDochy, J. Willis, and W. C. Patzert, 2008: Heat Waves in Southern California: Are They Becoming More Frequent and Longer Lasting? *Yearbook of the Association of Pacific Coast Geographers*, doi:10.1353/pcg.0.0001.

Tan, J., Y. Zheng, G. Song, L. S. Kalkstein, A. J. Kalkstein, and X. Tang, 2007: Heat wave impacts on mortality in Shanghai, 1998 and 2003. *International Journal of Biometeorology*, **51**, 193–2000.

Teskey, R., T. Wertin, I. Bauweraerts, M. Ameye, M. A. McGuire, and K. Steppe, 2015: Responses of tree species to heat waves and extreme heat events. doi: 10.1111/pce.12417.

Tosunoglu, F., and O. Kisi, 2017: Trend Analysis of Maximum Hydrologic Drought Variables Using Mann–Kendall and Şen's Innovative Trend Method. *River Research and Applications*, **33**, 597–610, doi:10.1002/rra.3106.

Trenberth, K. E., and J. T. Fasullo, 2012: Climate extremes and climate change: The Russian heat wave and other climate extremes of 2010. *Journal of Geophysical Research Atmospheres*, doi:10.1029/2012JD018020.

van der Velde, M., F. N. Tubiello, A. Vrieling, and F. Bouraoui, 2012: Impacts of extreme weather on wheat and maize in France: Evaluating regional crop simulations against observed data. *Climatic Change*, **113 (3-4)**, doi:10.1007/s10584-011-0368-2.

White, D., A. Roschelle, P. Peterson, D. Schlissel, B. Biewald, and W. Steinhurst, 2003: The 2003 blackout: Solutions that won't cost a fortune. *Electricity Journal*, **16 (9)**, doi:10.1016/j.tej.2003.10.002.

Whitman, S., G. Good, E. R. Donoghue, N. Benbow, W. Shou, and S. Mou, 1997: Mortality in Chicago attributed to the July 1995 heat wave. *American Journal of Public Health*, doi:10.2105/AJPH.87.9.1515.

Wolf, S., and Coauthors, 2016: Warm spring reduced carbon cycle impact of the 2012 US summer drought. *Proceedings of the National Academy of Sciences of the United States of America*, **113 (21)**, 5880–5885, doi:10.1073/pnas.1519620113.

Wreford, A., and W. Neil Adger, 2010: Adaptation in agriculture: Historic effects of heat waves and droughts on UK agriculture. *International Journal of Agricultural Sustainability*, **8**, 278–289, doi:10.3763/ijas.2010.0482.

Wu, X., L. Wang, R. Yao, M. Luo, S. Wang, and L. Wang, 2020: Quantitatively evaluating the effect of urbanization on heat waves in China. *Science of the Total Environment*, doi:10.1016/j.scitotenv.2020.138857.

Wu, Z., H. Lin, J. Li, Z. Jiang, and T. Ma, 2012: Heat wave frequency variability over North America: Two distinct leading modes. *Journal of Geophysical Research Atmospheres*, doi:10.1029/2011JD016908.

Yilmaz, B., 2019: Analysis of hydrological drought trends in the GAP region (south-eastern Turkey) by Mann-Kendall test and innovative sen method. *Applied Ecology and Environmental Research*, **17**, 3325–3342, doi:10.15666/aeer/1702_33253342.

Zamuda, C., and Coauthors, 2013: U.S. Energy Sector Vulnerabilities to Climate Change and Extreme Weather. Tech. rep.

Zhang, X., G. Hegerl, F. W. Zwiers, and J. Kenyon, 2005: Avoiding inhomogeneity in percentile-based indices of temperature extremes. *Journal of Climate*, doi: 10.1175/JCLI3366.1.

Zuo, J., S. Pullen, J. Palmer, H. Bennetts, N. Chileshe, and T. Ma, 2015: Impacts of heat waves and corresponding measures: A review. doi: 10.1016/j.jclepro.2014.12.078.

Appendices

Appendix-A

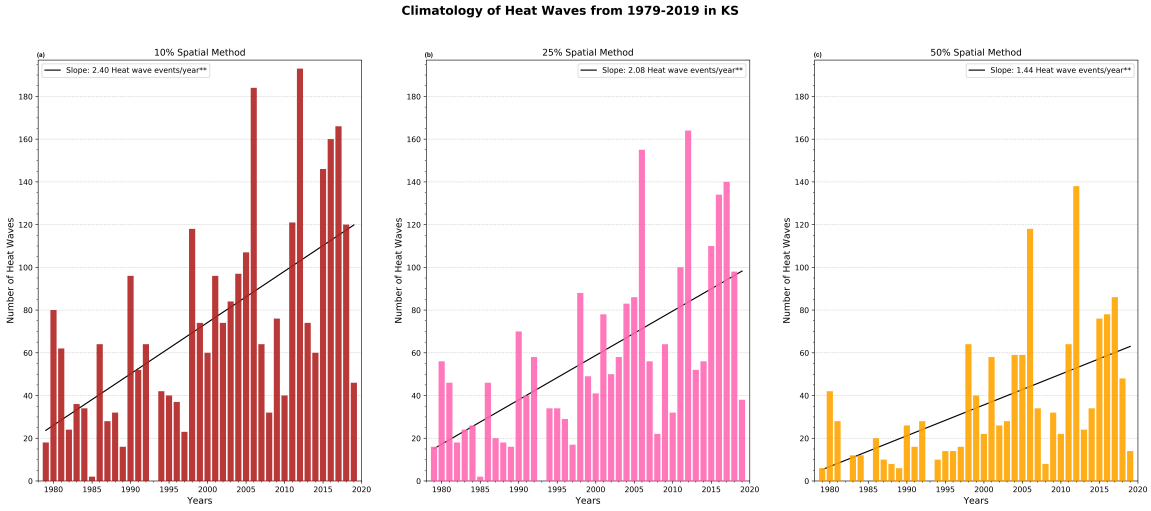

Figure A.1: Time Series from the climatology of heat wave events for Kansas. (a) Time Series of the climatology heat wave events established using the 10% spatial method. (b) Same as (a), but utilizing the 25% spatial method to produce the heat wave climatology. (c) Same as (a), but employing the 50% spatial method in the heat wave identification methodology. Trends indicated with single asterisk (*) are significant at the p <0.1 level, while those marked with a double asterisk (**) are significant at the p <0.05 level.

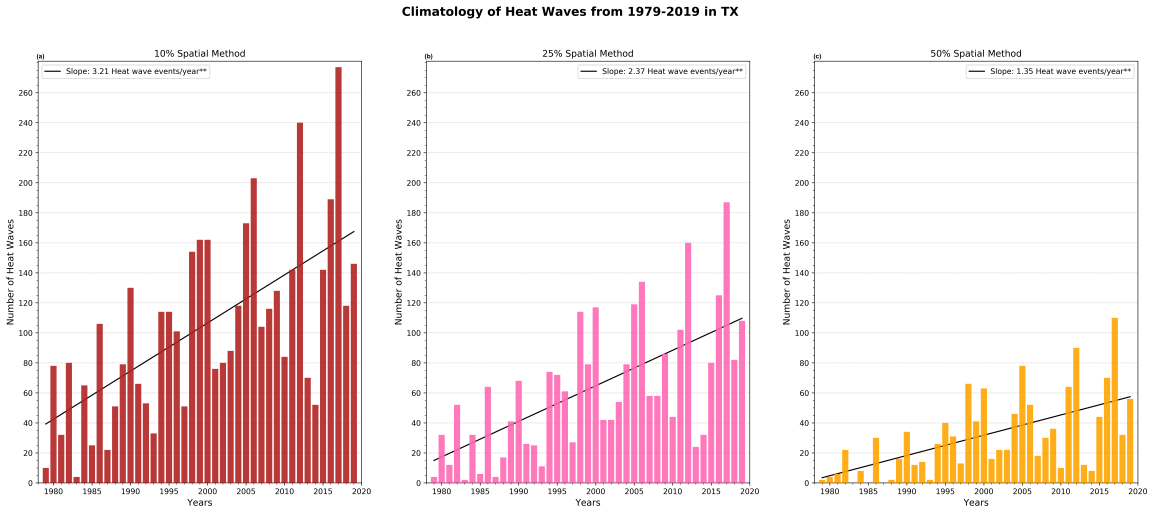

Figure A.2: Same as Figure A.1, but for Texas.

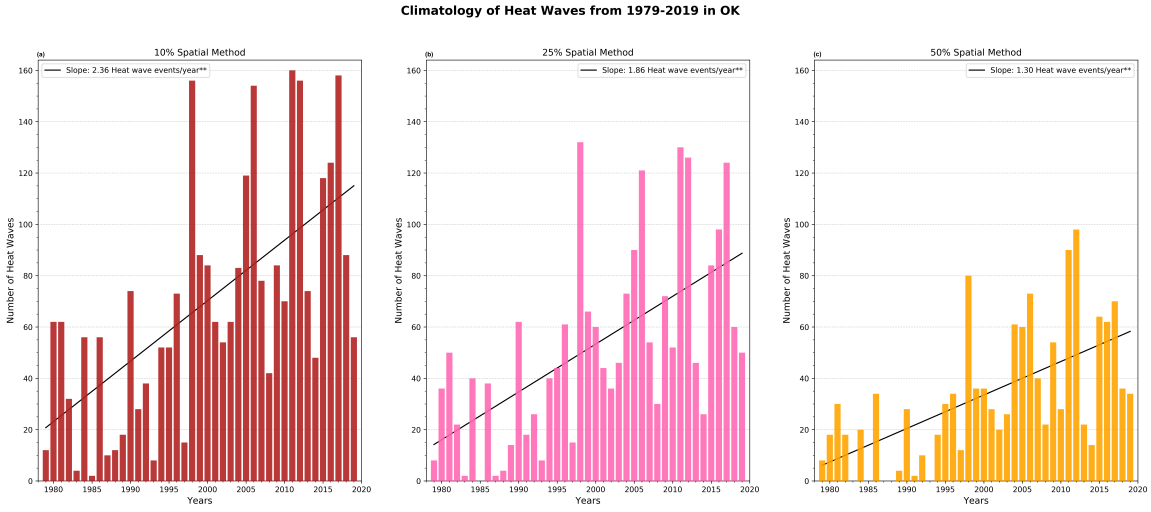

Figure A.3: Same as Figure A.1, instead for Oklahoma.

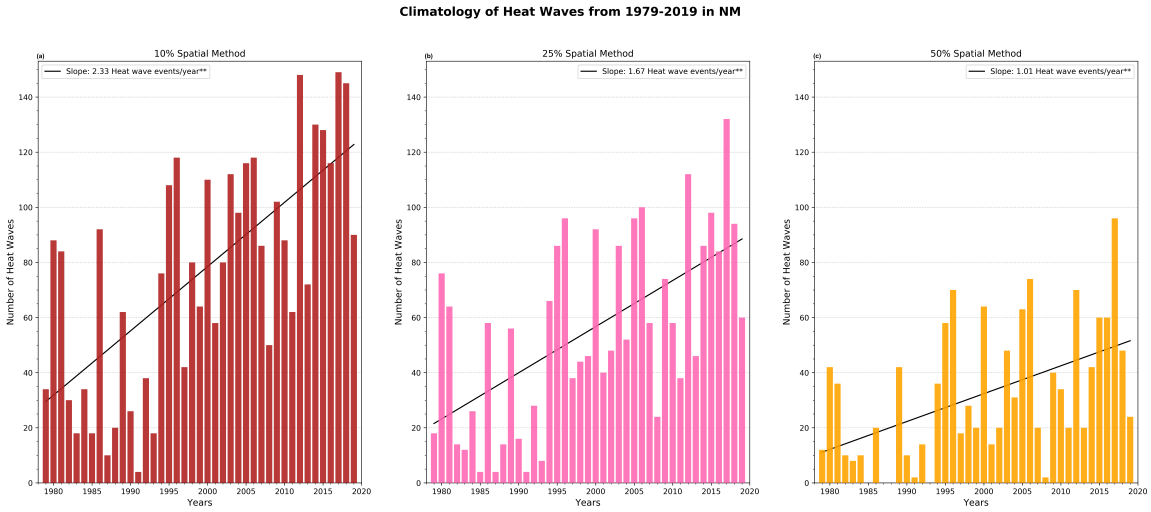

Figure A.4: Same as Figure A.1, but for New Mexico.

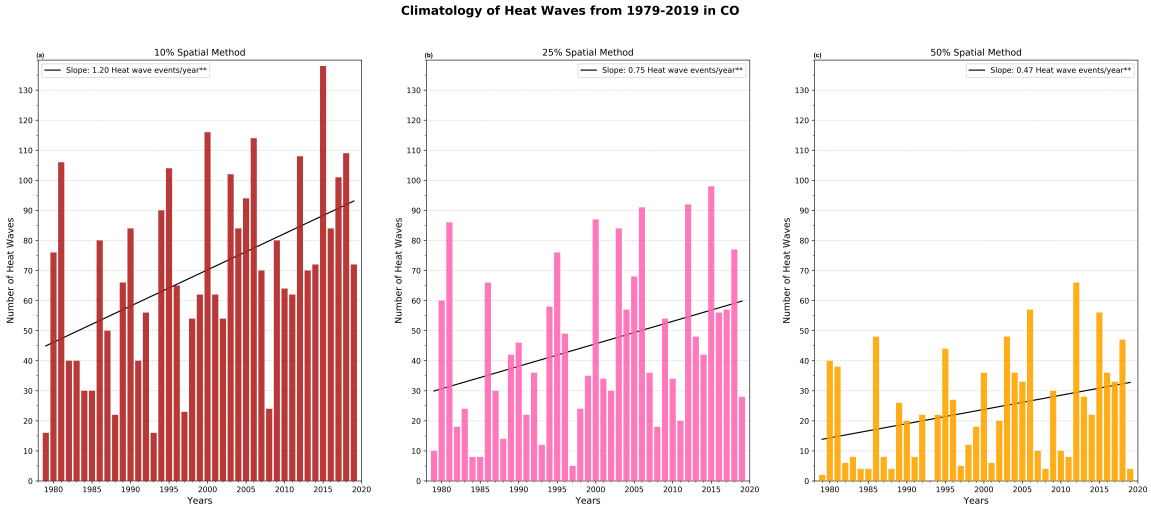

Figure A.5: Same as Figure A.1, but for Colorado.

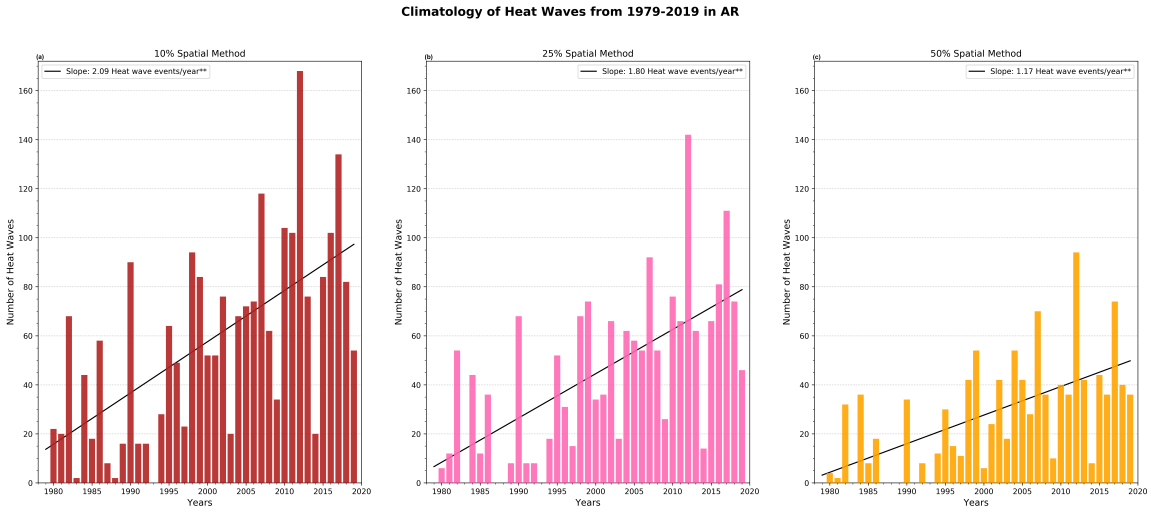

Figure A.6: Same as Figure A.1, instead for Arkansas.

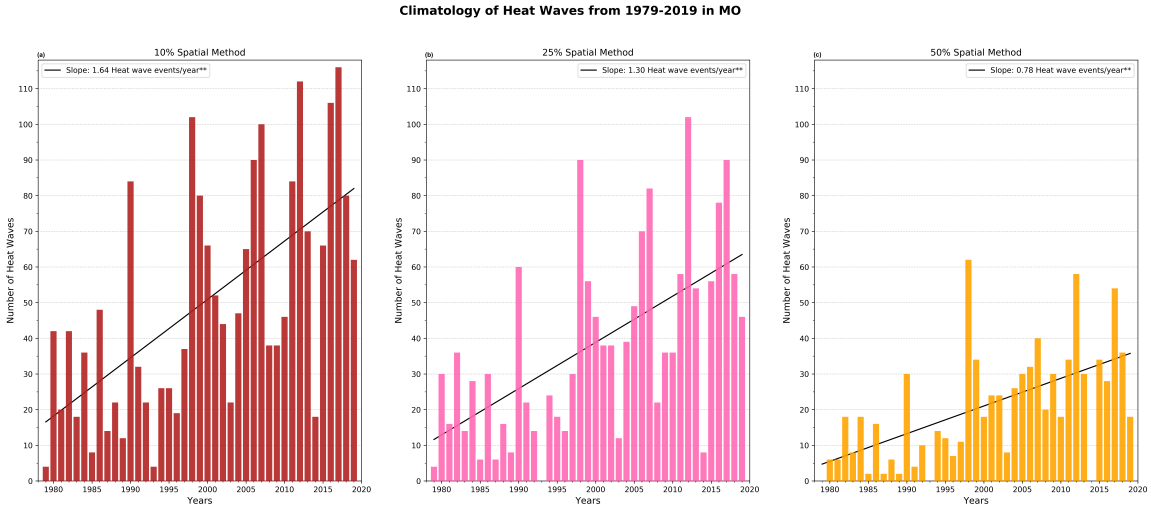

Figure A.7: Same as Figure A.1, instead for Missouri.

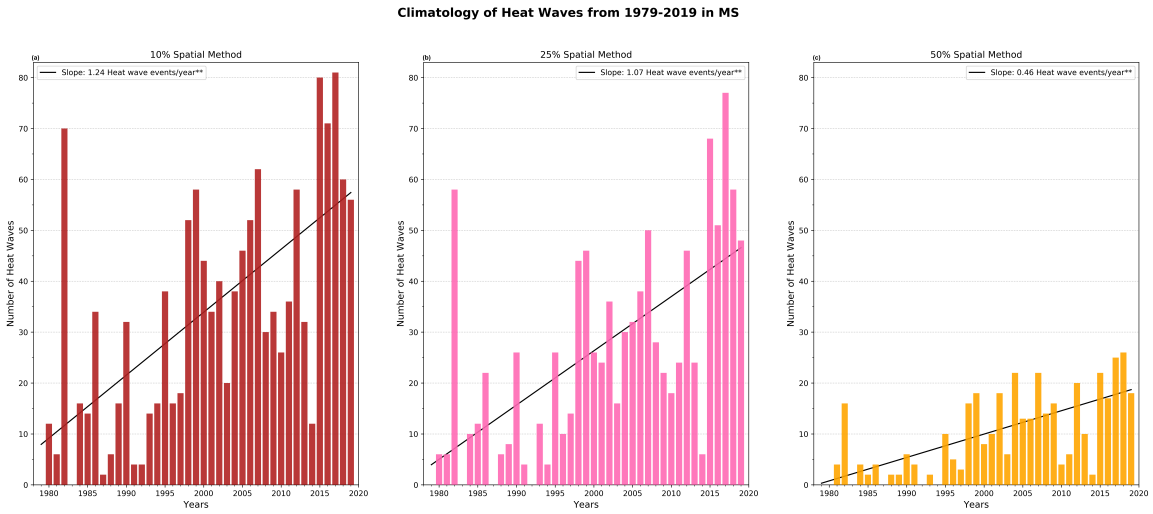

Figure A.8: Same as Figure A.1, instead for Mississippi.

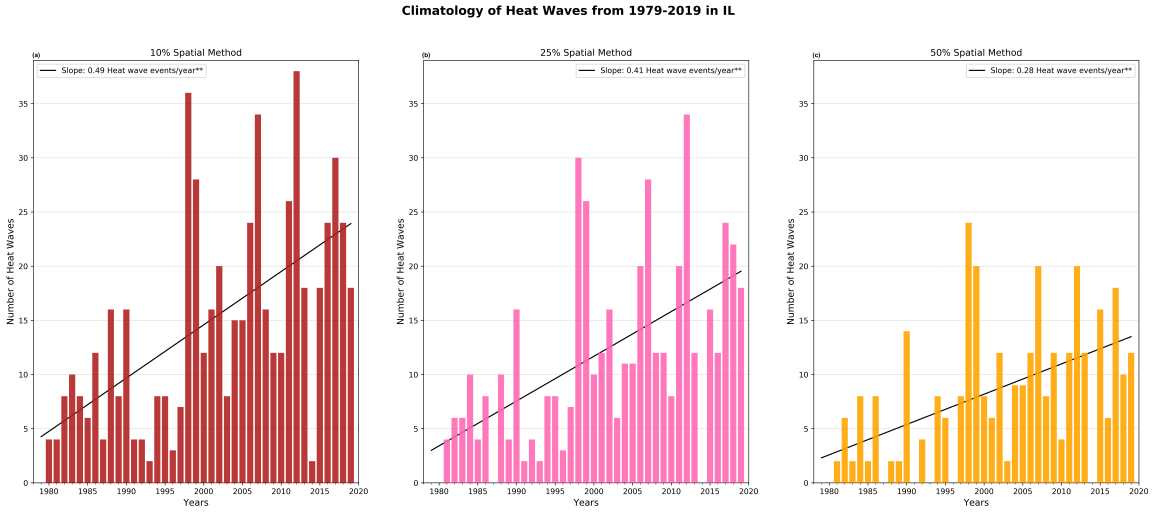

Figure A.9: Same as Figure A.1, but for Illinois.

Appendix-B

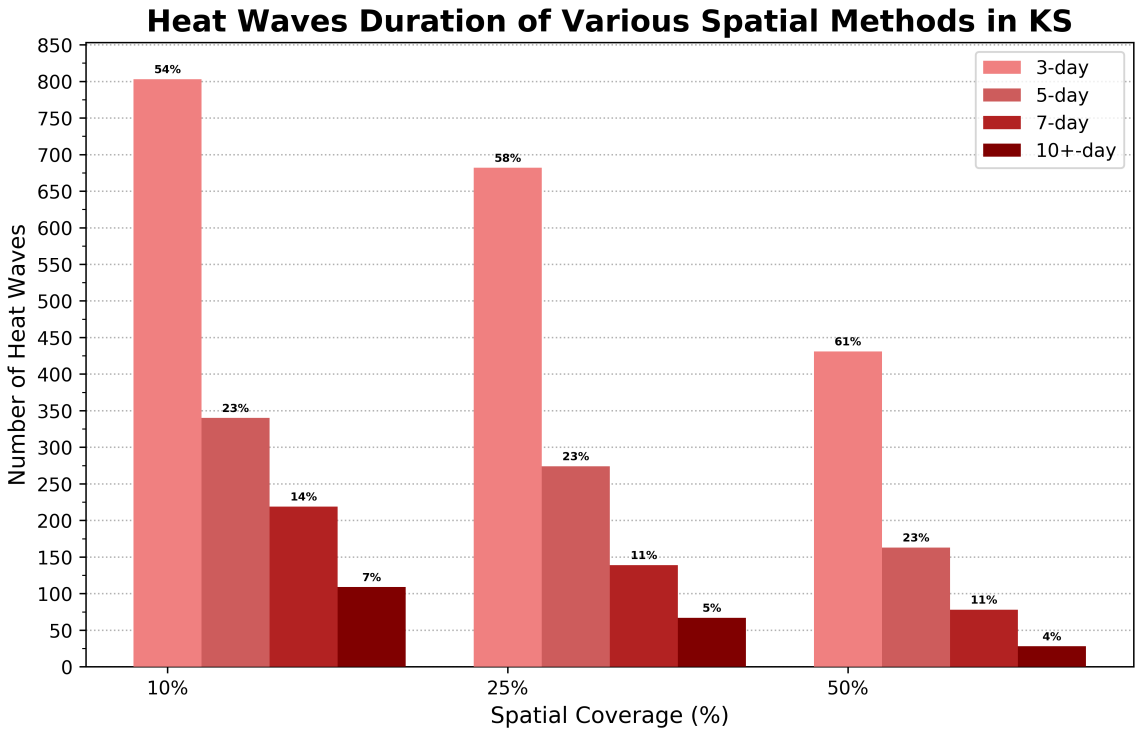

Figure B.1: Number of heat wave events from the study time period in each duration category for the state of Kansas for all three spatial methods (10%, 25%, and 50%). Percentage of heat wave events within the overall climatology that fall in each duration category displayed on top of each bar.

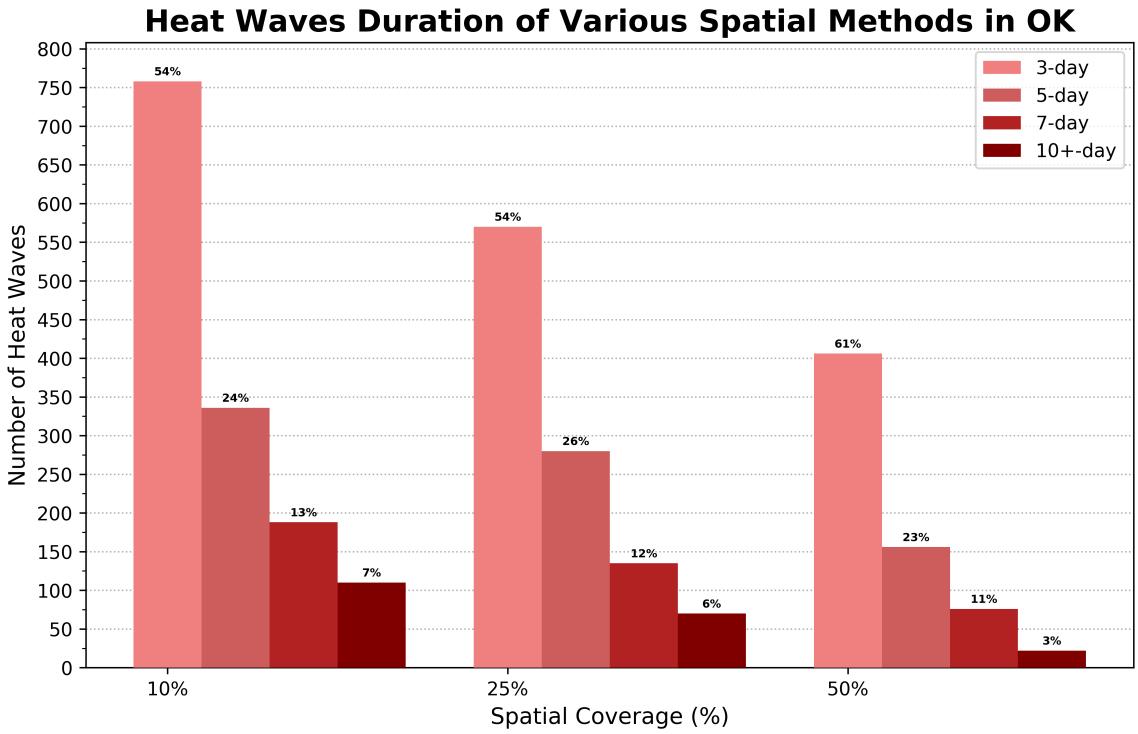

Figure B.2: Same as Figure B.1, but for Oklahoma.

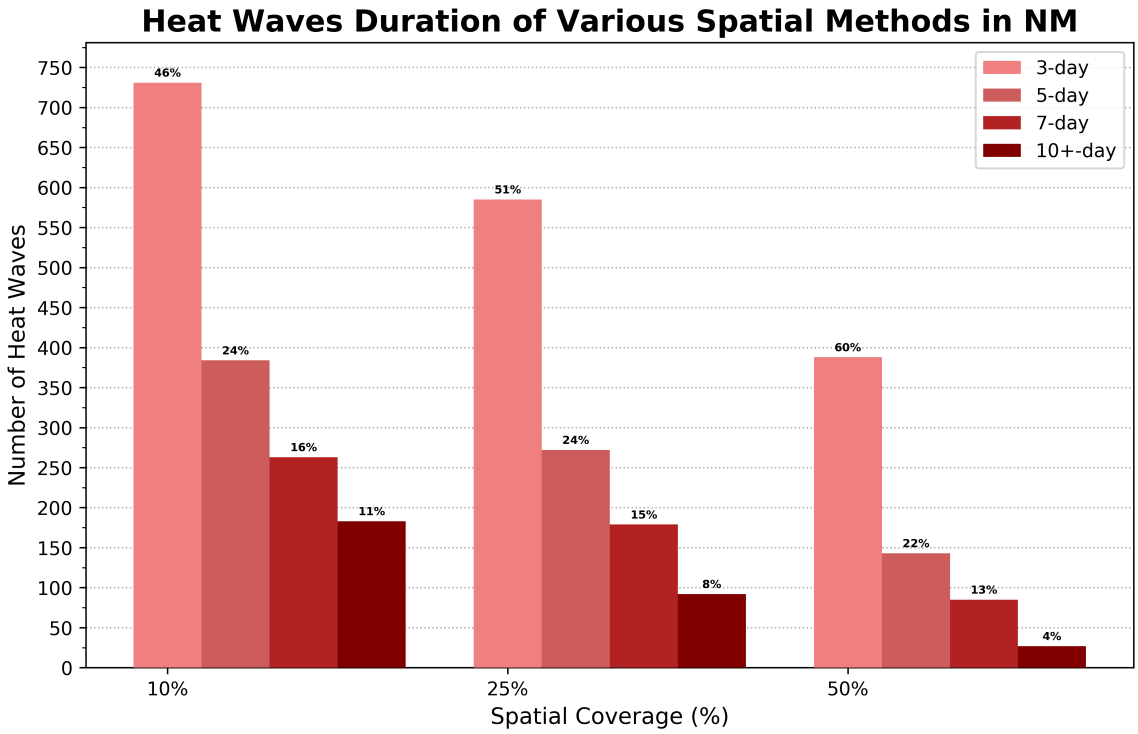

Figure B.3: Same as Figure B.1, but for New Mexico.

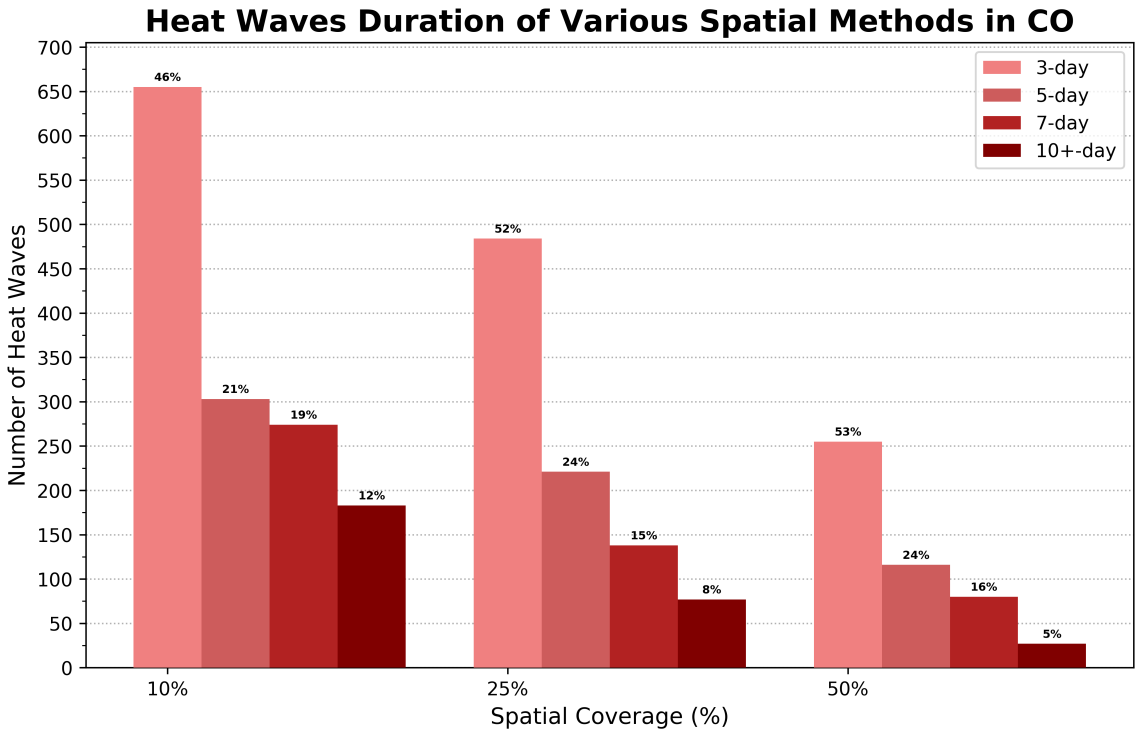

Figure B.4: Same as Figure B.1, but for Colorado.

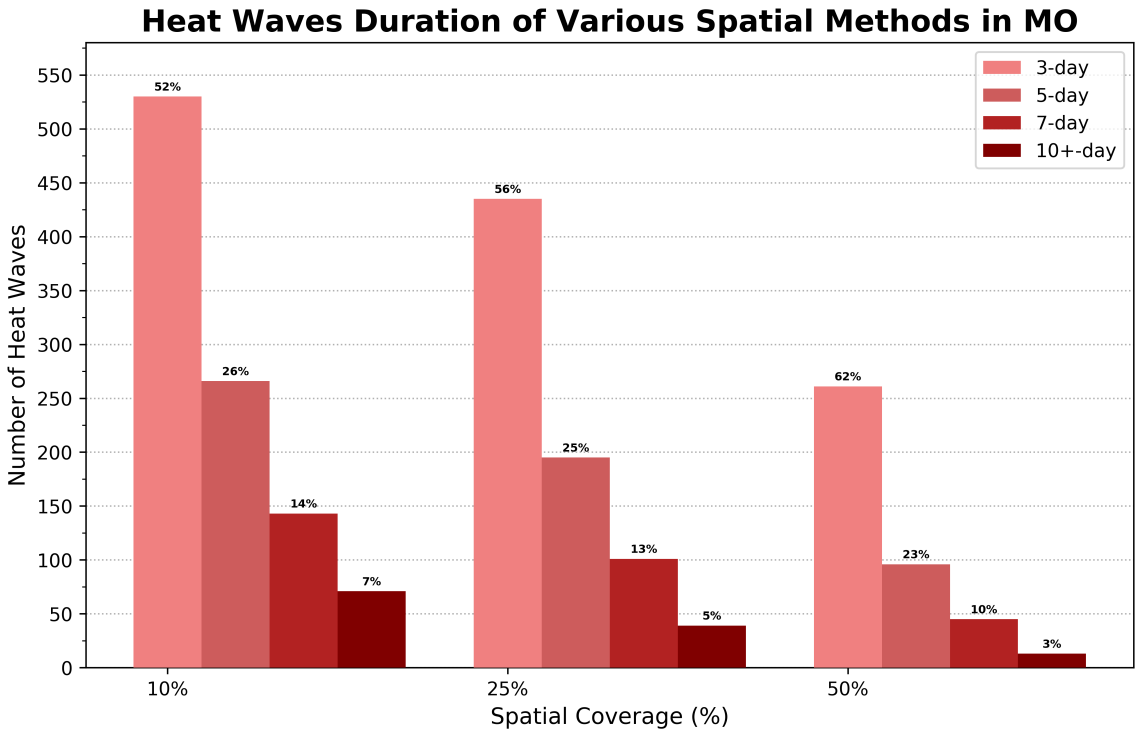

Figure B.5: Same as Figure B.1, instead for Missouri.

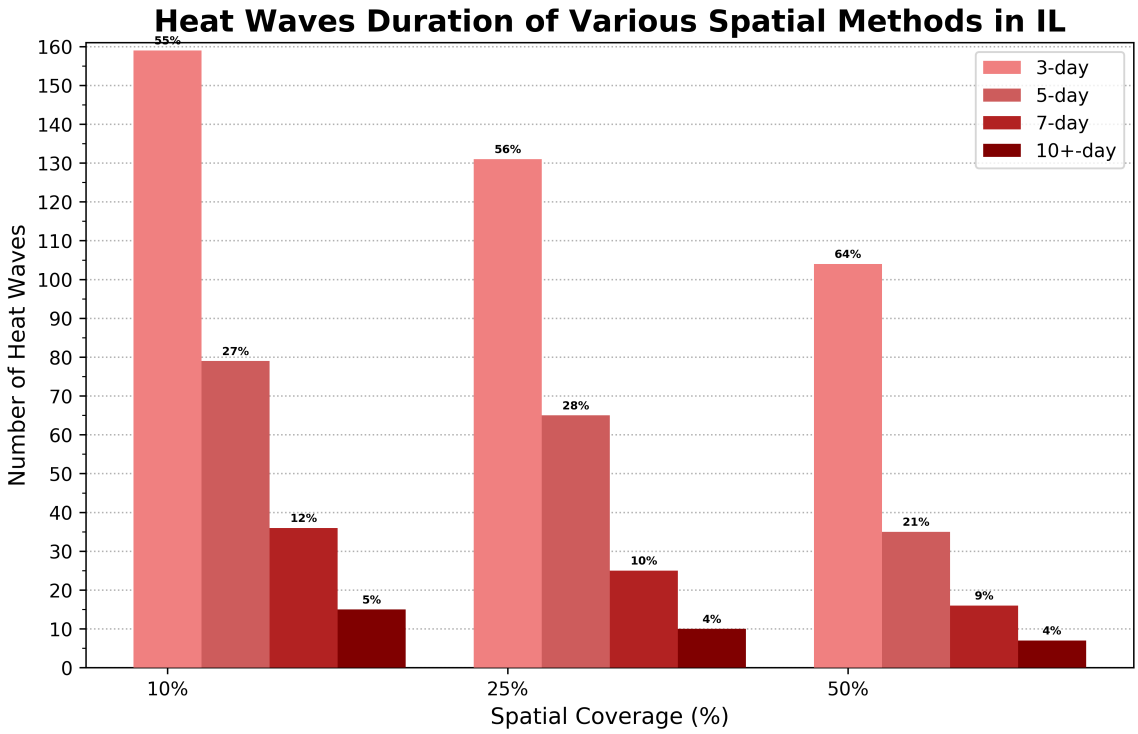

Figure B.6: Same as Figure B.1, instead for Illinois.

Appendix-C

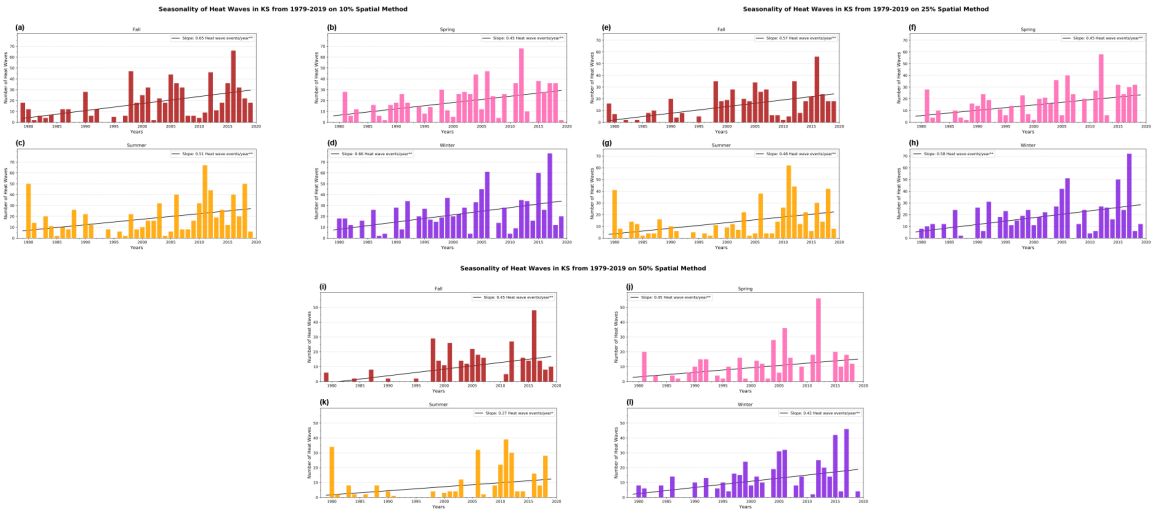

Figure C.1: Annual frequency of heat wave events during each season (i.e., fall, spring, summer, and winter) for all three spatial methods in Kansas. (a-d) all four seasons utilizing the 10% spatial coverage method, (e-h) all four seasons using the 25% spatial method, and (i-l) all four seasons employing the 50% spatial coverage method.Trends indicated with single asterisk (*) are significant at the p <0.1 level, while those marked with a double asterisk (**) are significant at the p <0.005 level.

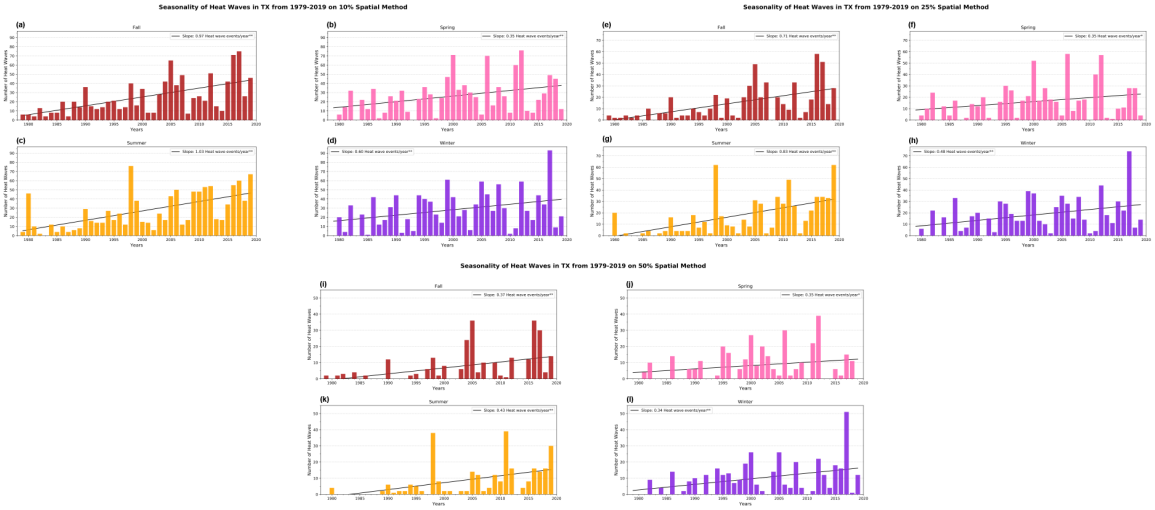

Figure C.2: Same as Figure C.1, but for Texas.

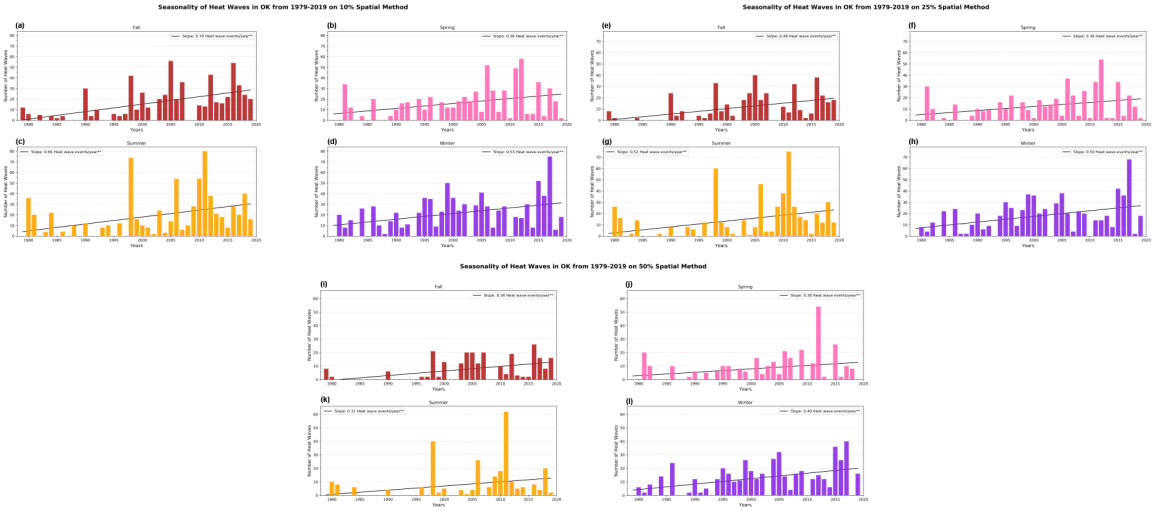

Figure C.3: Same as Figure C.1, but for Oklahoma.

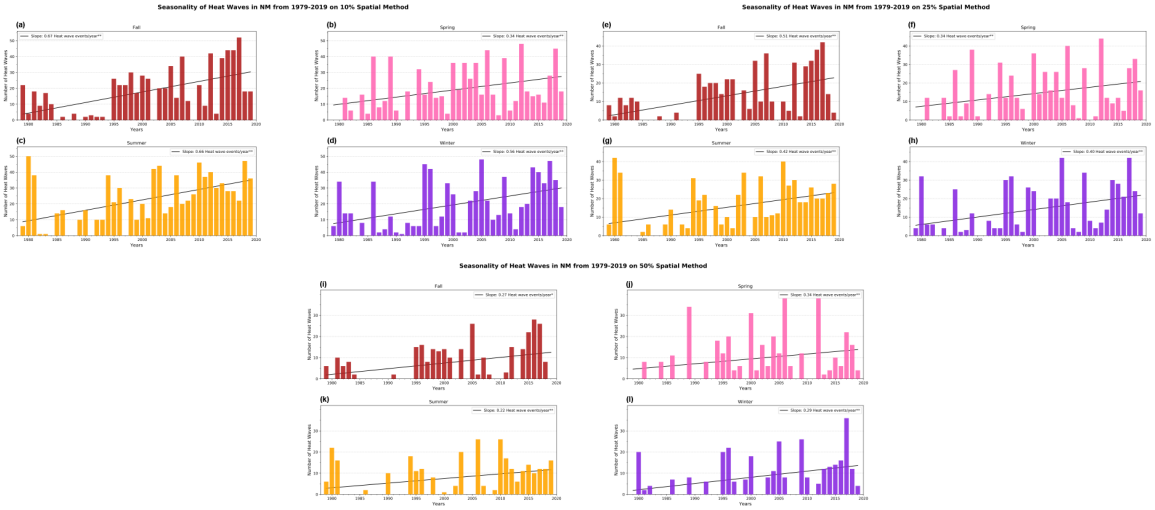

Figure C.4: Same as Figure C.1, but for New Mexico.

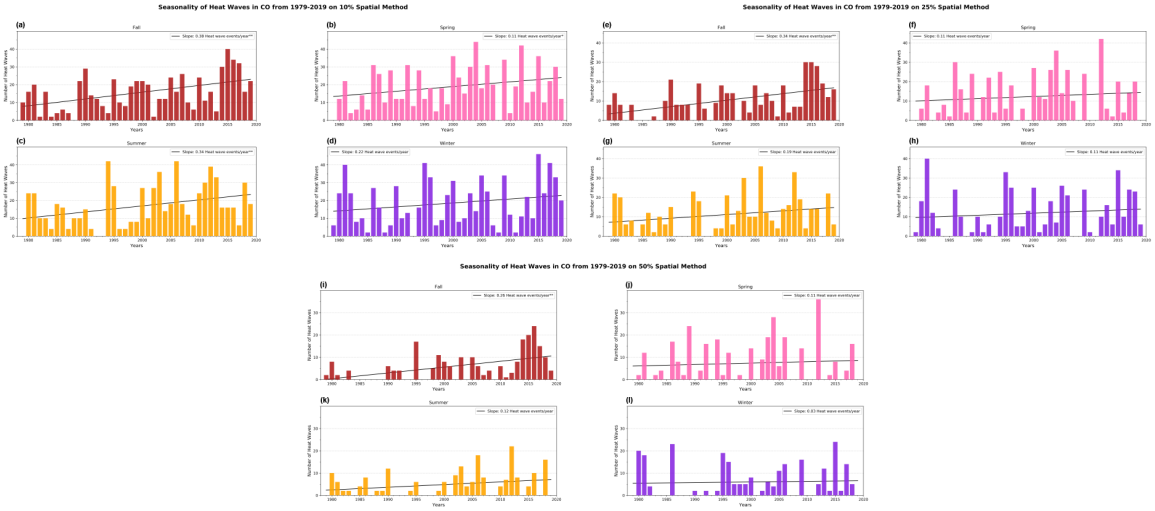

Figure C.5: Same as Figure C.1, instead for Colorado.

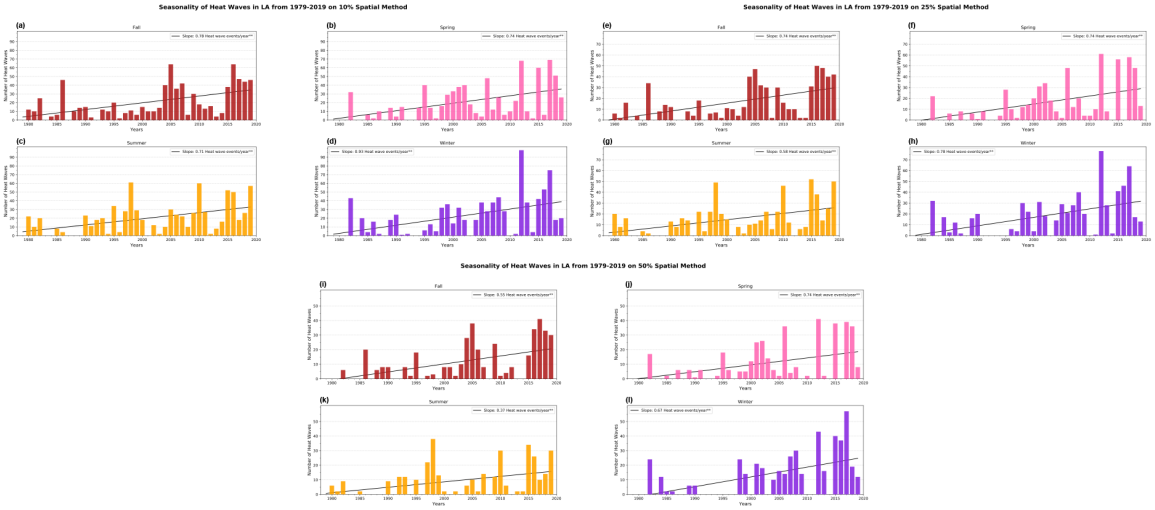

Figure C.6: Same as Figure C.1, but for Louisiana.

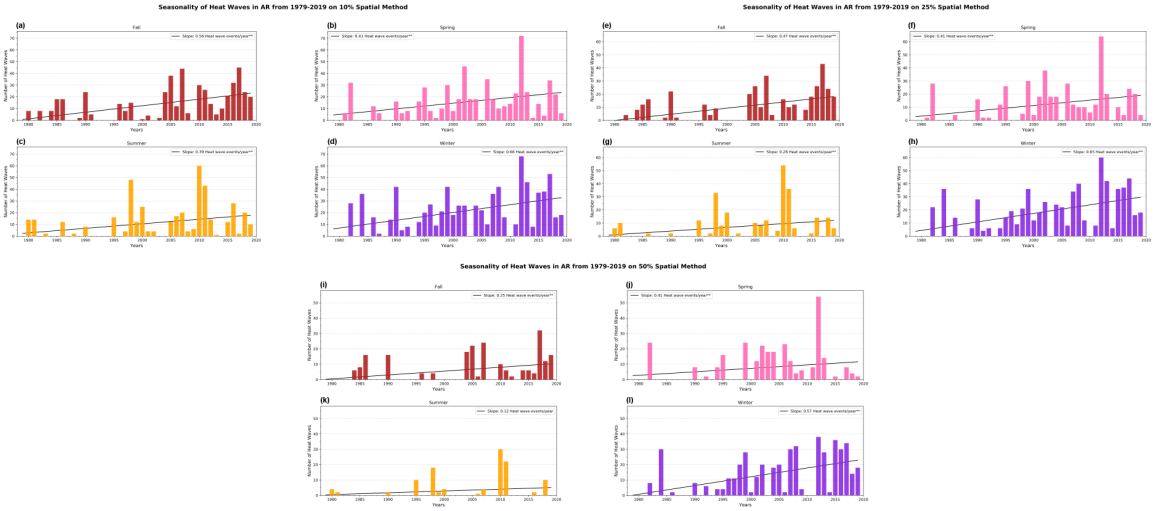

Figure C.7: Same as Figure C.1, but for Arkansas.

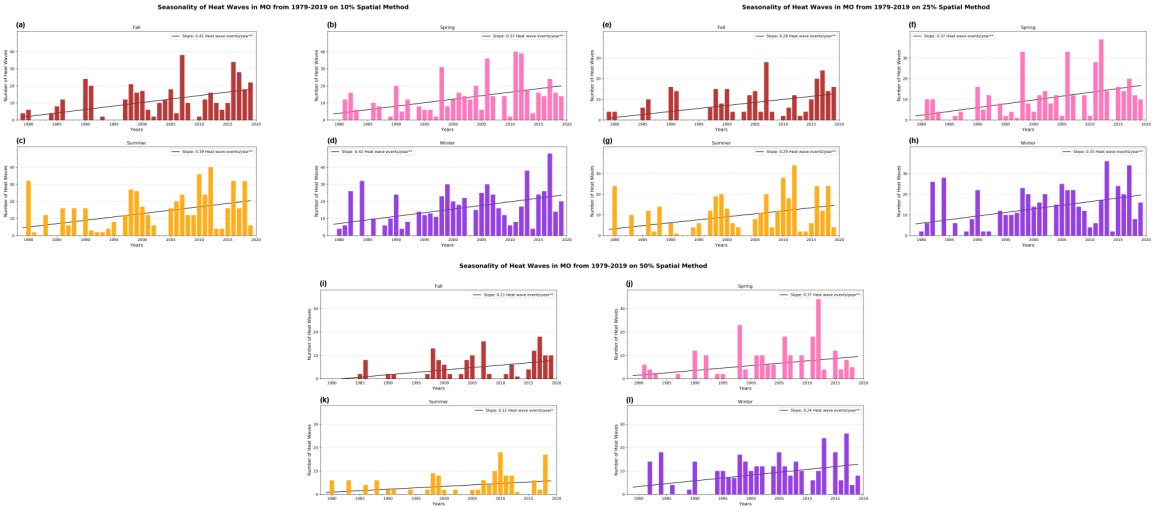

Figure C.8: Same as Figure C.1, instead for Missouri.

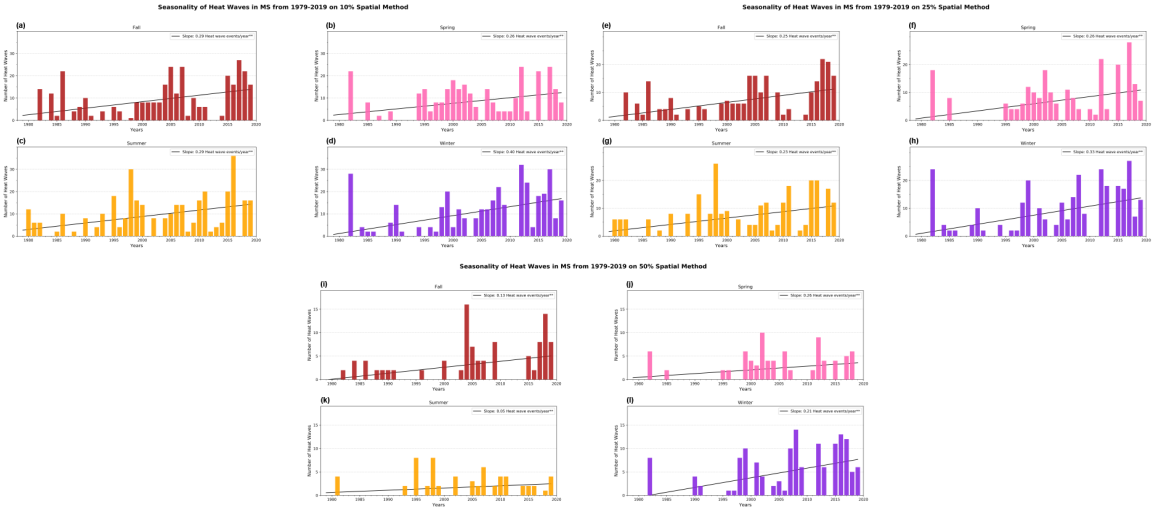

Figure C.9: Same as Figure C.1, instead for Mississippi.

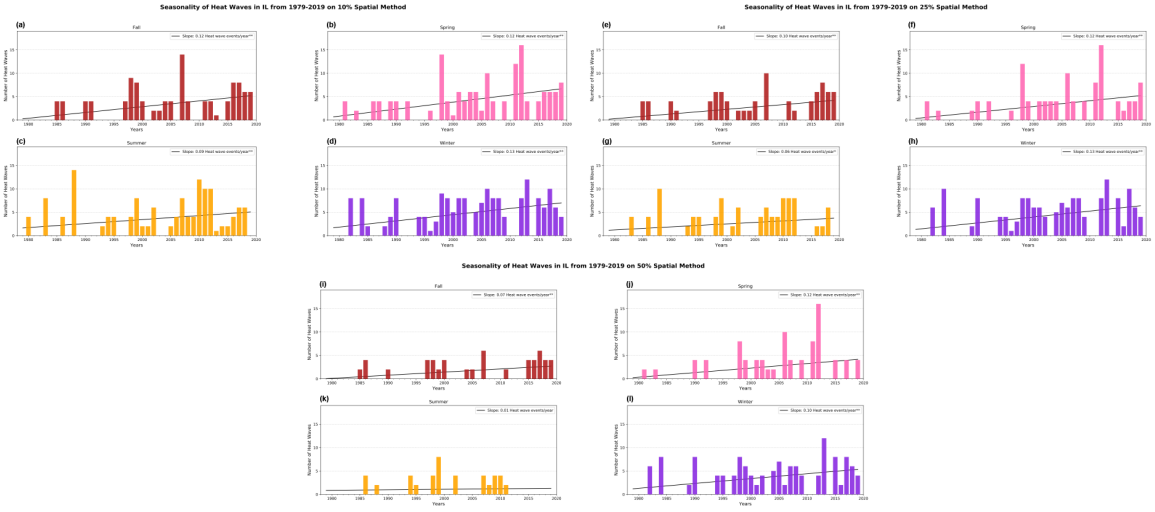

Figure C.10: Same as Figure C.1, instead for Illinois.